CONSTITUTIVE MODELING OF CREEP OF SINGLE CRYSTAL SUPERALLOYS

A Dissertation

by

SHARAT CHAND PRASAD

Submitted to the Office of Graduate Studies of
Texas A&M University
in partial fulfillment of the requirements for the degree of

DOCTOR OF PHILOSOPHY

August 2005

Major Subject: Mechanical Engineering

CONSTITUTIVE MODELING OF CREEP OF SINGLE CRYSTAL SUPERALLOYS

A Dissertation

by

SHARAT CHAND PRASAD

Submitted to the Office of Graduate Studies of
Texas A&M University
in partial fulfillment of the requirements for the degree of

DOCTOR OF PHILOSOPHY

Approved by:

Chair of Committee,	K. R. Rajagopal
Committee Members,	J. N. Reddy
	Ibrahim Karaman
	Jay R. Walton
Head of Department,	Dennis O'Neal

August 2005

Major Subject: Mechanical Engineering

ABSTRACT

Constitutive Modeling of Creep of Single Crystal Superalloys. (August 2005)
Sharat Chand Prasad, B.Tech., Indian Institute of Technology, Kanpur;
M.S., Texas A&M University
Chair of Advisory Committee: Dr. K. R. Rajagopal

In this work, a constitutive theory is developed, within the context of continuum mechanics, to describe the creep deformation of single crystal superalloys. The constitutive model that is developed here is based on the fact that as bodies deform the stress free state that corresponds to the current configuration (referred to as the "natural configuration", i.e., the configuration that the body would attain on the removal of the external stimuli) evolves. It is assumed that the material possesses an infinity of natural (or stress-free) configurations, the underlying natural configuration of the body changing during the deformation process, with the response of the body being elastic from these evolving natural configurations. It is also assumed that the evolution of the natural configurations is determined by the tendency of the body to undergo a process that maximizes the rate of dissipation. Central to the theory is the prescription of the forms for the stored energy and rate of dissipation functions. The stored energy reflects the fact that the elastic response exhibits cubic symmetry. Consistent with experiments, the elastic response from the natural configuration is assumed to be linearly elastic and the model also takes into account the fact that the symmetry of single crystals does not change with inelastic deformation. An appropriate form for the inelastic stored energy (the energy that is 'trapped' within dislocation networks) is also utilized based on simple ideas of dislocation motion. In lieu of the absence of any experimental data to corroborate with, the form for the inelastic stored energy is assumed to be isotropic. The rate of dissipation function is

chosen to be anisotropic, in that it reflects invariance to transformations that belong to the cubic symmetry group. The rate of dissipation is assumed to be proportional to the density of mobile dislocations and another term that takes into account the damage accumulation due to creep. The model developed herein is used to simulate uniaxial creep of <001>, <111> and <011> oriented single crystal nickel based superalloys for a range of temperatures. The predictions of the theory match well with the available experimental data for CMSX-4. The constitutive model is also implemented as a User Material (UMAT) in commercial finite element software ABAQUS to enable the analysis of more general problems. The UMAT is validated for simple problems and the numerical scheme based on an implicit backward difference formula works well in that the results match closely with those obtained using a semi-inverse approach.

To my mother, father and brother, Manish

ACKNOWLEDGMENTS

I would like to express my sincere gratitude to Prof. K.R. Rajagopal for giving me this excellent opportunity to work with him. During my four years of stay in the graduate school, I have learnt a great deal from his vast knowledge in mechanics, mathematics and life in general. His demand for perfection in everything has always inspired and challenged me to put forth my best effort. Prof. Rajagopal's lectures on continuum mechanics and elasticity were outstanding and his unique style of teaching always kept my enthusiasm sky high. His discourses on various aspects of mechanics both during the group meetings and during our personal interactions have helped me think critically. The freedom that he gave me in pursuing my ideas during the course of my research work has helped me prepare mentally to work as an independent researcher.

I would also like to gratefully acknowledge Prof. J.N. Reddy's support, encouragement and advice during the course of my research work. Prof. Reddy's lectures on non-linear finite element methods and composites inspired me a great deal about the computational aspects of engineering problems. His course on non-linear finite element method is one of the most challenging courses that I had during my stay in the graduate school. Prof. Reddy's well organized classes and assignments were extremely helpful in gaining a strong foothold in computational mechanics.

I would like to thank Prof. Jay R. Walton for serving on my committee. Prof. Walton's classes on applied mathematics and mathematical foundations of continuum mechanics helped me acquire the mathematical background needed for research work in continuum mechanics. His well organized classes and challenging assignments always fascinated me.

I would also like to thank Dr. Ibrahim Karaman for serving on my committee.

I also want to thank Dr. I. Joga Rao who was the co-principal investigator of

the project I worked on. His advice and help on various issues during the research work was very useful.

I would also take this opportunity to thank Dr. Luoyi Tao, Dr. J. Murali Krishnan and Dr. Krishna Kannan for their support, encouragement and advice and helping me out whenever I was stuck. My numerous discussions on various issues related to my research work and mechanics in general with Dr. Krishna Kannan, Dr. Saravanan Umakanthan, Dr. Anand Mohan, Dr. Pradeep Hariharkumar, Parag Ravindran, and Shankar C. Subramanian have helped me think clearly and analyze issues with a broader perspective.

I am also grateful for all the love, support and encouragement that I received from my family. I am deeply indebted to my parents who have always encouraged me to put my greatest effort into all my endeavors. They taught me the importance of knowledge and learning and the merit of being a good human being. My parent's lessons in science and mathematics during my early school years through high school inspired me to pursue a career in science and engineering. I am also grateful to my brother, Manish, who has always inspired me by always setting a high standard and leading by example and for telling me, no matter how well I do, that it is not good enough.

Some of the results of the current work were obtained using the Supercomputing facility at Texas A&M University. I wish to acknowledge their support. The financial support provided by United States Department of Energy through Contract # DE-FC26-01NT41344 is also gratefully acknowledged.

TABLE OF CONTENTS

CHAPTER Page

LIST OF TABLES

LIST OF FIGURES

FIGURE Page

FIGURE Page

FIGURE Page

FIGURE Page

CHAPTER I

INTRODUCTION

The demand to increase the efficiency of gas turbines used in power generation and aircraft applications has fueled research to develop advanced materials for gas turbine blades that can withstand high temperatures. In fact, higher efficiencies of such engines are possible if turbine blades can be designed to withstand inlet temperature of the order of 1500 ^{o}C or more. At such high temperatures, it is critical to use materials that have excellent creep capabilities.

The term "Superalloys" describe a group of alloys developed for applications that require high performance at elevated temperatures. Superalloys have a load bearing capacity up to 0.9 times their melting temperature. They retain their strength even after long exposure time at high temperatures and they have good low temperature ductility as well. There are three categories of superalloys that have been developed:

1. Nickel based superalloys
2. Iron-nickel based superalloys
3. Cobalt based superalloys

Superalloys are available as

1. Polycrystalline superalloys
2. Columnar grain directionally solidified superalloys
3. Single crystal superalloys

The journal model is *IEEE Transactions on Automatic Control.*

Table I. Some applications of superalloys [17, 18].

Aircraft/industrial gas turbines
Blades, Vanes, Disks, Bolts, Shafts, Cases, Combustors,
Afterburners, Thrust reversers
Steam turbines
Blades, Bolts, Reheaters
Automotive components
Turbochargers, Exhaust valves
Nuclear power systems
Control-rod drive mechanisms, Valve stems, Springs, Ducting
Space vehicles
Aerodynamically heated skins, Rocket engine parts
Medical components
Prosthetic devices
Metal processing
Hot work tools and dies

Because of their excellent thermal, fatigue and creep properties, superalloys are used in numerous applications. Table I lists some of the applications of superalloys.

Single crystal superalloys have the highest temperature capacity and hence they are used in the hottest sections of gas turbine engines. The most important of these alloys are the ones which are based on nickel and modeling the creep behavior of such alloys is the primary goal of current work. Henceforth focus will be laid on describing the behavior of single crystal nickel based superalloys.

Single crystal superalloys have superior thermal, fatigue and creep properties amongst the class of superalloys because grain boundaries have been eliminated. A

Table II. Generations of single crystal nickel based superalloys and their composition [18].

Alloy	Ni	Cr	Co	Mo	W	Al	Ti	Ta	Re	Nb	V	Hf
First generation												
PWA 1480	62.5	10	5		4	5	1.5	12				
René N4	62.6	9	8	2	6	3.7	4.2	4		0.5		
CMSX-2	66.6	8	4.6	0.6	7.9	5.6	0.9	5.8				
SRR 99	66.5	8.5	5		9.5	5.5	2.2	2.8				
Second generation												
PWA 1484	59.4	5	10	2	6	5.6		9	3			
René N5	61.8	7	8	2	5	6.2		7	3			0.2
CMSX 4	61.8	6.5	9	0.6	6	5.6	1	6.5	3			0.1
CMSX 6	70.4	10	5	3		4.8	4.7	2				0.1
Third generation												
CMSX-10	69.6	2	3	0.4	5	5.7	0.2	8	6	0.1		0.03
René N6	57.4	4.2	12.5	1.4	6	5.75	0	7.2	5.4	0	0	0.15

whole generation of single crystal nickel based superalloys have been developed over the last few decades with significant improvement in the operating temperature. Table II lists the generations of single crystal nickel based superalloys developed over last few decades.

The second and third generation of superalloys are characterized by increasing concentration of Rhenium which improves creep and fatigue resistance. Fourth generation superalloys with Ruthenium are also being developed with further enhancement in high temperature creep resistance.

Table II also lists the alloying elements that are added in single crystal nickel

Table III. Role of alloying elements in superalloys [17, 18].

Effects	Alloying elements
Solid solution strengthening	Co, Cr, Mo, W, Ta, Re
Formation of γ' (Ni_3Al, Ni_3Ti), the principle strengthening phase	Al, Ti
Raises solvus temperature of γ'	Co
Oxidation resistance	Al, Cr
Formation of hardening phase γ'' (Ni_3Nb)	Nb
Sulfidation resistance	Cr, Co
Retards γ' rafting	Re
Formation of topologically closed packed (TCP) phases[1]	Co, Mo, W, Re, Cr

based superalloys. Various alloying additions alter the thermal and mechanical behavior of superalloys. Since single crystal nickel based superalloys are multi-phase alloys, the presence of various alloying additions significantly alter the microstructure. Table III lists the role various alloying elements play in a modern single crystal nickel based superalloy.

A. Microstructure of superalloys

A typical modern superalloy (eg. CMSX-4) for turbine blades is a single crystal, which contains particles, based on the ordered γ' $L1_2$ structure, lying in a matrix based on a disordered face-centered cubic Ni_3Al. The γ' phase forms remarkably regular cubes packed in a rather regular cubic array and it occupies $65-70\%$ of the

[1] TCP phases are brittle phases which are detrimental to the mechanical properties of superalloys.

volume. The shape, size and arrangement of γ' precipitates in the matrix depend on the kind of heat treatment the alloy is subject to, and it can significantly affect the creep strength [8].

Table IV. Various phases present in single crystal nickel based superalloys [17, 18].

Phase	Crystal structure	Formula	Effects
γ'	Face centered cubic	$Ni_3(Al, Ti)$	Principal strengthening phase, volume fraction could be as high as 70 %
η	Hexagonal closed packed	Ni_3Ti	Causes some amount of hardening
γ''	Body centered tetragonal	Ni_3Nb	Principal hardening phase in certain alloys, careful precipitation is needed to avoid formation of δ phase
Ni_3Nb (δ)	Orthorhombic	Ni_3Nb	detrimental to properties when present in large amount
μ[2]	Rhombohedral	Co_2W_6	TCP phase, detrimental to mechanical properties

The two-phase structure of a superalloy contributes essentially to its excellent creep strength at high temperatures, the phase boundaries providing obstacles to dislocation motion. The volume fraction of the γ' phase is an important factor in optimizing superalloy composition to get the best creep strength. Usually a maximum

[2]Laves and σ are other TCP phases which appear in iron-nickel and cobalt based superalloys.

in the creep strength is reached between 70 and 80% volume fraction of γ' phase with further increase leading to a significant drop in strength (see [18]).

Although γ' is the principle hardening phase in single crystal nickel based superalloys, various alloying elements that are added during the formation of superalloys cause numerous other phases to precipitate. Table IV lists some of the phases that are present in single crystal nickel based superalloys. Addition of carbon and boron in polycrystalline superalloys (all three groups) lead to formation of carbide and boride phases which cause grain boundary strengthening. They also tie up with certain elements which may cause phase instability otherwise.

It has been observed by Pollock and Argon [64] that in the primary stage of creep in modern superalloys, and during most of the secondary creep, plastic deformation is confined to the γ channels. The γ' particles act as impenetrable obstacles. The γ' phase has another very remarkable property. Whereas most metals and alloys, including the γ matrix, have flow stresses that decreases steadily with increasing temperature, alloys related to Ni_3Al, and many other alloys with the $L1_2$ structure, show flow stresses that can increase by a factor of 5 as the temperature increases from room temperature to about 650 ^{o}C [53]. The high strength of γ' is especially valuable at high temperatures.

The lattice parameters of the γ matrix and the γ' precipitate are very similar, but not identical. The creep deformed microstructure and many mechanical properties depend on the lattice misfit (defined as $\delta = 2(a_{\gamma'} - a_\gamma)/(a_{\gamma'} + a_\gamma)$, where $a_{\gamma'}$ and a_γ are lattice parameters of γ' and γ phases respectively). The presence of various alloying elements strongly affects the value of the misfit. The misfit could be positive or negative depending on the particular composition of the superalloy. Moreover, the misfit changes with the kind of heat treatment, the alloy is subject to and it also varies with the temperature [58, 6]. The sign of the misfit plays an important role in

the evolution of microstructure as the material creeps.

One of the most important microstructural properties of nickel based superalloys containing high volume fraction of γ' precipitates is the ability of cubic γ' phase to transform into flat plates ("rafts") under the influence of stress and temperature. This process is known as "Rafting". The rafting behavior of γ' phase has been subject to numerous investigations since it was first observed in 1960s ([100]). This directional coarsening is especially important in nickel based superalloys because the morphological changes in the two phase microstructure alters the creep resistance of the material in the stress and temperature range where these alloys are used in applications such as turbine blades. Two types of rafting behavior in <001> oriented nickel based single crystals have been identified ([96, 95]).

1. Type N - Rafts develop transverse to the direction of the externally applied load;

2. Type P - Rafts develop parallel to the direction of the externally applied load.

Type N behavior is usually associated with negative misfit alloys stressed in tension, or positive misfit alloys stressed in compression. Conversely, type P behavior is associated with positive misfit alloys stressed in tension, and negative misfit alloys stressed in compression, i.e., the direction of rafting depends upon the direction of loading and the sign of lattice misfit. The differences in the microstructural evolution associated with a change from positive to negative misfit are an indication that the rafting is primarily dominated by internal stresses developed due to the misfit. In fact, the $\gamma - \gamma'$ interface plays an important role in creep property of superalloys [16, 55]. The evolution of rafts with creep depends on the applied stress and operating temperature. The kinetics of rafting and its dependence on various factors is still not fully understood at this point. Matan *et al.* [48] conducted experiments on CMSX-4

at 950 ^{o}C to determine the influence of applied stress. They observed that specimens which have attained a critical value of plastic strain continue to raft further even if the applied stress is removed, while rafts in specimens having strains lesser than the critical value cease to develop further. At temperatures beyond 950 ^{o}C, experiments conducted by Reed *et al.* [84] suggest that rafting is complete during very early stages of creep. Most of the experimental observations on rafting are available for loading along <001> orientation. The manner in which rafting takes place for loading away from <001> orientation is still not clear. Apart from this, the kinetics of rafting behavior for complex loading conditions, a scenario quite common in actual practice, is still not understood.

B. Creep properties

The creep behavior of single crystal superalloys is highly anisotropic. The inherent crystallography of single crystals leads to orientation dependent creep behavior. From a design point of view, it is imperative to use an orientation, which utilizes maximum strength of the superalloy. In fact it is known that the creep strength of a modern single crystal superalloy along the <001> orientation , which is also the preferred grain growth direction is favorable compared to the <011> or <111> orientations. There have been numerous experimental investigations into the creep behavior and the related microstructural aspects of the <001> oriented single crystal nickel based superalloys. Apart from this, experiments have also focussed on characterizing the behavior of single crystal turbine blades with centrifugal loading away from the exact <001> orientation. Such situations are common in actual practice where misalignment of up to 15^{o} [49] could occur due to variety of reasons.

A number of studies have been devoted to studying the creep performance

of <001> oriented superalloy single crystals. At lower temperatures, particularly in the vicinity of 750 ^{o}C, a considerable amount of primary creep can occur (see [42] and [20]). At temperatures between 850 ^{o}C and 1000 ^{o}C, loading along <001> yields a creep strain rate which increases monotonically with creep strain (i.e., tertiary creep is dominant), there being no evidence of a steady state regime (See [8], [55] and [86]). At temperatures beyond 1000 ^{o}C, Reed *et al.* [84] reported that rafting of γ' phase occurs very rapidly and is complete in the very initial stages of creep deformation. After this stage, strain rate decreases with increasing strain for a considerable amount of time. Reed *et al.* [84] concluded that this strain hardening effect arises as a consequence of rafting of γ' phase. The strain rate in this temperature range keeps decreasing with increasing strain until a critical strain is reached. After the critical strain is reached, the creep strain rate increase sharply with strain with failure occurring eventually. Moreover, this critical strain was found to be essentially constant in the temperature range of $1050 - 1200$ ^{o}C. Reed *et al.* [84] observed that the rapid increase in the creep strain in the later stages of creep is associated with highly localized deformations in the vicinity of the fracture surface. Furthermore, this creep deformation is associated with creep cavitation occurring at, or in the vicinity of casting porosity and topologically closed packed (TCP) phases.

As pointed out earlier, the inherent crystallography of single crystals leads to orientation dependent creep behavior. The degree of anisotropy is strongly influenced by the temperature (around 750-850 ^{o}C) and it is also known that at higher temperatures, the orientation dependence of creep behavior is less strong. Several studies have been devoted to study the effect of orientation on creep behavior of single crystal superalloys and identify the slip systems responsible for the observed deformation behavior. Experiments carried out by Kear and Piearcey [37] on first generation single crystal nickel based superalloy MAR-M200 revealed that creep re-

sistance close to the <001> and <111> orientations is substantially better than that close to the <011> orientation in the temperature range 760-871 ^{o}C. They also found that orientation has much less influence on creep life at 982 ^{o}C. It was also observed that at 760 ^{o}C, <001> orientation has the best creep life , however at temperatures 872 and 982 ^{o}C, <111> orientation displayed the best creep life. Significant amount of primary creep was observed close to the <001> orientation at 760 ^{o}C, however primary creep was absent for the <011> and <111> orientations. At temperatures beyond 760 ^{o}C, tertiary creep was dominant in all the orientations studied. Another experimental study on creep of MAR-M200 at 760 ^{o}C was performed by Leverant and Kear [41], wherein they studied the creep behavior of specimens oriented within 18^o of <001> orientation. They observed primary, secondary and tertiary creep regimes for all the orientations and noted that the primary and steady state creep rates increase in the following order: <001>, <001>/<0$\bar{1}$1> boundary, orientations between <001>/<0$\bar{1}$1> and <001>/<1$\bar{1}$1> boundaries, <001>/<1$\bar{1}$1> boundary. A similar study performed by MacKay and Maier [43] on another first generation single crystal nickel based superalloy MAR-M247 at temperature 774 ^{o}C showed that crystals having orientations within 25^o of the <001> orientation exhibited significantly longer creep lives when their orientations were closer to the <001>/<011> boundary of the stereographic triangle than to the <001>/< $\bar{1}$11> boundary. These observations were in accordance with the results for the creep of MAR-M200 ([37, 41]), the only difference being that MAR-M247 showed best creep life close to the <111> orientation whereas MAR-M200 showed best creep life close to the <001> orientation. Caron et al. [9] studied the effect of orientation on creep lives of first generation single crystal nickel based superalloy CMSX-2 at 760 ^{o}C and 750 MPa. Their experiments showed that the best creep life occurs close to the <001> orientation, however unlike the results for MAR-M200 and MAR-M247 [37, 41, 43], CMSX-2 exhibited very poor creep

life close to the <111> orientation. Moreover, orientations away from the <001> orientation (say by 20^o) did not cause significant reduction in creep life as was the case for MAR-M200 and MAR-M247 [37, 41, 43].

The effect of orientation on creep behavior of second generation single crystal nickel based superalloy CMSX-4 was studied by Matan et al. [47]. They studied the creep behavior for small misorientations away from the <001> orientation. Their investigation showed that at 750 ^{o}C, significant amount of primary creep takes place, the extent of which depends strongly upon small misorientations away from the <001>/<011> boundary of the stereographic triangle. At 950 ^{o}C, tertiary creep is dominant with very little primary creep. They also observed that orientation dependence is less strong at 950 ^{o}C. Recent creep tests carried out by Gunturi et al. [30] on CMSX-4 at 750 ^{o}C in crystallographic orientations distant from the <001> orientation showed that orientations distant from the <001>/<111> boundary had relatively lower creep lives while orientations closer to the <001>/<111> boundary had longer creep life.

C. Previous works on single crystals

Several models have been proposed to describe the response of single crystals. The notion of Bravais lattice has been associated with the structure of single crystals at the atomic level to model its behavior. The single crystals are not free of imperfections in that they have dislocations and inclusions which are responsible for the permanent inelastic deformation of single crystals. In polycrystals, the presence of grain boundaries complicate the material behavior significantly.

There are several studies on the kinematical aspects of crystals, under the assumption of uniformly distributed dislocations (see Bilby [4], Eshelby [22], Kondo [38],

Kröner [39] and Nabarro [52]). A dynamical theory based for single crystals based on the notion of a Cosserat continuum via the introduction of directors was established by Naghdi and Srinivasa [57]. The theory based on the notion of directors has several inherent difficulties such as introduction of new balance laws containing terms which are not physically motivated. Moreover there are associated difficulties with regard to specifying boundary conditions for quantities such as directors. Naghdi and Srinivasa [56] have also introduced a measure of the influence of dislocations on the plastic deformation of single crystals through the curl of the plastic deformation gradient.

Early experiments on single crystals were carried out by Ewing and Resenhain [23], Taylor and Elam [92, 93, 94], Piercy et al. [61], and Kocks [62]. Piercy et al. [61] and Kocks [62] studied multiple slips in single crystals. Various mechanisms have been proposed to explain the response of single crystals and a discussion on these can be found in papers by Asaro [1], Havner [31], Taylor [91] and Van Buereu [98], .

The most important issue to recognize, concerning the modeling of a single crystal is that it is not a simple material in the sense of Noll [60] (see also Truesdell and Noll [97]), that is the stress in the material can not be purely determined by the history of the deformation gradient. Several methods have been proposed to capture this non-simple behavior of the body (for example, the theory based on directors) but they are fraught with difficulties. One of the goals of the current work is to understand why the theory of simple materials fail for single crystals and to develop a rigorous approach to model such non-simple materials.

D. Current models for creep and shortcomings

There have been several attempts to model the creep behavior of single crystal superalloys. Phenomenological models have been developed both to describe the creep deformation of <001> oriented single crystals and to describe the orientation dependence of creep behavior. Dyson and Mclean [20] observed that the tertiary creep rate in most engineering materials including conventional nickel based superalloys increases monotonically with accumulated plastic strain. They concluded that strain softening is caused by active damage mechanisms (cavitation and development of cracks on the surface) and accumulation of dislocations. They excluded the possibility of γ' phase coarsening causing the strain softening as was thought earlier. They also presented an empirical model wherein the strain rate is determined by inelastic strain rather than time. Following their observations, several empirical models for creep in superalloys have been proposed that take into account the kinetics of the dislocation motion [19]. The models developed in [20] and [19] are isotropic models and hence cannot capture orientation dependent creep behavior. An extension of the isotropic model to capture the anisotropic creep behavior was developed by Ghosh and Mclean [27] and Ghosh *et al.* [26]. Since the level of primary creep observed in most single crystal superalloys is small, they restricted their extension of anisotropy to the analysis of tertiary creep only and not to the primary creep. Their model accounted for tertiary creep based on the accumulation of mobile dislocations with plastic strain. Reed *et al.* [84] extended the model developed by Ghosh and co-workers to include the effect of rafting at high temperature.

Several other models for creep of superalloys have been proposed based on the framework of continuum damage mechanics and single crystal plasticity. Bertram and Olschewski [2] proposed an anisotropic constitutive model for describing creep

behavior of single crystal superalloys. They constructed a three-dimensional model by a projection technique which is essentially a generalization of the four-parameter Burgers model. Their model was restricted to the undamaged material behavior of the primary and secondary creep phase. Qi and Bertram [66] extended the model using the theory of continuum damage mechanics to incorporate the damage induced in the material through the introduction of a fourth order tensor that assesses damage.

Recently Maclachlan and Knowles [44] have proposed a model based on single crystal plasticity wherein they incorporate the damage induced due to creep through a fourth order damage operator.

Most of the models for creep of single crystal superalloys fail to take into account the symmetry of single crystals and the fact that the symmetry does not change as the single crystal undergoes inelastic deformation. Apart from this, most of these models are empirical in nature and lacked a three dimensional framework. These models also lack thermodynamical underpinnings. Although models based on single crystal plasticity are three dimensional and they incorporate the symmetry of single crystals, such models require extensive details of slip systems which are operating. Also, the model requires information about self and latent hardening of slip systems that are active which lead to a overwhelming number of material parameters (The model developed by Maclachlan and Knowles [44] has 42 material parameters).

The effect of high temperature rafting on creep was incorporated in models developed by Reed *et al.* [84] and Maclachlan and Knowles [44] who used a dislocation hardening mechanism first proposed by Gilman [28]. Apart from including the effect of rafting on creep in a macroscopic way, there have been several works devoted to describe the kinetics of the rafting behavior itself but most of them are limited to the elastic regime (see for example [63, 34, 35, 24, 25, 15, 54]). Such approaches are fraught with difficulties as the elastic regime is very difficult to detect in modern su-

peralloys and rafting is always associated with significant amount of inelastic strain. Such a drawback was emphasized by the work of Carry and Strudel [10, 11], Ignat and co-workers [33, 7] and others where it was shown that interaction of dislocations created during creep deformation with γ/γ' interface play an important role in morphological changes of precipitates. The models developed by Socrate and Parks [89] and Veron *et al.* [99] attempted to account for the inelastic strain, but their work was empirical in nature, lacked a 3D framework and was within the purview of small strain theory.

E. Goals of the current work

In this work, the aim is to develop a constitutive theory within the context of continuum mechanics, to predict the creep deformation of single crystal superalloys. The goal of such continuum theories is to describe the macroscopic behavior of a material without explicitly going into the complex details at the microscopic level, while at the same time taking cognizance of the microstructure , albeit in a homogenized sense.

The constitutive model is within a thermodynamic setting and it exploits the fact that the configuration that the body would attain on the removal of external stimuli, referred to as "natural configuration", evolves, with the response of the body being non-dissipative (in more general situations non entropy producing) from these evolving "natural configurations". The evolution of these natural configurations is determined by the tendency of the body to undergo a process that maximizes the rate of dissipation.

As mentioned before, it is important to recognize that single crystals can not be modeled by theory of simple materials. The lattice structure and the material symmetry remains the same when a single crystal is subject to inelastic deformation.

This experimental fact was recognized by the seminal work of Taylor and Elam [92] in as early as 1923. The current work aims to take cognizance of this essential empirical fact and develop a constitutive theory that complies with this observation.

Another goal of the current work is to evaluate the theories based on single crystal plasticity which explicitly take into account elaborate details of the motion of dislocations on various slip systems and model the self and latent hardening of these systems during the inelastic deformation process. Such an elaborate detail is not needed to model the inelastic behavior of single crystals and a phenomenological continuum mechanics based model which take cognizance of the microstructure in a homogenized sense will suffice. As pointed out earlier, one of the shortcomings of incorporating elaborate details regarding motion of dislocations on slip systems and the hardening of slip systems is that one ends up with an overwhelming number of material parameters.

F. Outline of the dissertation

The dissertation is organized as follows. In Chapter II, the preliminaries that form the backbone of the current work is discussed. The kinematics, kinetics, balance laws in continuum mechanics, second law of thermodynamics and the notion of frame invariance is discussed. The theory of simple materials and why it can not be used for modeling the response of single crystals and how the current framework is robust enough to fill this lacunae are also discussed. In chapter III, an isothermal constitutive model for high temperature creep of single crystal superalloys is developed. In Chapter IV, the specific problem of creep deformation of single crystal superalloys for loading along the <001>, <111> and <011> orientations is solved and the results are presented. Chapter V deals with incorporating the constitutive model in finite

element software ABAQUS as a User Material (UMAT) to enable its use for solving more general problems. A comparison between the results obtained using ABAQUS and those obtained using a semi-inverse method is made. In Chapter VI, a thermo-mechanical model for describing the creep of single crystal superalloys is developed. The summary of the dissertation and recommendations for future work is presented in Chapter VII.

G. Notations

The notations used in this dissertation are similar to those used in standard continuum mechanics texts. Vectors and tensors (second order and fourth order tensors) are represented with bold faced letters. For example,

a - Vector,

T - Second order tensor,

K - fourth order tensor.

The gradient and divergence operator with respect to initial reference configuration are denoted as:

$GRAD\ \mathbf{a} = \frac{\partial \mathbf{a}}{\partial \mathbf{X}}$, $[GRAD\ \mathbf{a}]_{ij} = \frac{\partial a_i}{\partial X_j}$,

$DIV\ \mathbf{T} = \frac{\partial \mathbf{T}}{\partial \mathbf{X}}$, $[DIV\ \mathbf{T}]_i = \frac{\partial T_{ij}}{\partial X_j}$.

The gradient and divergence operator with respect to current configuration are denoted as:

$grad\ \mathbf{a} = \frac{\partial \mathbf{a}}{\partial \mathbf{x}}$, $[grad\ \mathbf{a}]_{ij} = \frac{\partial a_i}{\partial x_j}$,

$div\ \mathbf{T} = \frac{\partial \mathbf{T}}{\partial \mathbf{x}}$, $[div\ \mathbf{T}]_i = \frac{\partial T_{ij}}{\partial x_j}$.

CHAPTER II

PRELIMINARIES

In this chapter, some of the basic concepts of continuum mechanics are summarized. The basic definitions related to the kinematics and kinetics of bodies are introduced. The basic balance laws of physics namely the balance of mass, balance of linear and angular momentum and balance of energy are also discussed in brief. The role second law of thermodynamics plays in imposing restrictions on the response of materials is discussed. After going through the basic notions of classical continuum mechanics, the notion of "natural configurations" is discussed in some detail. Some insight is provided into the roles of stored energy and rate of dissipation as they are central to the constitutive theory that will be developed within the framework of multiple natural configurations to describe the high temperature creep response of superalloys.

A. Kinematics

Kinematics deals with the geometry of motion and the deformation of material bodies without resorting to any description of the outside influence which causes it.

The idea of a material body is central to continuum mechanics. A body $\mathcal{B}$ is an open set in a topological space $\boldsymbol{\mathcal{X}}$, which has a mass (a non-negative Borel measure) defined over it. The elements of the body are called particles. An invertible mapping κ from the space of the bodies $\boldsymbol{\mathcal{X}}$ to a three dimensional Euclidean space is called a placer and the image of $\mathcal{B}$ obtained through the placer, $\kappa(\mathcal{B})$, is called a configuration of the body. It is a common practice to choose a particular configuration as the "reference configuration" and define various quantities from it.

Let $\kappa_R(\mathcal{B})$ and $\kappa_t(\mathcal{B})$ denote (see Fig. 1) the reference and the current configuration of the body $\mathcal{B}$. Henceforth, for the sake of convenience, $\mathcal{B}$ in the notation $\kappa_R(\mathcal{B})$,

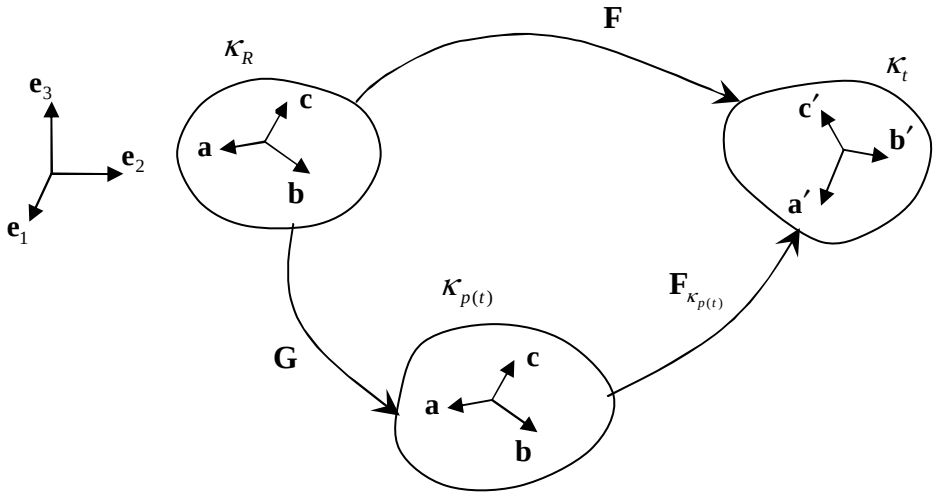

Fig. 1. Natural configurations associated with the body.

etc will be suppressed. The motion of a body can be defined as a one-to-one mapping that assigns to each point $\mathbf{X} \in \kappa_R$, a point $\mathbf{x} \in \kappa_t$, for each t, i.e.

$$\mathbf{x} = \boldsymbol{\chi}_{\kappa_R}(\mathbf{X}, t) \ . \tag{2.1}$$

The subscript κ_R is also dropped, for the sake of convenience. It is also assumed that the motion is sufficiently smooth to render all the following operations meaningful.

The velocity of the particle is given by

$$\mathbf{v}(\mathbf{X}, t) = \frac{\partial \boldsymbol{\chi}}{\partial t} \ , \tag{2.2}$$

while its acceleration is given by

$$\mathbf{a}(\mathbf{X}, t) = \frac{\partial^2 \boldsymbol{\chi}}{\partial^2 t} \ . \tag{2.3}$$

The deformation gradient, $\mathbf{F}_{\kappa_R}$ is defined through

$$\mathbf{F}_{\kappa_R} = \frac{\partial \boldsymbol{\chi}}{\partial \mathbf{X}} = \mathbf{F} \ . \tag{2.4}$$

The left and right Cauchy-Green stretch tensors $\mathbf{B}_{\kappa_R}$ and $\mathbf{C}_{\kappa_R}$ are defined through

$$\mathbf{B}_{\kappa_R} = \mathbf{F}_{\kappa_R}\mathbf{F}^T_{\kappa_R} \ , \quad \mathbf{C}_{\kappa_R} = \mathbf{F}^T_{\kappa_R}\mathbf{F}_{\kappa_R} \ . \tag{2.5}$$

The Green-St. Venant strain, $\mathbf{E}_{\kappa_R}$ is defined through $\mathbf{C}_{\kappa_R}$ as

$$\mathbf{E}_{\kappa_R} = \frac{1}{2}(\mathbf{C}_{\kappa_R} - \mathbf{I}) \ . \tag{2.6}$$

Let $\kappa_{p(t)}$ be the stress-free state (natural configuration) associated with the current configuration κ_t of the body. The mapping $\mathbf{G}$ (see Fig. 1) is defined through

$$\mathbf{G} = \mathbf{F}_{\kappa_R \to \kappa_{p(t)}} = \mathbf{F}^{-1}_{\kappa_{p(t)}}\mathbf{F} \ . \tag{2.7}$$

In a manner similar to that used in Eq. (2.5), the left and right Cauchy-Green stretch tensor associated with the instantaneous response from the natural configuration $\kappa_{p(t)}$ is defined as

$$\mathbf{B}_{\kappa_{p(t)}} = \mathbf{F}_{\kappa_{p(t)}}\mathbf{F}^T_{\kappa_{p(t)}} \ , \quad \mathbf{C}_{\kappa_{p(t)}} = \mathbf{F}^R_{\kappa_{p(t)}}\mathbf{F}_{\kappa_{p(t)}} \ . \tag{2.8}$$

The Green-St. Venant strain, $\mathbf{E}_{\kappa_{p(t)}}$ from the natural configuration is defined through

$$\mathbf{E}_{\kappa_{p(t)}} = \frac{1}{2}(\mathbf{C}_{\kappa_{p(t)}} - \mathbf{I}) \ . \tag{2.9}$$

The velocity gradients, $\mathbf{L}$ and $\mathbf{L}_p$, are defined through

$$\mathbf{L} = \dot{\mathbf{F}}_{\kappa_R}\mathbf{F}^{-1}_{\kappa_R} \ , \tag{2.10}$$

and

$$\mathbf{L}_p = \dot{\mathbf{G}}\mathbf{G}^{-1} \ , \tag{2.11}$$

where the dot signifies the usual material time derivative. The symmetric parts of $\mathbf{L}$ and $\mathbf{L}_p$ are given, respectively, through:

$$\mathbf{D} = \frac{1}{2}(\mathbf{L} + \mathbf{L}^T), \quad \mathbf{D}_p = \frac{1}{2}(\mathbf{L}_p + \mathbf{L}_p^T) \ . \tag{2.12}$$

The skew parts of $\mathbf{L}$ and $\mathbf{L}_p$ are given, respectively, through:

$$\mathbf{W} = \frac{1}{2}(\mathbf{L} - \mathbf{L}^T), \quad \mathbf{W}_p = \frac{1}{2}(\mathbf{L}_p - \mathbf{L}_p^T) \ . \tag{2.13}$$

B. Kinetics

The purpose of kinetics is to link the motion and the deformation of a material body to the outside influence which actually cause such a motion or deformation. The concept of force is central to kinetics and it manifests either as a body force $\mathbf{b}$ or surface tractions $\mathbf{t}$. The body force $\mathbf{b}$ is due to the action of influences which are not in direct contact with the body or a part of it which is being considered (the most common example is the force due to gravity). The tractions $\mathbf{t}$ on the other hand describe forces which act through the surface $\mathcal{S}$ that separates a body from its outside environment.

The famous theorem due to Cauchy established the relation between the stress tensor and the traction $\mathbf{t}$ on the surface $\mathcal{S}$ as

$$\mathbf{t}(\mathbf{x}, t, \mathcal{S}) = \mathbf{T}^T(\mathbf{x}, t)\mathbf{n} \ , \tag{2.14}$$

where $\mathbf{n}$ is the unit normal to $\mathcal{S}$ at the material point $\mathbf{x}$, in the current configuration. The second order tensor, $\mathbf{T}$ is known as the *Cauchy stress tensor*.

C. Balance laws

The manner in which a material body responds to the outside influence is governed by certain balance laws of physics. These are balance of mass, balance of linear and angular momentum and balance of energy[1].

1. Balance of mass

The balance of mass states the physically observed phenomena that mass is temporally constant for any given material body. The balance of mass states that

$$\rho_R = \rho \det(\mathbf{F}) \ , \tag{2.15}$$

where ρ_R and ρ are the mass densities in the reference and current configuration, respectively. Equation (2.15) is the Lagrangian form for the balance of mass. The Eulerian statement in the local form for the balance of mass is given by

$$\frac{\partial \rho}{\partial t} + \operatorname{div}(\rho \mathbf{v}) = 0 \ . \tag{2.16}$$

If the material is incompressible, the body can undergo only isochoric motions, which implies that the density is a constant. Appealing to equation (2.16) immediately leads to

$$\operatorname{div}(\mathbf{v}) = 0 \ , \tag{2.17}$$

or equivalently

$$\det(\mathbf{F}) = 1 \ . \tag{2.18}$$

[1]The balance of mass and energy do not necessarily hold individually (for example during radioactive decay).

2. Balance of linear and angular momentum

The balance of linear momentum is basically Newton's second law of motion written for a continuum. The Eulerian statement for the balance of linear momentum in its local form is

$$\mathrm{div}(\mathbf{T}^T) + \rho\mathbf{b} = \rho\dot{\mathbf{v}} \ , \tag{2.19}$$

where the dot signifies the usual material time derivative and $\mathbf{b}$ is the body force per unit volume.

In the absence of body couples, the balance of angular momentum reduces to

$$\mathbf{T} = \mathbf{T}^T \ , \tag{2.20}$$

i.e. the Cauchy stress tensor is symmetric[2].

3. Balance of energy

The notion of conservation of energy assumes a central role in physics. It stipulates that the change in the energy of a system is equal to the transfer of the energy to the system. The transfer of energy could occur in various forms such as heat transfer or mechanical working. In describing the response of a body, one may need to specify a constitutive equation for various modes of energy transfer such as mechanical, thermal, chemical, electrical, etc. However, within the confines of a thermomechanical process, only the mechanical and thermal modes come into picture. For a thermomechanical process, the balance of energy, in its local form takes the following form:

$$\rho\dot{\epsilon} + \mathrm{div}(\mathbf{q}) = \mathbf{T}\cdot\mathbf{L} + \rho r \ , \tag{2.21}$$

[2]Cauchy stress tensor could be non symmetric in bodies such as micro-polar fluids. Also, in mixture theory [80], partial stresses of individual constituents is not symmetric unless the angular momentum supply is zero.

where ϵ is the internal energy, $\mathbf{q}$ is the heat flux vector and r is the radiant heating.

D. Second law of thermodynamics

The second law of thermodynamics is commonly introduced in continuum mechanics in the form of Clausius Duhem inequality (see Truesdell and Noll [97]). However, in the current work, it will be introduced as an equality by introducing a balance law for entropy. This approach follows from the work of Green and Naghdi [29] and Rajagopal and Srinivasa [79]. The balance law for entropy takes the form

$$\rho\dot{\eta} + \operatorname{div}\Big(\frac{\mathbf{q}}{\theta}\Big) = \rho\frac{r}{\theta} + \rho\xi \ , \tag{2.22}$$

where η is the entropy, θ is the absolute temperature and ξ is the rate of entropy production.

Combining the balance of energy, Eq. (2.21), and the balance of entropy, Eq. (2.22) and eliminating the radiant heating term r, reduced energy-dissipation equation is obtained:

$$\mathbf{T}\cdot\mathbf{L} - \rho\dot{\epsilon} + \rho\theta\dot{\eta} - \frac{\mathbf{q}\cdot\operatorname{grad}(\theta)}{\theta} = \rho\theta\xi := \zeta \geq 0 \ , \tag{2.23}$$

where ζ is the rate of dissipation. The rate of entropy production ξ and the rate of dissipation ζ is constrained to be non-negative for a physically acceptable process. In any physical process, entropy production could take place due to a variety of reasons, for e.g., due to mechanical working, heat conduction, phase change, chemical reactions etc. For reversible processes, the rate of entropy production and hence the rate of dissipation is identically zero. However, for irreversible processes, the rate of entropy production is greater than zero.

The term $-\frac{\mathbf{q}\cdot grad(\theta)}{\theta}$ in (2.23) is the rate of entropy production due to conduction. It is a non-negative quantity, which is positive when temperature gradient exist in

the body and zero when there is no temperature gradient. It is usually assumed that the rate of dissipation can be split into a part that is due to heat conduction (ζ_c) and another part due to mechanical working (ζ_m). Such a split leads us to

$$\mathbf{T} \cdot \mathbf{L} - \rho\dot{\psi} - \rho\eta\dot{\theta} = \zeta_m \geq 0 \ , \tag{2.24}$$

$$-\frac{\mathbf{q} \cdot grad(\theta)}{\theta} = \zeta_c \geq 0 \ . \tag{2.25}$$

Assuming the heat flux vector to be of the form

$$\mathbf{q} = -\Lambda \ grad(\theta) \ , \tag{2.26}$$

where Λ is the thermal conductivity and is required to be non-negative, ensures that condition (2.25) is met.

E. Material frame indifference

The notion of material frame indifference requires that the physical quantities such as scalars, vectors and tensors that are used in a constitutive theory should remain invariant to superposed rigid body motion (Truesdell and Noll [97]).

Let us consider a material point $\mathbf{X}$ which is occupying some position in the current configuration. The location of the material point $\mathbf{X}$ in the current configuration is seen as $(\mathbf{x}, t)$ and $(\mathbf{x}^*, t^*)$ in two frames which are related to each other through rigid body motion of the form

$$\mathbf{x}^* = \mathbf{c}(t) + \mathbf{Q}(t)(\mathbf{x} - \mathbf{x}_o), \ t^* = t - t_o \ , \tag{2.27}$$

where $\mathbf{c}(t)$ is an arbitrary vector function of time, $\mathbf{Q}(t)$ is an arbitrary orthogonal tensor and t_o is a constant.

A scalar, vector or a tensor is said to be frame-indifferent if under a change of

frame they are related through:

$$\phi^* = \phi \ , \quad \mathbf{v}^* = \mathbf{Q}\mathbf{v} \ , \quad \mathbf{T}^* = \mathbf{Q}\mathbf{T}\mathbf{Q}^T \ . \tag{2.28}$$

It follows from Eq. (2.28) and the definition of deformation gradient that

$$\mathbf{F}^*_{\kappa_R} = \mathbf{Q}\mathbf{F}_{\kappa_R} \ . \tag{2.29}$$

As the underlying natural configuration associated with the body is continuously evolving and the Cauchy stress is represented with respect to the stress free configuration or the natural configuration, it is also required that the invariance requirement on $\mathbf{F}$ and $\mathbf{F}_{\kappa_{p(t)}}$ are the same, i.e.,

$$\mathbf{F}^*_{\kappa_{p(t)}} = \mathbf{Q}\mathbf{F}_{\kappa_{p(t)}} \ . \tag{2.30}$$

It follows from Eqs. (2.7), (2.29) and (2.30) that

$$\mathbf{G}^* = \mathbf{G} \ . \tag{2.31}$$

The various quantities such as specific Helmholtz potential and rate of dissipation function that will be used in our constitutive theory will be required to satisfy the constraint due to material frame indifference:

$$\begin{aligned} \psi(\mathbf{F}^*_{\kappa_{p(t)}}, \mathbf{G}^*, \theta^*) &= \psi(\mathbf{Q}\mathbf{F}_{\kappa_{p(t)}}, \mathbf{G}, \theta) \ , \\ \xi(\mathbf{F}^*_{\kappa_{p(t)}}, \mathbf{G}^*, \mathbf{L}^*_p, \theta^*) &= \xi(\mathbf{Q}\mathbf{F}_{\kappa_{p(t)}}, \mathbf{G}, \mathbf{L}_p, \theta) \ . \end{aligned} \tag{2.32}$$

F. Theory of simple materials and single crystals

A material is said to be a simple material (see Noll [60]) if the stress $\mathbf{T}$ can be determined purely by the history of the deformation gradient and within a thermodynamic

context, the history of the temperature, i.e.,

$$\mathbf{T} = \mathcal{F}_{\tau=0}^{\infty}[\mathbf{F}(t-\tau), \theta(t-\tau)] \ . \tag{2.33}$$

Classical models for elastic solids take the form

$$\mathbf{T} = \mathbf{f}(\mathbf{F}, \theta) \ , \tag{2.34}$$

and it belongs to the class of models given by (2.33). The classical viscous fluid model

$$\mathbf{T} = \mathbf{f}(\rho, \mathbf{D}) \ , \tag{2.35}$$

also belong to the same class. Moreover most of the models developed to describe viscoelastic materials such as fluids of grade n also belong to the class of simple fluids. The models given by (2.33) are inadequate to describe the inelastic response of materials. Traditional models for polycrystalline plasticity do not fall into the class (2.33) (see Rajagopal and Srinivasa [72]).

We shall now discuss an important property of single crystals that implies that the model cannot belong to the class defined by (2.33), and this concerns with the inability of such models to depict the evolution of the anisotropy of the single crystal as it undergoes inelastic deformation. Let us now begin by defining the notion of symmetry group at a material point.

The symmetry group associated with a material point belonging to the material, which reflects the physical symmetry of the material, is defined through

$$\mathcal{G}_{\kappa} = \{\mathbf{H} \subset \mathcal{U} \mid \mathbf{f}_{\kappa}(\mathbf{F}_{\kappa}\mathbf{H}) = \mathbf{f}_{\kappa}(\mathbf{F}_{\kappa})\} \ , \tag{2.36}$$

where $\mathcal{U}$ is the unimodular group and the dependence on temperature is suppressed. If κ_1 and κ_2 are two configurations of the body (see Fig. 2), then it follows that $\mathcal{G}_{\kappa_1}$

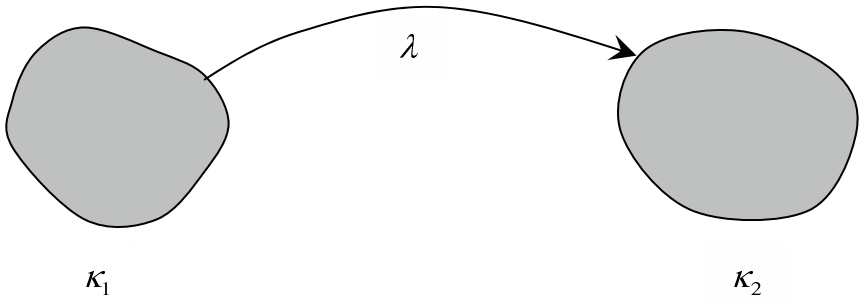

Fig. 2. Noll's rule for simple materials.

and $\mathcal{G}_{\kappa_2}$ are related through the gradient of the mapping λ from κ_1 to κ_2 (Noll's rule):

$$\mathcal{G}_{\kappa_2} = \mathbf{P}\mathcal{G}_{\kappa_1}\mathbf{P}^{-1} \ , \tag{2.37}$$

where

$$\mathbf{P} := \nabla\lambda \ . \tag{2.38}$$

If a single crystal were to be a simple material, and if κ_1 and κ_2 represent two configurations of the single crystal, then $\mathcal{G}_{\kappa_1}$ and $\mathcal{G}_{\kappa_2}$ should be related by Noll's rule. Now, if a single crystal is sheared and the corresponding mapping $\mathbf{P}$ determined, then we can ask if $\mathcal{G}_{\kappa_1}$ and $\mathcal{G}_{\kappa_2}$ are related by Noll's rule. If shear along a slip plane of the crystal leaves the material symmetry unchanged, it immediately follows that (2.37) is not met.

Experiments have clearly shown that the lattice structure and hence the material symmetry remains the same when a single crystal is sheared sufficiently so that "slip" takes place (see Fig. 3). In their seminal paper on single crystals, Taylor and Elam [92] made the following observations:

> "moreover, measurements of the inclination of two different crystal planes during the present experiments showed that the angle between

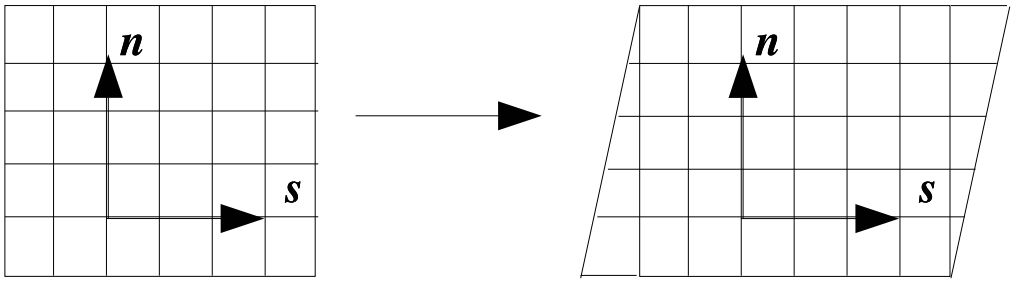

Fig. 3. Shearing of the lattice of a single crystal.

them remained practically constant during the whole course of the distortion."

"The fact that the material preserves its cubic symmetry during the distortion"

G. The framework of multiple natural configurations

For materials undergoing large deformations, Eckart [21] seems to have been the first to recognize that many materials can possess multiple stress free states (natural configurations), that he called variable relaxed states, and studied them in some detail. However, he did not worry about symmetry considerations of the variable relaxed states or the role that the evolution of the symmetry plays in the constitutive relation for the material. Nor was Eckart interested in placing the evolution of material structure within a thermodynamic framework. A detailed discussion of the central role played by natural configurations in a variety of dissipative processes with associated symmetry changes and the change of the response characteristics of the body has been considered by Rajagopal [67, 68]. In fact the notion of "Natural configurations" is central to the development of constitutive theories in continuum mechanics. The

crucial role it plays in describing the response of a broad range of material behaviors has not been recognized and delineated in detail until the recent work of Rajagopal [67, 68]. Invoking the notion of "natural configurations" has led to the development of constitutive theories which has filled the lacunae that existed in incorporating the microstructural details from a continuum perspective. It has led to development of constitutive theories with rigorous thermodynamic underpinnings without resorting to any ad hoc means such as invoking "internal variables" into the theory. The phenomenal success of such a framework in describing the response of a disparate class of materials can be seen in a series of papers by Rajagopal and coworkers: the response of multi-network polymers [102, 81], twinning [70, 71], traditional plastic response [72, 73], solid to solid phase transitions [70, 71], shape memory alloys [74], viscoelastic response [75], anisotropic response of liquids [76], crystallization of polymers [83], superplastic response [69], response of asphalt mixtures [51], growth and adaptation of biological materials [82] and response of superalloys [65]. The classical theories of elasticity and linearly viscous fluid arise naturally as sub-cases.

The framework of multiple natural configurations exploits the fact that the configuration that the body would attain on the removal of external stimuli, referred to as "natural configuration", evolves, with the response of the body being non-dissipative (in more general situations non entropy producing) from these evolving natural configurations. The evolution of these natural configurations is determined by the tendency of the body to undergo a process that maximizes the rate of dissipation. Different natural configurations are accessed during different processes. It is suffice to say that the notion of natural configuration is a primitive in our framework and it can be thought of as one of the state variables in the constitutive theory.

CHAPTER III

A CONTINUUM MODEL FOR CREEP OF SUPERALLOYS

A. Development of constitutive model

Let us now start with the reduced energy dissipation equation (see Green and Naghdi [29]):

$$\mathbf{T}\cdot\mathbf{L}-\rho\dot{\psi}-\rho\eta\dot{\theta}-\frac{\mathbf{q}\cdot\mathrm{grad}(\theta)}{\theta}=\rho\theta\xi:=\zeta\geq 0\ , \tag{3.1}$$

which is a different version of Eq. (2.23) obtained by substituting $\psi=\epsilon-\theta\eta$, where ψ is the Helmholtz potential.

In what follows, the effect of temperature is ignored and an isothermal model is developed. The motivation to develop an isothermal model stems from the fact that all the creep experiments are done at a constant temperature. The material parameters that will appear in the constitutive model will be different for different temperatures. In chapter VI, a framework for a non-isothermal model has been developed.

Splitting the entropy production part as that due to thermal effects and a part due to mechanical dissipation lead us to,

$$\mathbf{T}\cdot\mathbf{L}-\rho\dot{\psi}=\zeta_{mech}\geq 0\ . \tag{3.2}$$

Equation (3.2) is the starting point for the development of a isothermal constitutive model.

The form for the stored energy of the crystalline materials is assumed to be

$$\psi=\psi(\mathbf{F}_{\kappa_{p(t)}},\mathbf{G})\ . \tag{3.3}$$

It is assumed that the Helmholtz potential can be decomposed in the following way:

$$\psi=\hat{\psi}+\tilde{\psi}\ , \tag{3.4}$$

where

$$\hat{\psi} = \hat{\psi}_{\kappa_{p(t)}}(\mathbf{F}_{\kappa_{p(t)}}) \ , \tag{3.5}$$

is related to the elastic stored energy, and

$$\tilde{\psi} = \mathcal{F}^{\infty}_{\tau=0}[\mathbf{G}(t-\tau)] \ , \tag{3.6}$$

is related to the inelastic stored energy. A standard rearrangement will yield

$$\left[\mathbf{T} - \rho\frac{\partial\hat{\psi}}{\partial\mathbf{F}_{\kappa_{p(t)}}}\mathbf{F}^{T}_{\kappa_{p(t)}}\right]\cdot\mathbf{L} + \rho\mathbf{F}^{T}_{\kappa_{p(t)}}\frac{\partial\hat{\psi}}{\partial\mathbf{F}_{\kappa_{p(t)}}}\cdot\mathbf{L}_p - \rho\frac{d\tilde{\psi}}{dt} = \zeta_{mech} \geq 0 \ . \tag{3.7}$$

It is now assumed that the Cauchy stress is of the form

$$\mathbf{T} = \rho\frac{\partial\hat{\psi}}{\partial\mathbf{F}_{\kappa_{p(t)}}}\mathbf{F}^{T}_{\kappa_{p(t)}} = \rho\mathbf{F}_{\kappa_{p(t)}}\frac{\partial\hat{\psi}}{\partial\mathbf{E}_{\kappa_{p(t)}}}\mathbf{F}^{T}_{\kappa_{p(t)}} \ . \tag{3.8}$$

On using equation (3.8), equation (3.7) can be reduced to

$$(\mathbf{F}^{T}_{\kappa_{p(t)}}\mathbf{T}\mathbf{F}^{-T}_{\kappa_{p(t)}})\cdot\mathbf{L}_p - \rho\frac{d\tilde{\psi}}{dt} = \zeta_{mech} \ . \tag{3.9}$$

Decomposing $(\mathbf{F}^{T}_{\kappa_{p(t)}}\mathbf{T}\mathbf{F}^{-T}_{\kappa_{p(t)}})$ into symmetric and skew parts and using the polar decomposition $(\mathbf{F}_{\kappa_{p(t)}} = \mathbf{V}_{\kappa_{p(t)}}\mathbf{R}_{\kappa_{p(t)}})$ leads to

$$\mathbf{A}\cdot\mathbf{D}_p + \boldsymbol{\tau}\cdot\mathbf{W}_p - \rho\frac{d\tilde{\psi}}{dt} = \zeta_{mech} \ , \tag{3.10}$$

where

$$\mathbf{A} = (\mathbf{F}^{T}_{\kappa_{p(t)}}\mathbf{T}\mathbf{F}^{-T}_{\kappa_{p(t)}})_{sym} = \frac{1}{2}\mathbf{R}^{T}_{\kappa_{p(t)}}(\mathbf{V}_{\kappa_{p(t)}}\mathbf{T}\mathbf{V}^{-1}_{\kappa_{p(t)}} + \mathbf{V}^{-1}_{\kappa_{p(t)}}\mathbf{T}\mathbf{V}_{\kappa_{p(t)}})\mathbf{R}_{\kappa_{p(t)}} \ , \tag{3.11a}$$

$$\boldsymbol{\tau} = (\mathbf{F}^{T}_{\kappa_{p(t)}}\mathbf{T}\mathbf{F}^{-T}_{\kappa_{p(t)}})_{skew} = \frac{1}{2}\mathbf{R}^{T}_{\kappa_{p(t)}}(\mathbf{V}_{\kappa_{p(t)}}\mathbf{T}\mathbf{V}^{-1}_{\kappa_{p(t)}} - \mathbf{V}^{-1}_{\kappa_{p(t)}}\mathbf{T}\mathbf{V}_{\kappa_{p(t)}})\mathbf{R}_{\kappa_{p(t)}} \ . \tag{3.11b}$$

For a material that is elastically isotropic, $\mathbf{T}$ will be an isotropic function of $\mathbf{V}_{\kappa_{p(t)}}$ so that $\boldsymbol{\tau} = \mathbf{0}$.

The rate of dissipation due to creep is assumed to be of the form

$$\zeta_{mech} = \zeta_1(\theta, \mathbf{D}_p) + \zeta_2(\theta, \mathbf{W}_p) \ , \tag{3.12}$$

i.e., the rate of dissipation depends both upon the rate at which the material stretches as well as the rate at which the orientation changes. For a specimen loaded in any arbitrary orientation, the crystal lattice rotates. However, for uniaxial creep loading along orientations <001>, <111> and <011>, there is no associated rotation of the crystal lattice.

Equation (3.12) with equation (3.10) yields

$$\mathbf{A} \cdot \mathbf{D}_p - \rho \frac{d\tilde{\psi}}{dt} = \zeta_1(\theta, \mathbf{D}_p) \ , \quad \boldsymbol{\tau} \cdot \mathbf{W}_p = \zeta_2(\theta, \mathbf{W}_p) \ . \tag{3.13}$$

B. Specific constitutive relations

1. The Helmholtz potential $\hat{\psi}$

The specific form for the elastic stored energy consistent with a crystal having cubic symmetry is

$$\hat{\psi} = \frac{1}{2\rho}\big[c_{12}(\text{tr } \mathbf{E}_{\kappa_{p(t)}})^2 + 2c_{44}(\text{tr } \mathbf{E}^2_{\kappa_{p(t)}}) + (c_{11} - c_{12} - 2c_{44})\big((\mathbf{a} \cdot \mathbf{E}_{\kappa_{p(t)}}\mathbf{a})^2 + (\mathbf{b} \cdot \mathbf{E}_{\kappa_{p(t)}}\mathbf{b})^2 + (\mathbf{c} \cdot \mathbf{E}_{\kappa_{p(t)}}\mathbf{c})^2\big)\big] \ , \tag{3.14}$$

where $\mathbf{a}$, $\mathbf{b}$ and $\mathbf{c}$ are orthogonal unit vectors along the principal cubic axes and c_{11}, c_{12} and c_{44} are three independent parameters characterizing the elastic response.

2. Inelastic part of the stored energy $\tilde{\psi}$

The form for the inelastic stored energy captures the part of mechanical work that is trapped in the dislocation networks. Models due to Lee [40], Brown *et al.* [5] and Mason *et al.* [46] account for this kind of energy storage mechanism in the body by

multiplying the "plastic work" by an ad hoc factor whose value is approximately 0.8. The current work utilizes a rigorous form for such an energy storage mechanism without resorting to any ad hoc means. The energy that is stored in dislocation networks is of tremendous importance during the inelastic deformation of single crystal superalloys as such superalloys are multi phase materials with their microstructure engineered in such a way to ensure solid solution hardening and precipitation hardening.

We will assume the following form for the inelastic part of the free energy $\tilde{\psi}$ developed by Mollica *et al.*, [50] and subsequently used by Prasad *et al.*, [65]:

$$\tilde{\psi} = \psi_1 a(s) + \psi_2 \int_0^s e^{\eta(x-s)} (\mathbf{E}_p(s) - \mathbf{E}_p(x)) \cdot \mathbf{N}(x) dx \ , \tag{3.15}$$

where the scalar variable $s = s(t)$ is referred to as "inelastic strain pathlength" and is defined as

$$\dot{s} = (\mathbf{D}_p \cdot \mathbf{D}_p)^{\frac{1}{2}} \ , \tag{3.16}$$

ψ_1, ψ_2 and η are material constants and

$$\mathbf{E}_p = \int_0^t \mathbf{D}_p(\tau) d\tau \ , \tag{3.17}$$

$$\mathbf{N} = \frac{\mathbf{D}_p}{(\mathbf{D}_p \cdot \mathbf{D}_p)^{\frac{1}{2}}} \ . \tag{3.18}$$

$\mathbf{E}_p$ is a measure of accumulated inelastic strain with reference to reference configuration and it can be described as a measure of the total amount of slip that has taken place on slip systems which are active [59].

Also, $a(s)$ is the density of the dislocation network (defined as the total length of dislocation lines per unit volume [85]) and assumes the following form:

$$a(s) = a_o(1 + \beta_2(1 - e^{-\alpha_1 s})) \ . \tag{3.19}$$

The motivation to choose such a form stems from the experimental observation that the dislocation density increases with monotonic inelastic deformation and reaches a saturation value after a while.

The time rate of change of $\tilde{\psi}$ (3.15) is given by

$$\begin{aligned}\rho\frac{d\tilde{\psi}}{dt} &= \rho\left[\psi_1\left(a' + \eta a\right) - \eta\tilde{\psi}\right](\mathbf{D}_p \cdot \mathbf{D}_p)^{\frac{1}{2}} + \left(\rho\psi_2 \int_0^s e^{\eta(x-s)}\mathbf{N}(x)dx\right) \cdot \mathbf{D}_p \ , \\ &:= h(s)(\mathbf{D}_p \cdot \mathbf{D}_p)^{\frac{1}{2}} + \boldsymbol{\alpha} \cdot \mathbf{D}_p \ ,\end{aligned} \tag{3.20}$$

where $(\cdot)'$ denotes the total derivative with respect to s.

The tensor

$$\boldsymbol{\alpha} = \rho\psi_2 \int_0^s e^{\eta(x-s)}\mathbf{N}(x)dx \ , \tag{3.21}$$

is the backstress tensor. On taking the time derivative of (3.21), it can be seen that the backstress, $\boldsymbol{\alpha}$ would satisfy the following evolution equation:

$$\dot{\boldsymbol{\alpha}} = \rho\psi_2\mathbf{D}_p - \eta(\mathbf{D}_p \cdot \mathbf{D}_p)^{\frac{1}{2}}\boldsymbol{\alpha} \ , \tag{3.22}$$

which is a generalized version of the non-linear kinematic hardening rule [12]. Although no experimental data concerning the inelastic stored energy is available, to our knowledge, for single crystal superalloys, there are experimental data for polycrystalline metals [3, 101]. Apart from the experiments, several attempts have been made to model the inelastic stored energy (see for example, papers by Chaboche [13, 14] and Kamlah and Haupt [36]). The inelastic stored energy might not be significant at high temperatures at which creep occurs as only a small fraction of energy is stored (dissipation mechanisms being dominant).

3. Rate of dissipation

Following form for the rate of dissipation is assumed:

$$\zeta_1 = \mathbf{D}_p \cdot \mathbf{K}\mathbf{D}_p \ , \quad \zeta_2 = \eta_2 \mathbf{W}_p \cdot \mathbf{W}_p \ , \tag{3.23}$$

where $\mathbf{K}$ is a fourth order tensor reflecting cubic symmetry that is a function of the temperature, the inelastic history of the material and the driving force:

$$\mathbf{K} = k_{12}\mathbf{I} \otimes \mathbf{I} + 2k_{44}\mathbf{I}_4 + (k_{11} - k_{12} - 2k_{44})\boldsymbol{\mathcal{N}} \ , \tag{3.24}$$

where $\mathbf{I}_4$ is the fourth order identity tensor, and the fourth order tensor $\boldsymbol{\mathcal{N}}$ has the form

$$\mathcal{N}_{ijkl} = a_i a_j a_k a_l + b_i b_j b_k b_l + c_i c_j c_k c_l \ . \tag{3.25}$$

a_i, b_i and c_i are the components of the orthogonal unit vectors $\mathbf{a}$, $\mathbf{b}$ and $\mathbf{c}$.

The evolution equation for the natural configuration is determined by the tendency of the body to undergo a process that maximizes the rate of dissipation. The idea of maximization of rate of dissipation is not a fundamental principle of thermodynamics. However it is also not ad hoc either. It is a generalization of a notion due to Gibbs that an isolated system tends to a state of maximal entropy. A further assumption is made that the way, the body gets to the state of maximal entropy is by producing entropy at the maximal possible rate (see Rajagopal and Srinivasa [77, 78]).

Maximizing the rate of dissipation subject to the constraint $tr(\mathbf{D}_p) = 0$ (inelastic deformation being isochoric) gives the following equations for $\mathbf{D}_p$ and $\mathbf{W}_p$:

$$\mathbf{A} = p\mathbf{I} + \mathbf{A}^* \ , \tag{3.26a}$$

$$\mathbf{A}^* = \boldsymbol{\alpha} + \mathbf{K}\mathbf{D}_p + h(s)\frac{\mathbf{D}_p}{(\mathbf{D}_p \cdot \mathbf{D}_p)^{\frac{1}{2}}} \ , \tag{3.26b}$$

$$p = \frac{1}{3} tr(\mathbf{A} - \mathbf{A}^*) \ , \tag{3.26c}$$

and

$$\mathbf{W}_p = \frac{1}{\eta_2} \boldsymbol{\tau} \ . \tag{3.27}$$

The rate of dissipation functions ζ_1 and ζ_2 defined through (3.23) are required to be non-negative. Our constitutive assumption for the rate of dissipation ensures that it is non-negative. It can be seen from equation (3.23) that the rate of dissipation is dependent on the fourth order tensor $\mathbf{K}$ which is anisotropic. It is assumed that two mechanisms contribute to the rate of dissipation in the following way:

The first mechanism is related to the dissipation caused by mobile dislocations. There is a rapid multiplication of dislocations in the γ matrix at the beginning of creep. It is observed that the γ' phase is "hard" for significant amount of creep strains and hence no dislocation activity is associated with it. As the deformation increases, these dislocations start moving in the γ matrix. Further deformation results in these dislocations being stuck and bowed. This causes "hardening" of the material. In order to describe the loss of mobility of the dislocations with accumulating "creep strain", it is assumed that the mean velocity of the dislocations remains constant at constant stress while the density of dislocations, which are mobile decay exponentially. That is, only a fraction of the total remains mobile. Let f be this fraction. In accordance with the work of Gilman [28], following form for the mobile fraction is assumed:

$$f = e^{\alpha_2 s}, \tag{3.28}$$

where α_2 is the attrition coefficient.

The density of mobile dislocations, $a_m(s)$ is then given by

$$a_m(s) = a(s)f = a_o(1 + \beta_2(1 - e^{-\alpha_1 s}))e^{-\alpha_2 s}. \tag{3.29}$$

The first mechanism of dissipation is assumed to be proportional to the inelastic strain pathlength, $s(t)$ in the following way:

$$\zeta_1 \propto a_m(s). \tag{3.30}$$

Apart from this, the dissipation mechanism, in general, also depends upon the driving force, as most dislocation interactions become less inhibitory with increasing driving force.

The second mechanism associated with dissipation is related to the damage accumulation by creep cavitation. With the creep strain accumulating, the material starts getting "damaged" by means of highly localized deformation in the vicinity of crack surfaces. As reported in numerous experiments, this creep elongation at the later stage of deformation is associated with creep cavitation occurring at, or in the vicinity of casting porosity and topologically closed-packed phases. Hence this stage is marked by a rapid increase in the strain ("softening"). Moreover, experiments clearly indicate that the effect of highly localized damage due to creep cavitation becomes dominant only after a certain critical strain is reached. The second mechanism of dissipation is assumed to be proportional to the inelastic strain pathlength, $s(t)$ in the following way:

$$\zeta_1 \propto e^{\alpha_3 s}. \tag{3.31}$$

Moreover, it is also assumed that this second mechanism of dissipation remains active throughout the creep process but becomes dominant only in the later stages of creep. This second mechanism, in general, is also dependent on the driving force.

The coefficients associated with the tensor $\mathbf{K}$ have the following form:

$$\begin{aligned} k_{11} - k_{12} &= \frac{1}{\beta_1 e^{\kappa_1 tr(\mathbf{A})} a(s) e^{-\alpha_2 s} + \beta_3 e^{\kappa_2 tr(\mathbf{A})} e^{\alpha_3 s}} \,, \\ k_{44} &= \frac{0.5}{\Lambda_1 e^{\Gamma_1 tr(\mathbf{A})} a(s) e^{-\Omega_2 s} + \Lambda_3 e^{\Gamma_2 tr(\mathbf{A})} e^{\Omega_3 s}} \,. \end{aligned} \tag{3.32}$$

It should be noted that $k_{11} - k_{12}$ and k_{44} have the same form. The material parameters ψ_1, ψ_2, η, β_2 and α_1 which are associated with the inelastic stored energy do not change with the orientation of the crystal. The form for the rate of dissipation function is motivated based on creep deformation when the specimen is loaded along the <001> and the <111> directions. The coefficients $k_{11} - k_{12}$ and k_{44} reflect the dissipation which takes place when the specimen is loaded in the <111> and the <001> direction, respectively. Such a description is a simplistic one and we will see that it captures the creep deformation of single crystal superalloys reasonably well. The dependence of rate of dissipation on dislocation motion is much more intricate when the specimen is loaded along arbitrary directions.

4. Instantaneous rate of energy storage, R

One of the important quantities in any inelastic process is the ratio of rate of energy stored to the rate of work done by the externally applied tractions. The rate at which work is done during the inelastic process by the applied tractions per unit mass is given by

$$w_i(t) = \frac{\mathbf{T} \cdot \mathbf{L}}{\rho}. \tag{3.33}$$

The rate of dissipation per unit mass is given by

$$w_d(t) = \frac{\zeta_{mech}}{\rho} = \frac{1}{\rho}(\mathbf{D}_p \cdot \mathbf{K}\mathbf{D}_p + \eta_2 \mathbf{W}_p \cdot \mathbf{W}_p). \tag{3.34}$$

The rate of energy stored per unit mass is given by $\dot{\psi}$. The instantaneous rate of energy storage, R is then given by

$$R = \frac{w_s(t)}{w_i(t)} = 1 - \frac{w_d(t)}{w_i(t)}, \tag{3.35}$$

where the equation of balance of energy is utilized in the form of reduced energy dissipation equation (equation (3.2)). Although no experiments have been conducted, to our knowledge, on single crystal superalloys to measure such a quantity, there are some experimental results for polycrystalline metals (see Williams [101]) which can provide some guidance in our choice for the same for single crystal superalloys.

CHAPTER IV

CREEP OF SUPERALLOYS LOADED ALONG THE <001>, <111> AND <011> ORIENTATIONS

A. Problem formulation for loading along the <001>, <111> and <011> orientations

Creep deformation of single crystal superalloys under loading in any arbitrary direction is fully three dimensional. However, uniaxial creep loading along the orientations <001>, <111> and <011> gives rise to a simple deformation field and there is no associated rotation of the crystal lattice.

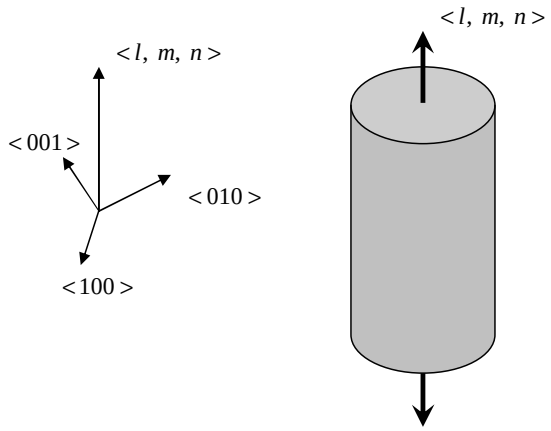

Fig. 4. Creep of a specimen loaded along the direction $<l, m, n>$ under constant load.

We will assume the following form for the deformation in rectangular coordinates (see Fig. 4):

$$x(t) = \phi_1(t)X \ , \quad y(t) = \phi_2(t)Y \ , z(t) = \phi_3(t)Z \ , \tag{4.1}$$

where $(X,\ Y,\ Z)$ is a material point in the configuration κ_R and $(x,\ y,\ z)$, the corresponding material point in the configuration κ_t.

The deformation gradient associated with the above motion is given by

$$\mathbf{F} = \text{diag}(\ \phi_1(t),\ \phi_2(t),\ \phi_3(t))\ . \tag{4.2}$$

The elastic response consistent with the above deformation is given by

$$x(t) = \lambda_1 X^*(t)\ ,\quad y(t) = \lambda_2 Y^*(t)\ , z(t) = \lambda_3 Z^*(t)\ , \tag{4.3}$$

where $(X^*,\ Y^*,\ Z^*) \in \kappa_{p(t)}$. The deformation gradient and the corresponding Green-St. Venant strain tensor associated with the elastic response from the natural configuration is given by

$$\mathbf{F}_{\kappa_{p(t)}} = \text{diag}(\ \lambda_1,\ \lambda_2,\ \lambda_3)\ ,\quad \mathbf{E}_{\kappa_{p(t)}} = \frac{1}{2}\text{diag}(\ \lambda_1^2 - 1,\ \lambda_2^2 - 1,\ \lambda_3^2 - 1)\ . \tag{4.4}$$

Specimens with orientation along <001> and <111> exhibit no shear strains and the transverse strains are equal (i.e., $\phi_1 = \phi_2$ and $\lambda_1 = \lambda_2$). For specimens loaded along <011>, there is no associated shear strains but the two transverse strains are not equal.

We will assume that the creep deformation takes place at constant stress, that is,

$$\mathbf{T} = \text{diag}(\ 0,\ 0,\ T_{zz})\ , \tag{4.5}$$

which leads to

$$\mathbf{A} = \text{diag}(\ 0,\ 0,\ T_{zz})\ ,\quad \boldsymbol{\tau} = \mathbf{0}\ ,\quad p = \frac{1}{3}T_{zz}\ . \tag{4.6}$$

Substituting the form for the elastic stored energy (Eq. (3.14)) into the constitutive equation for the elastic response (Eq. (3.8)), we obtain the governing equations for the elastic response from the natural configuration:

$$\begin{aligned} &c_{12}(\text{tr}\ \mathbf{E}_{\kappa_{p(t)}})\mathbf{F}_{\kappa_{p(t)}}\mathbf{F}^T_{\kappa_{p(t)}} + 2c_{44}\mathbf{F}_{\kappa_{p(t)}}\mathbf{E}_{\kappa_{p(t)}}\mathbf{F}^T_{\kappa_{p(t)}} \\ &+(c_{11} - c_{12} - 2c_{44})\mathbf{F}_{\kappa_{p(t)}}(\boldsymbol{\mathcal{N}}\mathbf{E}_{\kappa_{p(t)}})\mathbf{F}^T_{\kappa_{p(t)}} = \mathbf{T}\ . \end{aligned} \tag{4.7}$$

The unit vectors along the principal cubic axes, which constitutes the fourth order tensor $\boldsymbol{\mathcal{N}}$ are given by

$$\mathbf{a} = \left(\frac{\Lambda_2}{\Lambda_1},\ 0,\ \frac{l}{\Lambda_1}\right),\ \ \mathbf{b} = \left(-\frac{ml}{\Lambda_1\Lambda_2},\ \frac{n}{\Lambda_2},\ \frac{m}{\Lambda_1}\right),\ \ \mathbf{c} = \left(-\frac{nl}{\Lambda_1\Lambda_2},\ -\frac{m}{\Lambda_2},\ \frac{n}{\Lambda_1}\right), \tag{4.8}$$

where

$$\Lambda_1 = \sqrt{l^2 + m^2 + n^2}\ ,\quad \Lambda_2 = \sqrt{m^2 + n^2}\ , \tag{4.9}$$

with the loading axis along $l\mathbf{a} + m\mathbf{b} + n\mathbf{c}$.

The tensor $\mathbf{G}$, for the assumed deformation is given by

$$\mathbf{G} = \mathrm{diag}\left(\frac{\phi_1(t)}{\lambda_1},\ \frac{\phi_2(t)}{\lambda_2},\ \frac{\phi_3(t)}{\lambda_3}\right). \tag{4.10}$$

The symmetric and skew part of $\mathbf{L}_p$ are given by

$$\mathbf{D}_p = \mathrm{diag}\left(\frac{\dot{\phi}_1(t)}{\phi_1(t)},\ \frac{\dot{\phi}_2(t)}{\phi_2(t)},\ \frac{\dot{\phi}_3(t)}{\phi_3(t)}\right),\quad \mathbf{W}_p = \mathbf{0}\ , \tag{4.11}$$

and the time derivative of inelastic strain pathlength s is given by

$$\dot{s} = \sqrt{\left(\frac{\dot{\phi}_1(t)}{\phi_1(t)}\right)^2 + \left(\frac{\dot{\phi}_2(t)}{\phi_2(t)}\right)^2 + \left(\frac{\dot{\phi}_3(t)}{\phi_3(t)}\right)^2}\ . \tag{4.12}$$

A straightforward application of constitutive relations (3.26a)-(3.26c) will lead us to

$$\left(\frac{h}{\dot{s}} + 2k_{44}\right)\frac{\dot{\phi}_i(t)}{\phi_i(t)} + (\boldsymbol{\mathcal{N}}\mathbf{D}_p)_i = (\mathbf{A})_i - p - (\boldsymbol{\alpha})_i\ , \tag{4.13a}$$

$$(\dot{\boldsymbol{\alpha}})_i = \rho\psi_2\frac{\dot{\phi}_i(t)}{\phi_i(t)} - \eta\dot{s}(\boldsymbol{\alpha})_i\ ,\ i = 1-3\ \text{(no sum on } i)\ , \tag{4.13b}$$

$$\dot{\tilde{\psi}} = \frac{1}{\rho}\left(h\dot{s} + (\boldsymbol{\alpha})_1\frac{\dot{\phi}_1(t)}{\phi_1(t)} + (\boldsymbol{\alpha})_2\frac{\dot{\phi}_2(t)}{\phi_2(t)} + (\boldsymbol{\alpha})_3\frac{\dot{\phi}_3(t)}{\phi_3(t)}\right), \tag{4.13c}$$

where $()_i$ denotes the i-th diagonal element of the respective second order tensors. Equations (4.12) and (4.13a)-(4.13c) form the set of governing non-linear ordinary

differential equations.

The instantaneous rate of energy storage, R which is the ratio of rate of energy stored to the rate of work done by applied tractions is given by

$$R = 1 - \frac{w_d(t)}{w_i(t)} = 1 - \frac{\zeta_{mech}}{\mathbf{T} \cdot \mathbf{L}} \ , \tag{4.14}$$

where $w_d(t)$ is the rate of dissipation per unit mass and $w_i(t)$ is the specific stress power.

B. Results for loading along the <001> orientation

The creep strain was obtained by integrating equations (4.12)-(4.13c) over time. Equations (4.12)-(4.13c) are solved using a solver (ODE15S) for initial value problems in MATLAB.

The results were obtained for a range of temperatures, which are pertinent to the problem under consideration. The material parameters, in general, are functions of temperature. Simulation was carried out at three different temperatures at various stress values and the results are compared with the experimental results for CMSX-4 ([90] and [32]). The values of parameters characterizing the elastic response at different temperatures are listed in Table V and the values of material parameters for different temperatures are listed in Table VI.

Table V. Parameters characterizing the elastic response of CMSX-4 at various temperatures [88].

θ	750^{o}C	800^{o}C	950^{o}C	982^{o}C	1000^{o}C
c_{11} (GPa)	229.7	223	214.8	213.2	208.4
c_{12} (GPa)	149.3	145.6	141.4	140.9	138.4
c_{44} (GPa)	115	112	107	106	104

Table VI. Material parameters for CMSX-4 at various temperatures for loading along the <001> orientation.

θ	750^oC	982^oC	1000^oC
δ_1	1.8	1.07	3
δ_2	1.5×10^5	1.02×10^4	5×10^4
η	40	39.21	50
κ_1	1.7×10^{-8}	1.42×10^{-8}	1.2×10^{-7}
κ_2	2.77×10^{-8}	2.87×10^{-8}	1.7×10^{-8}
β_1	1×10^{-23}	8.27×10^{-19}	8.77×10^{-26}
β_2	1800	478	272
α_1	3	2.95	1.1
α_2	66	0	1817
β_3	1×10^{-29}	7.9×10^{-21}	3.53×10^{-18}
α_3	25.2	27.61	39.1

The variation of creep strain, instantaneous rate of energy storage and inelastic stored energy with time are presented for different temperatures at various stresses. The variation of creep strain with time for $\theta = 750, 982$ and $1000\ ^o$C are shown in Figs. 5, 6 and 7. It can be seen that the predictions of the model agree well with the experimental data for the different temperatures considered here. Figs. 8, 9 and 10

depict the variation of the inelastic stored energy with respect to the inelastic strain pathlength. Also, Figs. 11, 12 and 13 represent the variation of third component of backstress tensor with inelastic strain pathlength. Variation of the instantaneous rate of energy storage with inelastic strain pathlength is also studied. It can be seen from Figs. 14, 15 and 16 that the material stores energy in the initial stages of deformation but as the deformation proceeds most of the energy is dissipated. Moreover, it can be observed that the fraction of energy stored decreases at higher temperatures. That is, at higher temperatures most of the work done by the applied tractions is dissipated. This is to be expected as the dislocation motion which is primarily the source of dissipation becomes less and less inhibitory as the temperature increases. The inelastic stored energy increases with inelastic deformation but its value seems to be attaining a saturation value. The driving force doesn't seem to have significant effect on the variation of inelastic stored energy as the curves for the different stresses lie almost on top of each other. The driving force however, has significant effect on the rate of dissipation as dissipation mechanisms themselves are strongly dependent on the driving force.

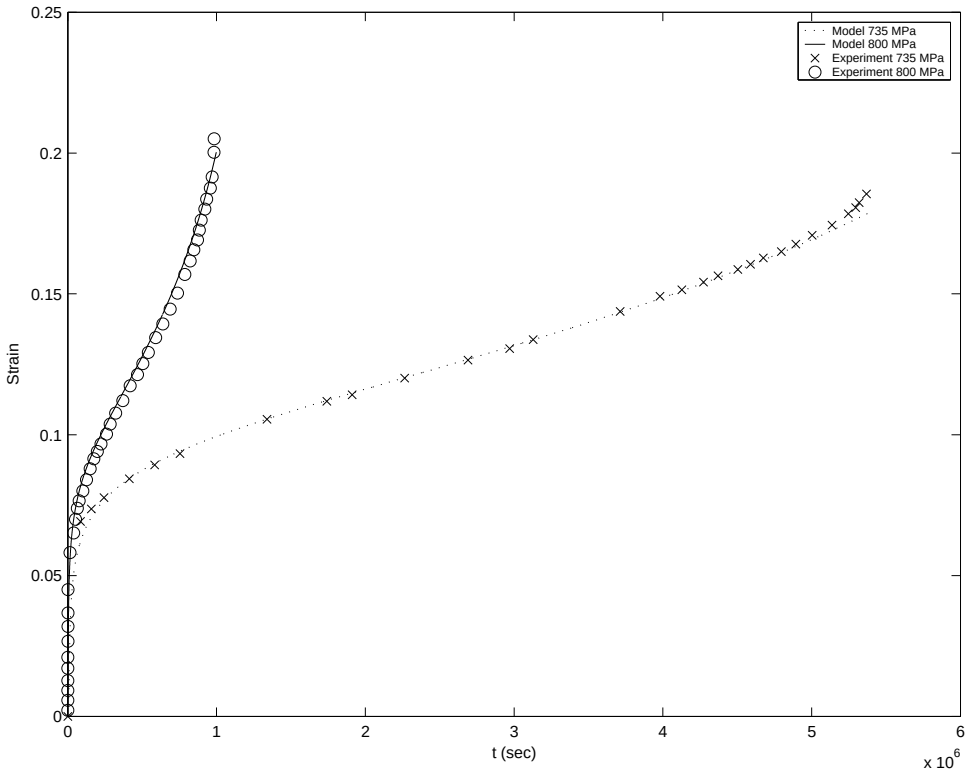

Fig. 5. Strain vs. time for CMSX-4 for loading along the <001> orientation, $\theta = 750\ ^{o}$C: Comparison of the predictions of the model with experimental results of Svoboda and Lucas [90] and Henderson and Lindblom [32].

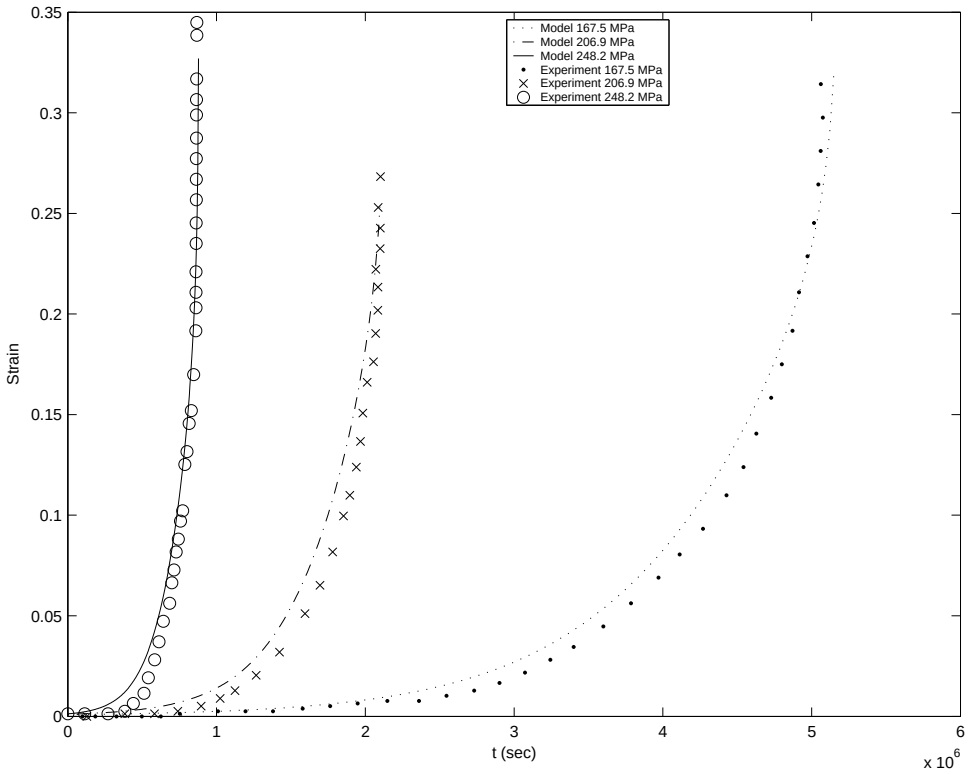

Fig. 6. Strain vs. time for CMSX-4 for loading along the <001> orientation, $\theta = 982\ ^{o}$C: Comparison of the predictions of the model with experimental results of Svoboda and Lucas [90] and Henderson and Lindblom [32].

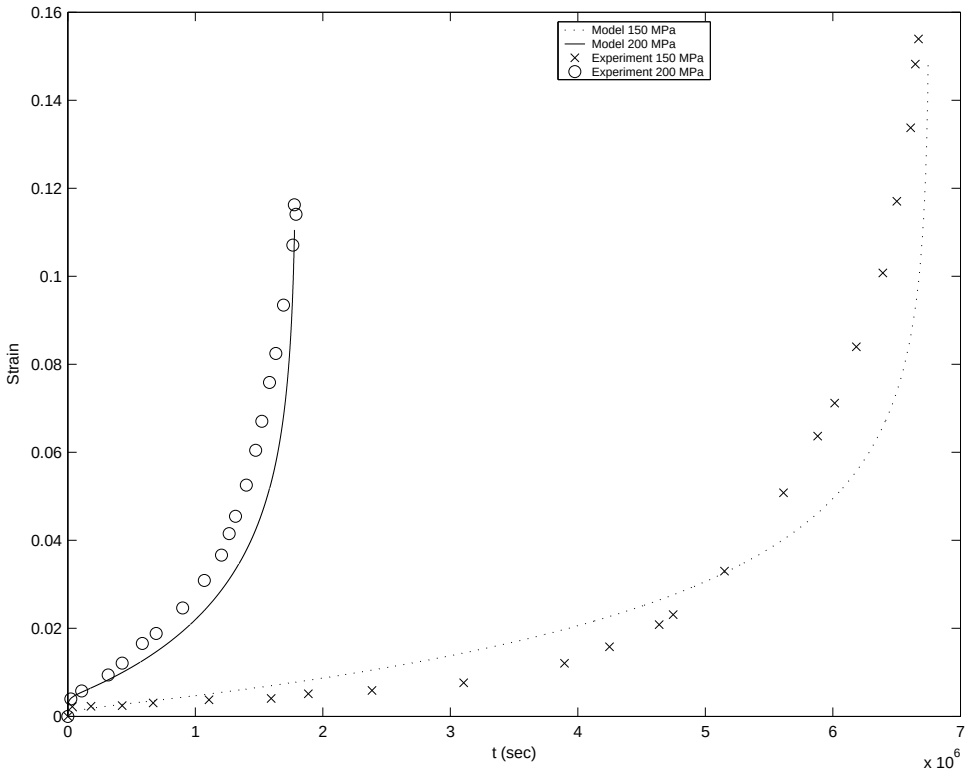

Fig. 7. Strain vs. time for CMSX-4 for loading along the <001> orientation, $\theta = 1000\ ^{o}$C: Comparison of the predictions of the model with experimental results of Svoboda and Lucas [90] and Henderson and Lindblom [32].

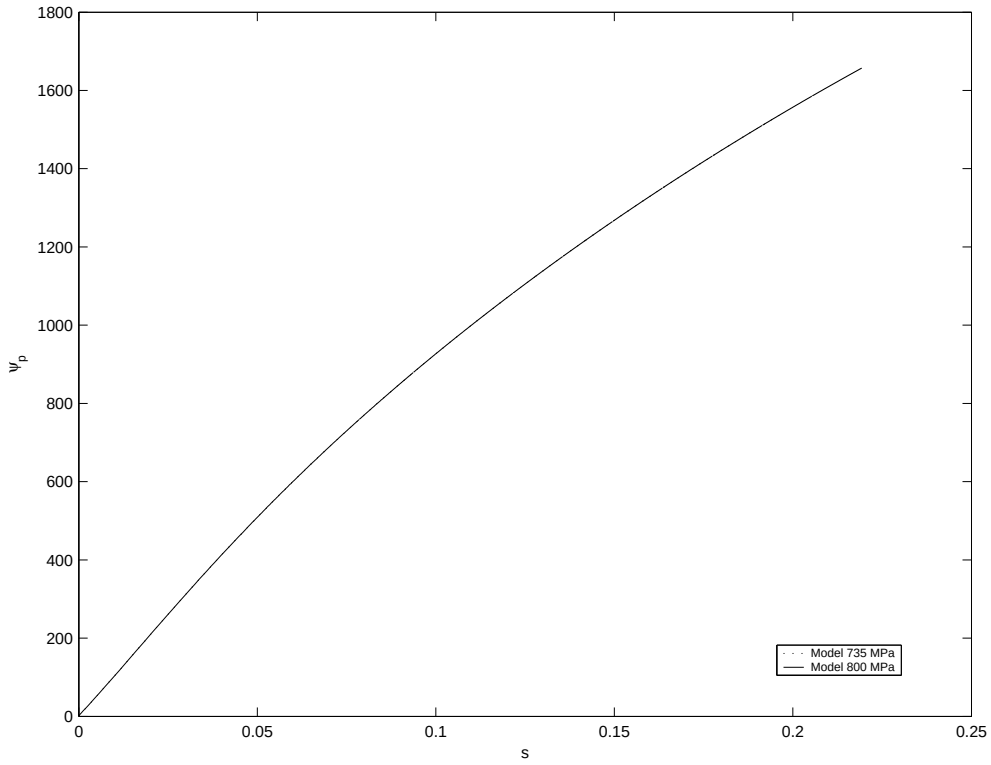

Fig. 8. Inelastic stored energy vs. inelastic strain pathlength for CMSX-4 for loading along the <001> orientation, $\theta = 750\ ^o$C: Predictions of the model.

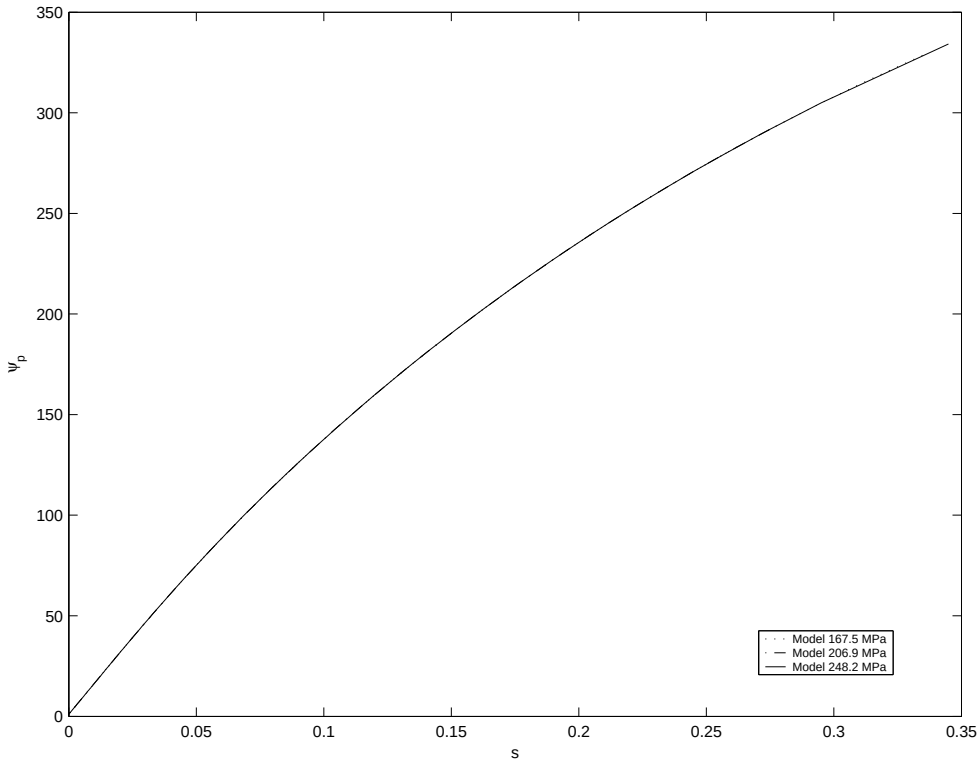

Fig. 9. Inelastic stored energy vs. inelastic strain pathlength for CMSX-4 for loading along the <001> orientation, $\theta = 982\ ^o$C: Predictions of the model.

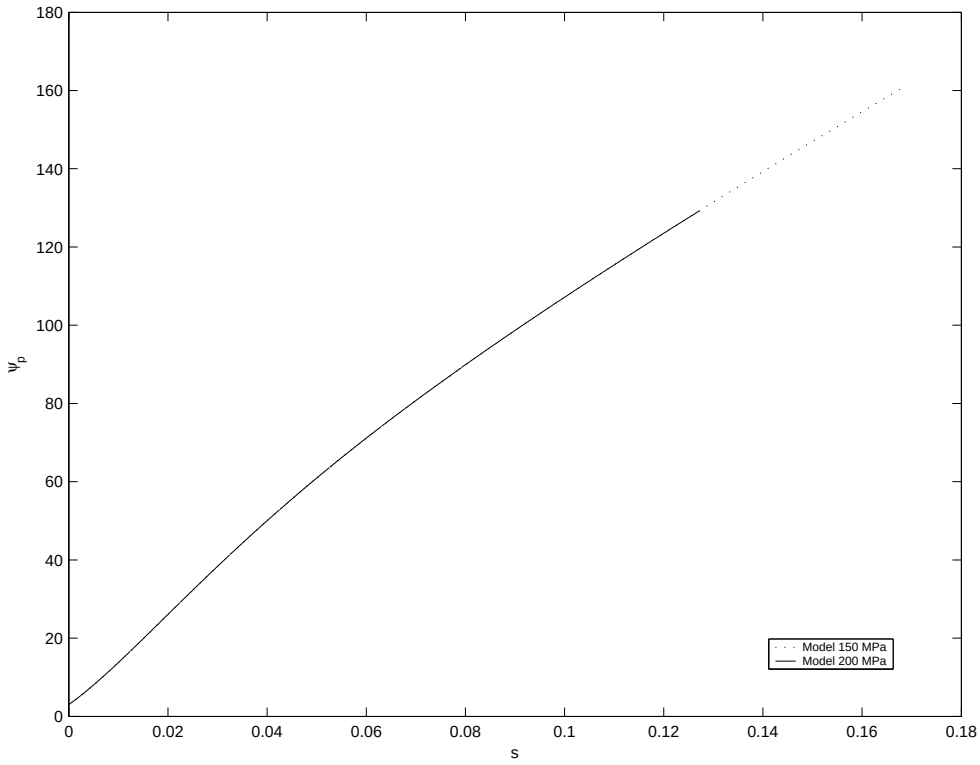

Fig. 10. Inelastic stored energy vs. inelastic strain pathlength for CMSX-4 for loading along the <001> orientation, $\theta = 1000\ ^o$C: Predictions of the model.

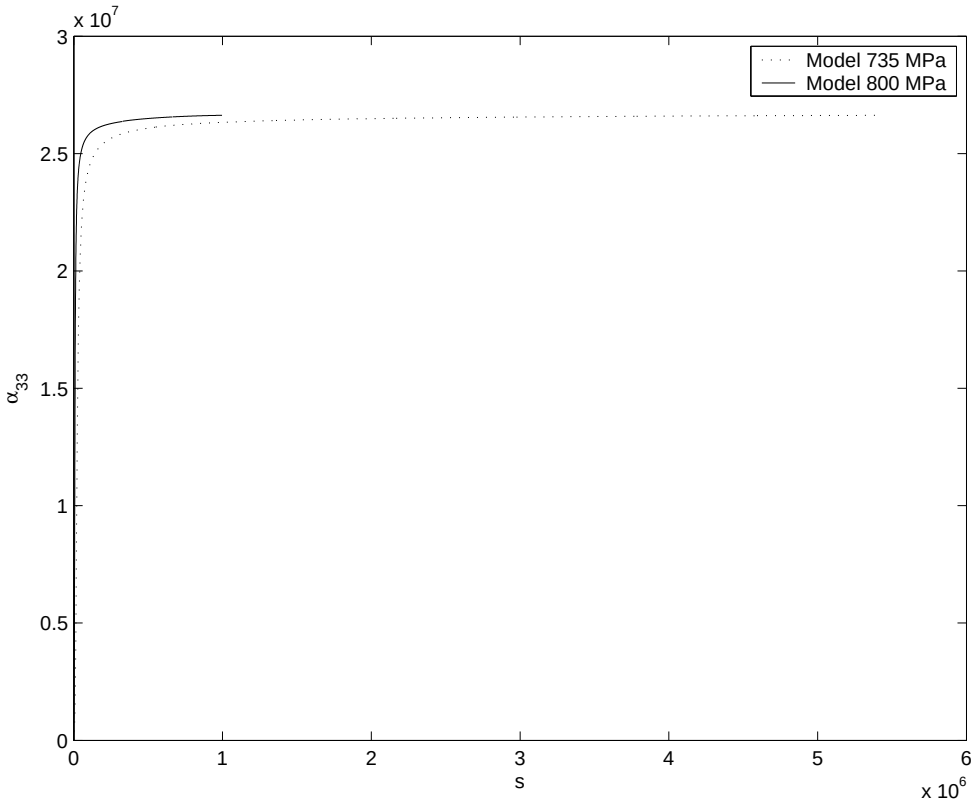

Fig. 11. Third component of backstress vs. inelastic strain pathlength for CMSX-4 for loading along the <001> orientation, $\theta = 750\ ^{o}$C: Predictions of the model.

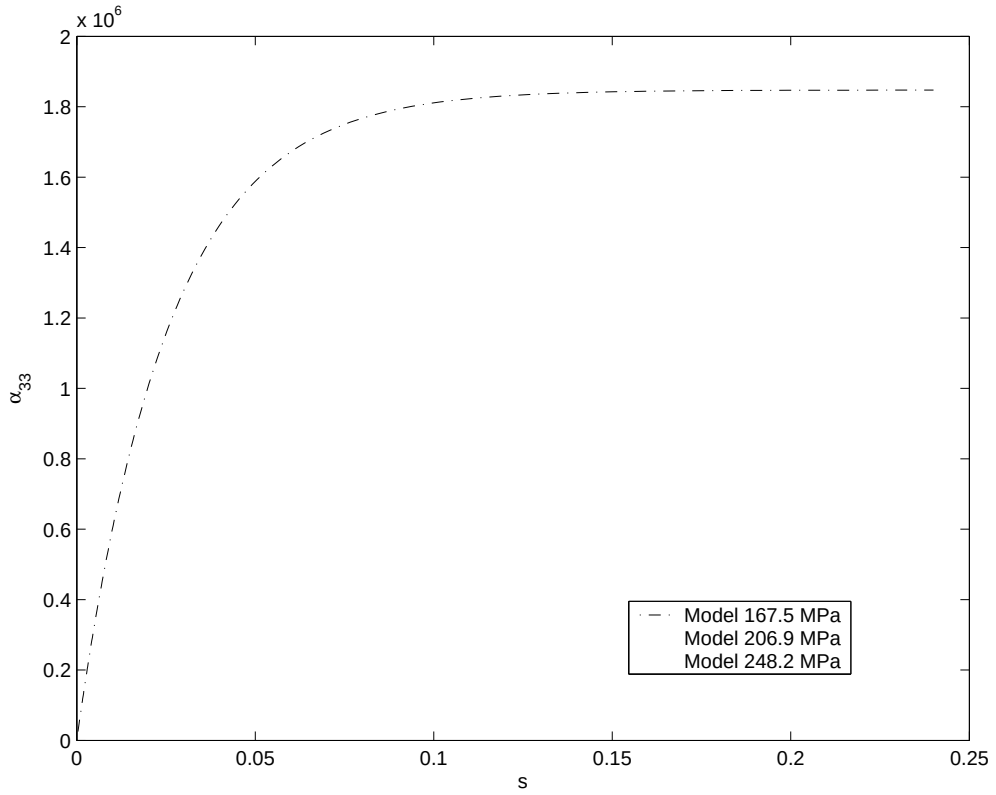

Fig. 12. Third component of backstress vs. inelastic strain pathlength for CMSX-4 for loading along the <001> orientation, $\theta = 982$ ^{o}C: Predictions of the model.

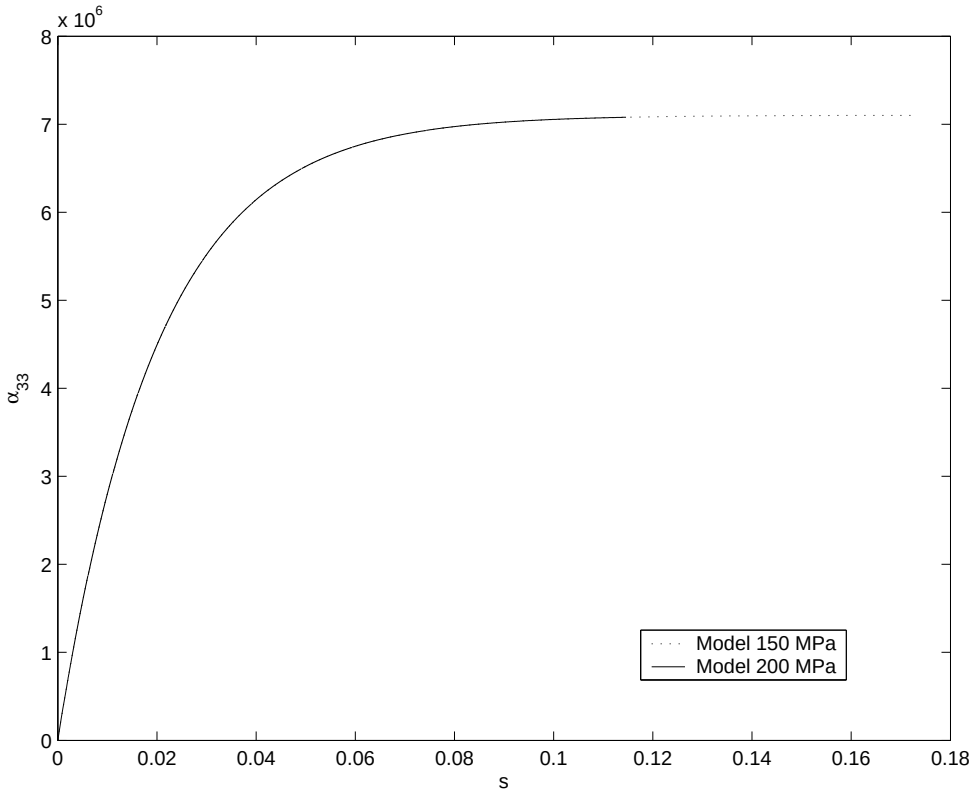

Fig. 13. Third component of backstress vs. inelastic strain pathlength for CMSX-4 for loading along the <001> orientation, $\theta = 1000\ ^{o}$C: Predictions of the model.

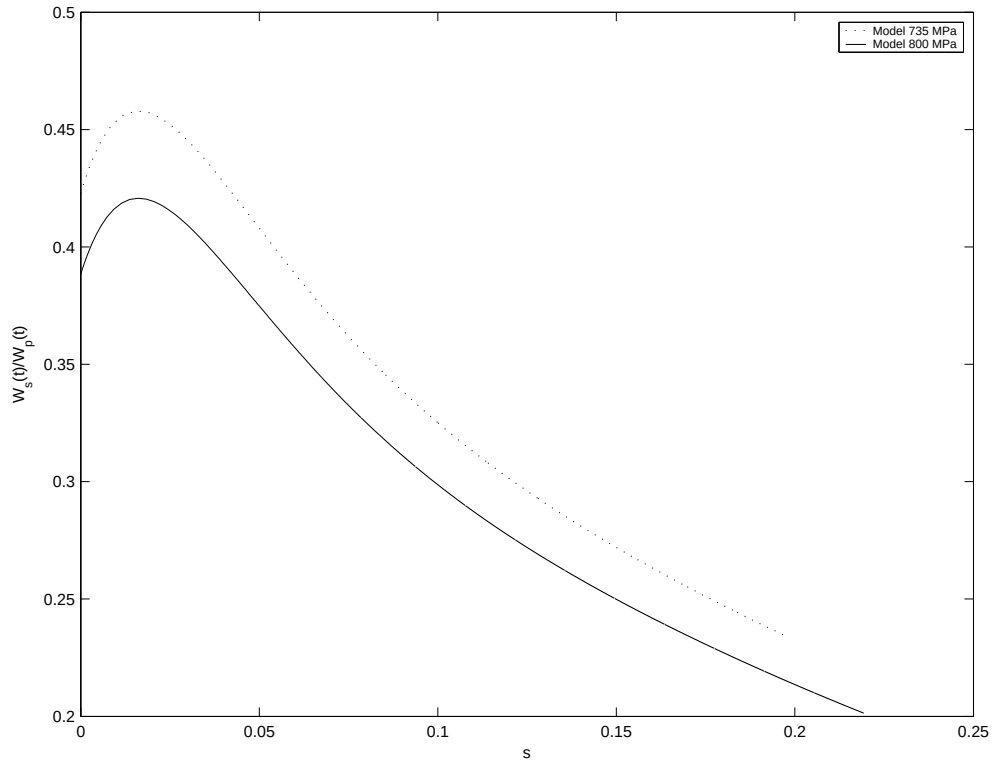

Fig. 14. Instantaneous rate of energy storage vs. inelastic strain pathlength for CM-SX-4 for loading along the <001> orientation, $\theta = 750\ ^{o}$C: Predictions of the model.

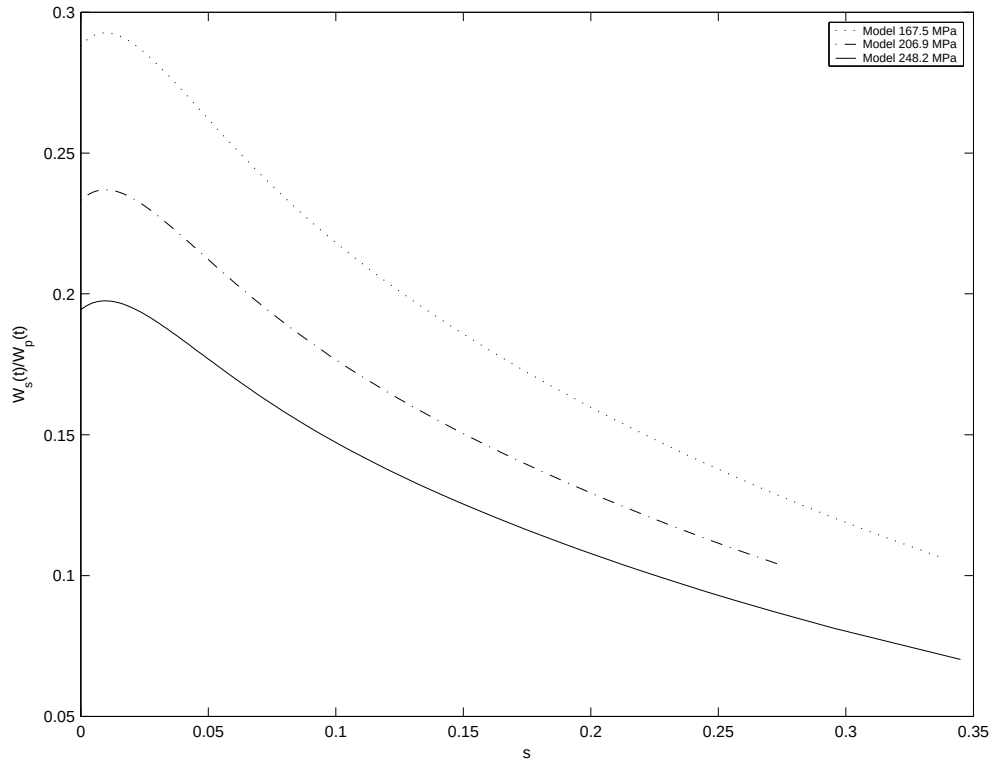

Fig. 15. Instantaneous rate of energy storage vs. inelastic strain pathlength for CM-SX-4 for loading along the <001> orientation, $\theta = 982\ ^{o}$C: Predictions of the model.

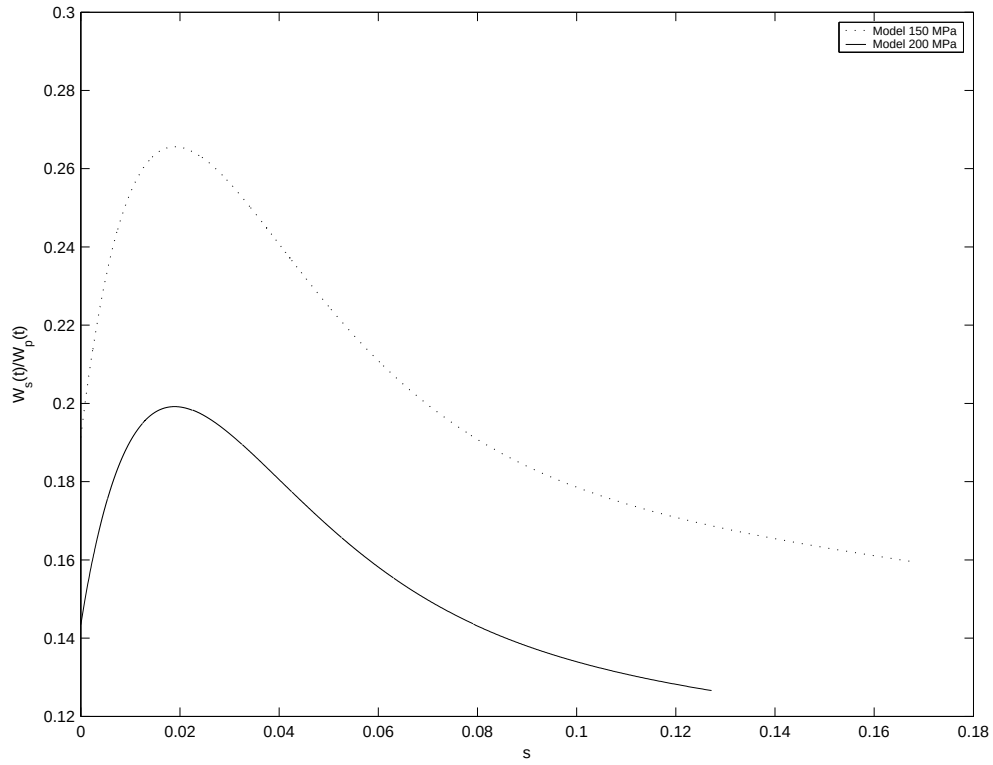

Fig. 16. Instantaneous rate of energy storage vs. inelastic strain pathlength for CM-SX-4 for loading along the <001> orientation, $\theta = 1000\ ^{o}$C: Predictions of the model.

C. Results for loading along the <001>, <111> and <011> orientations

The set of ordinary differential equations are solved using an initial value problem solver in MATLAB (ODE15s). The material parameters associated with coefficient k_{44} are fixed by matching the results with experiments for loading along the <001> orientation. Similarly, the parameters in the expression for $k_{11} - k_{12}$ are fixed by matching the results with experiments for loading along the <111> orientation. Hence, the orientations <001> and <111> are complete for determining the material constants for the current set of orientations studied. Once the complete set of materials parameters are obtained from the <001> and <111> data set, these are used to simulate the uniaxial creep along the <011> orientation. The results for single crystal nickel based superalloy CMSX-4 for loading along the <001>, <111> and <011> orientations for various values of stresses at 800 ^{o}C and 950 ^{o}C are obtained and compared with the available experimental results ([87, 45]). The values of material parameters for different temperatures are listed in Table VII. It is worth emphasizing that the material parameters are fixed with respect to one experiment and they are then used to predict the results for a different experiment.

The variation of the creep strain with time is shown in Figs. 17-22. It can be seen that the predictions of the model agree well with the experimental data for the temperatures considered here. The experimental data for loading along <011> orientation acts as a test case for measuring the efficacy of our model. Although no such data is available for 800 ^{o}C, we find that the prediction of the model are satisfactory for loading along the <011> orientation at 950 ^{o}C (see Fig. 22). Figs. 23 and 24 depict the variation of the inelastic stored energy ($\tilde{\psi}$) with inelastic strain pathlength. The inelastic energy increases with inelastic deformation and eventually attains a saturation value. Neither the driving force nor the orientation seems to

have any effect on the variation of inelastic stored energy as the curves for different stresses and loading orientations lie almost on top of each other. Figs. 25 and 26 show the variation of the third component of backstress tensor with inelastic strain pathlength. For certain orientations, the driving force seems to have little or no effect on the backstress, though for comparable stress values, the value of the backstress is somewhat lower for the <011> orientation than for the <001> and the <111> orientations. Variation of the instantaneous rate of energy storage with inelastic strain pathlength is depicted in Figs. 27 and 28. It can be seen that the material stores energy in the initial stages of deformation but as the deformation proceeds most of the energy is dissipated. For certain orientations, the fraction of energy stored decreases as the stress increases. This is expected as the dislocation motion which is primarily the source of dissipation becomes less and less inhibitory as the stress increases.

Table VII. Material parameters for CMSX-4 at various temperatures.

Parameter / θ	800 ^{o}C	950 ^{o}C
ψ_1	1.5	3
ψ_2	1.5 x 10^5	5 x 10^4
η	40	40
α_1	3	2
β_2	100	245
β_1	4.47 x 10^{-25}	6.5 x 10^{-19}
κ_1	1.1 x 10^{-7}	3.85 x 10^{-8}
κ_2	4.85 x 10^{-8}	4.8 x 10^{-8}
α_2	1700	0
β_3	3.7 x 10^{-22}	7.85 x 10^{-21}
α_3	27	30
Λ_1	7.43 x 10^{-25}	3.1 x 10^{-20}
Γ_1	1.12 x 10^{-7}	6.3 x 10^{-8}
Γ_2	6.09 x 10^{-8}	4.15 x 10^{-8}
Ω_2	400	0
Λ_3	1.55 x 10^{-22}	1.3 x 10^{-20}
Ω_3	20	30

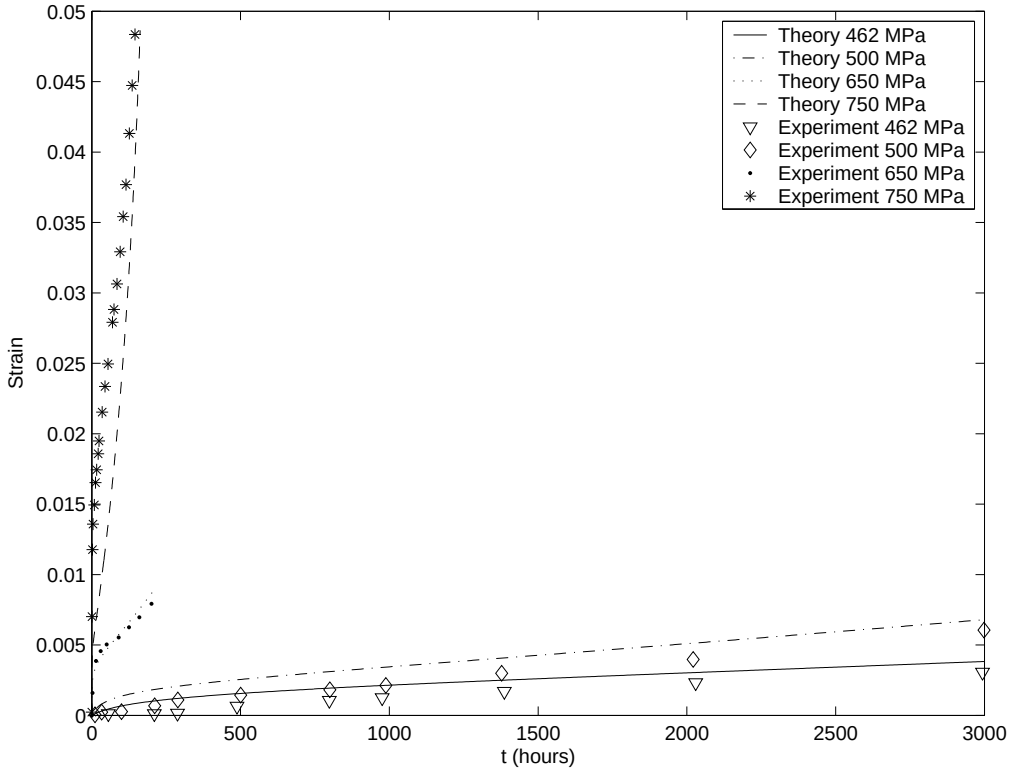

Fig. 17. Strain vs. time for CMSX-4 for loading along the <001> orientation, $\theta = 800\ ^{o}$C: Comparison of the predictions of the model with experimental results of Schubert et al., [87].

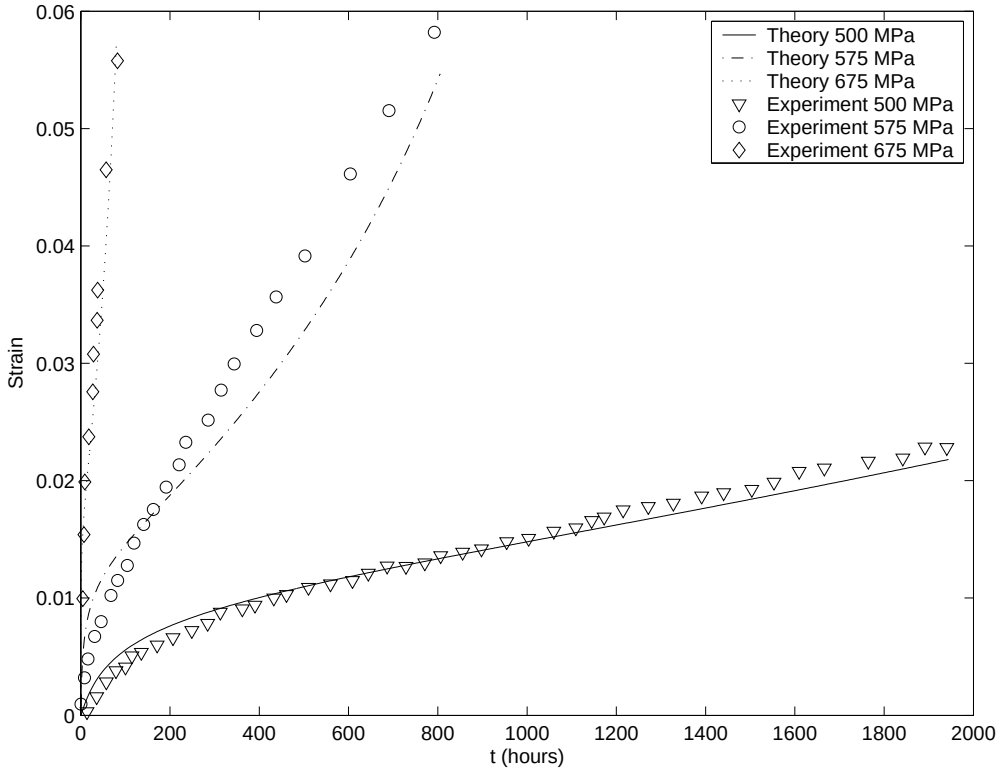

Fig. 18. Strain vs. time for CMSX-4 for loading along the <111> orientation, $\theta = 800\ ^{o}$C: Comparison of the predictions of the model with experimental results of Schubert et al., [87].

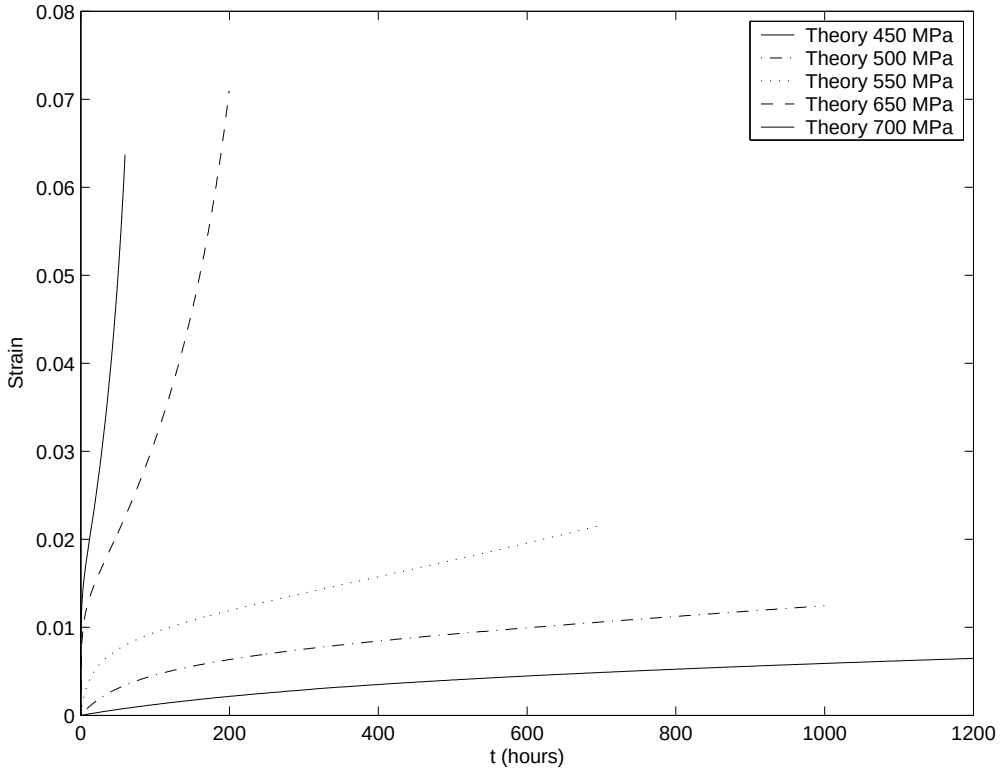

Fig. 19. Strain vs. time for CMSX-4 for loading along the <011> orientation, $\theta = 800\ ^{o}$C: Predictions of the model.

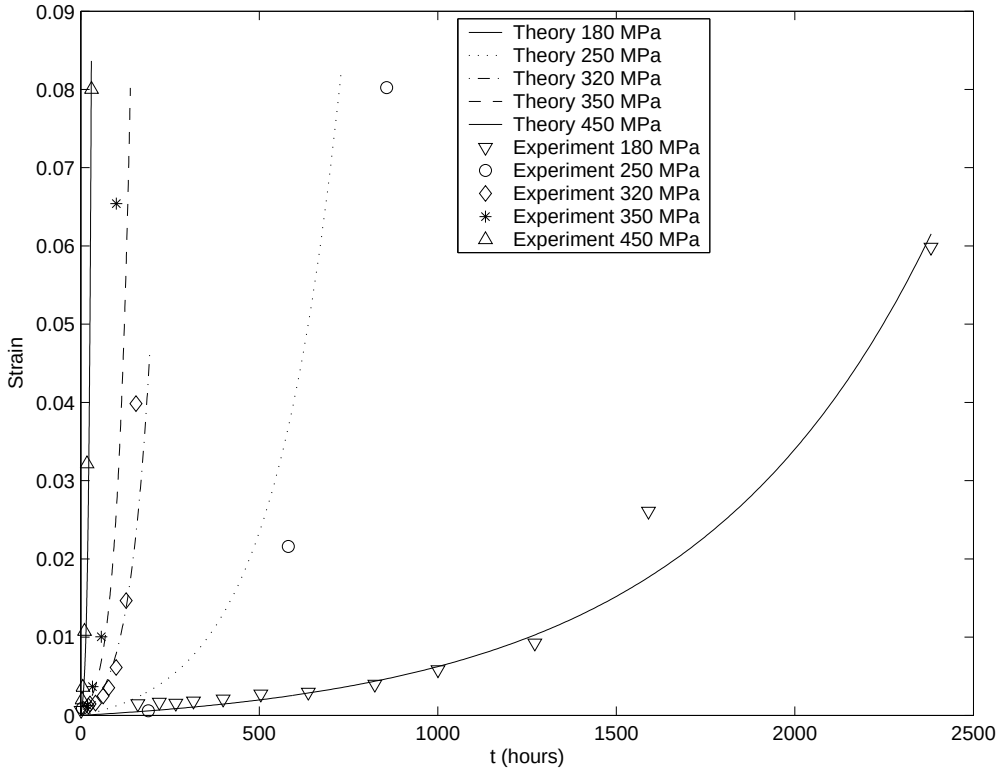

Fig. 20. Strain vs. time for CMSX-4 for loading along the <001> orientation, $\theta = 950\ ^{o}$C: Comparison of the predictions of the model with experimental results of MacLachlan et al., [45].

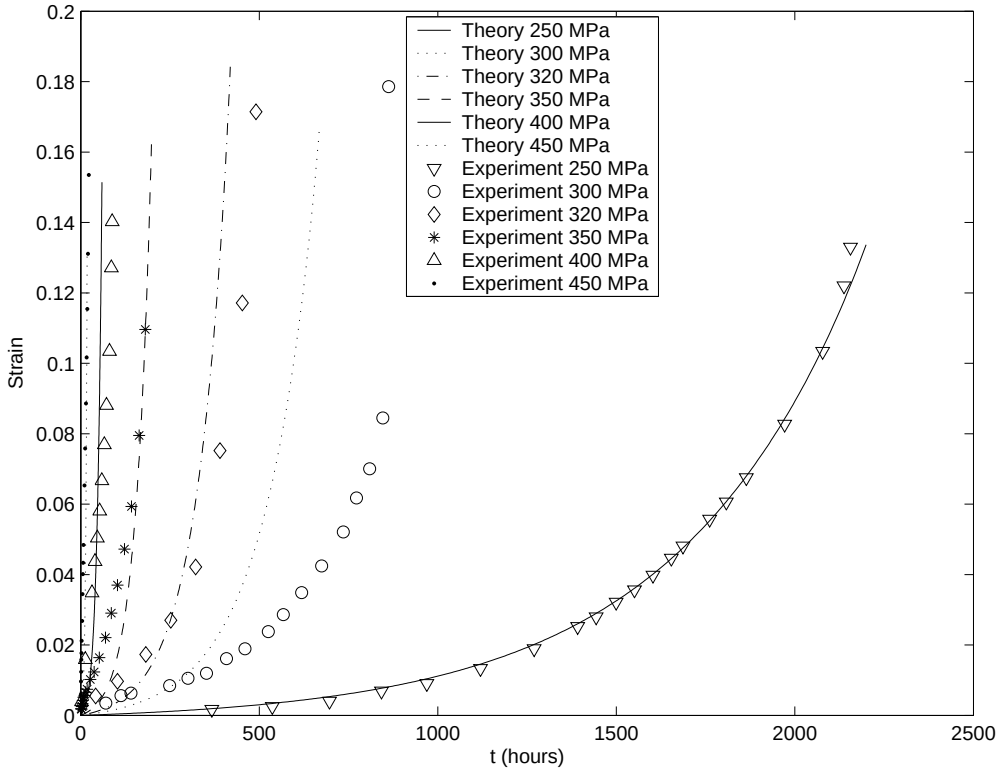

Fig. 21. Strain vs. time for CMSX-4 for loading along the <111> orientation, $\theta = 950\ ^{o}$C: Comparison of the predictions of the model with experimental results of MacLachlan et al., [45].

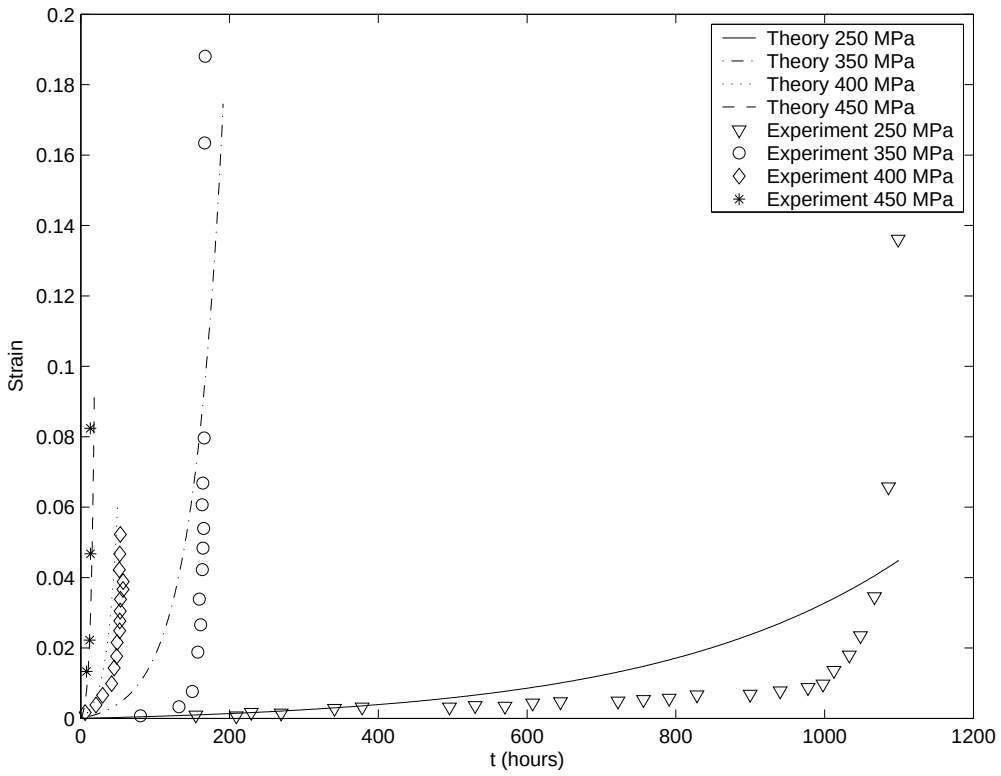

Fig. 22. Strain vs. time for CMSX-4 for loading along the <011> orientation, $\theta = 950\ ^{o}$C: Comparison of the predictions of the model with experimental results of MacLachlan et al., [45].

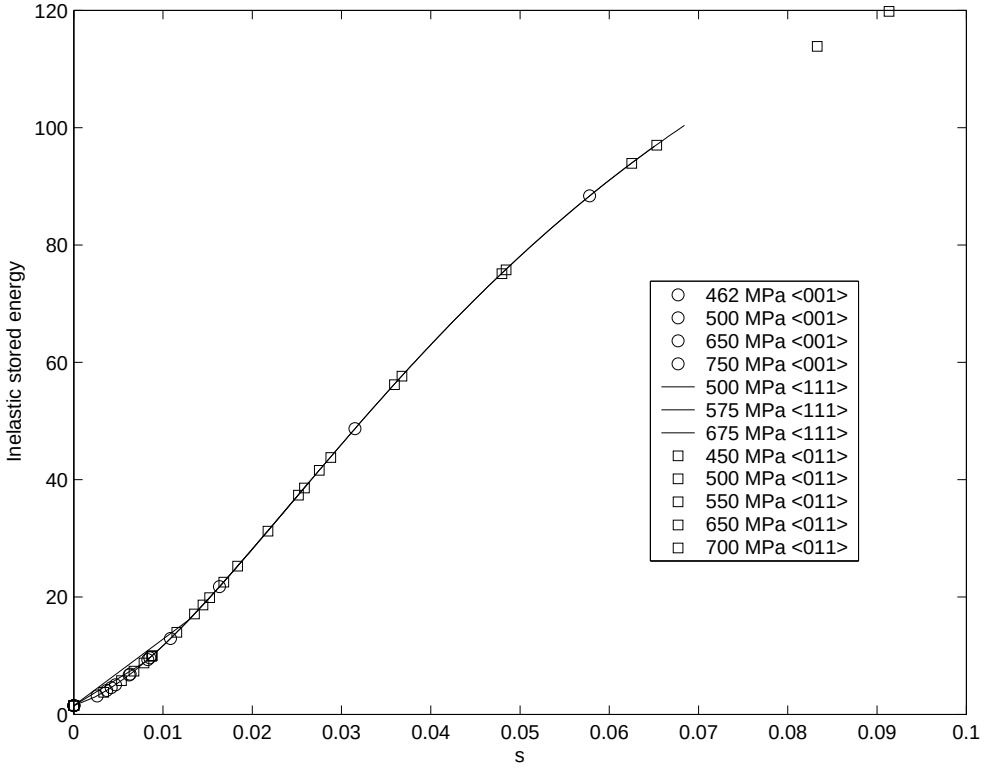

Fig. 23. Inelastic stored energy vs. inelastic strain pathlength for CMSX-4 , $\theta = 800\ ^{o}$C: Predictions of the model.

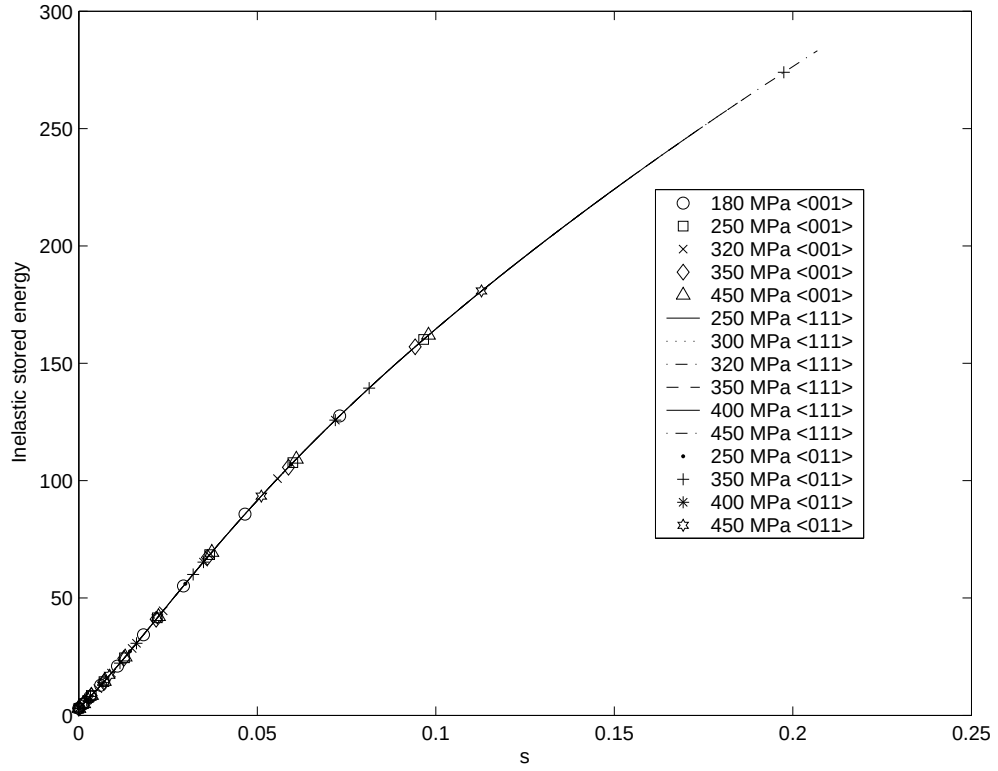

Fig. 24. Inelastic stored energy vs. inelastic strain pathlength for CMSX-4 , $\theta = 950\ ^{o}$C: Predictions of the model.

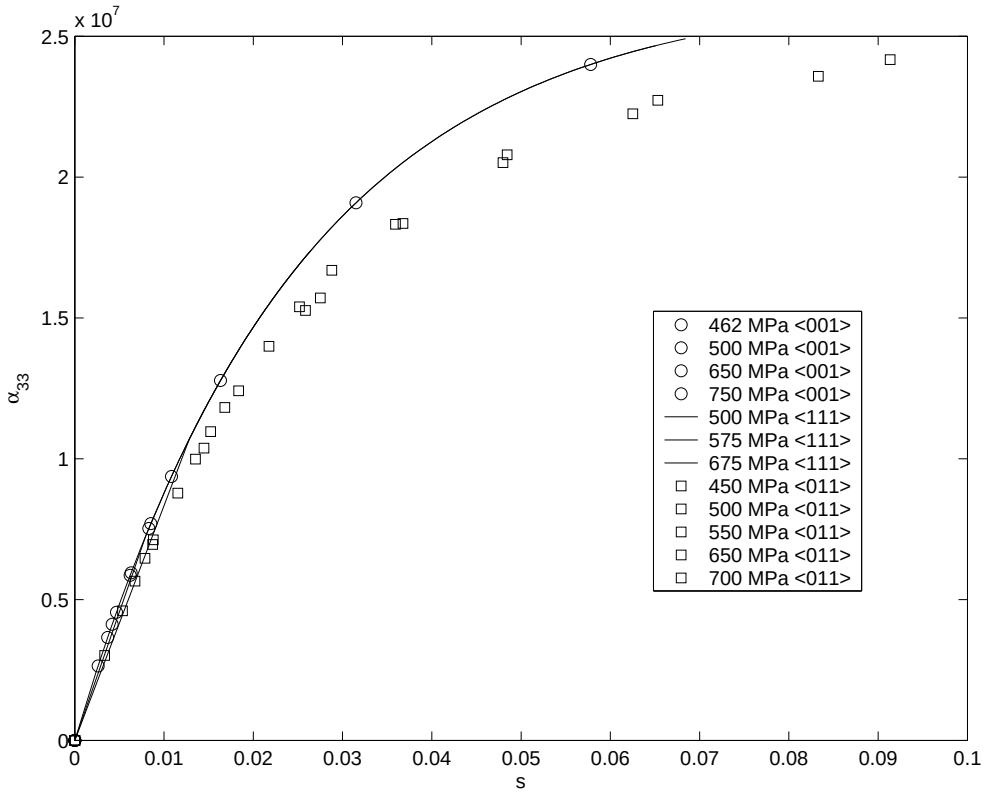

Fig. 25. Third component of backstress vs. inelastic strain pathlength for CMSX-4 , $\theta = 800\ ^{o}$C: Predictions of the model.

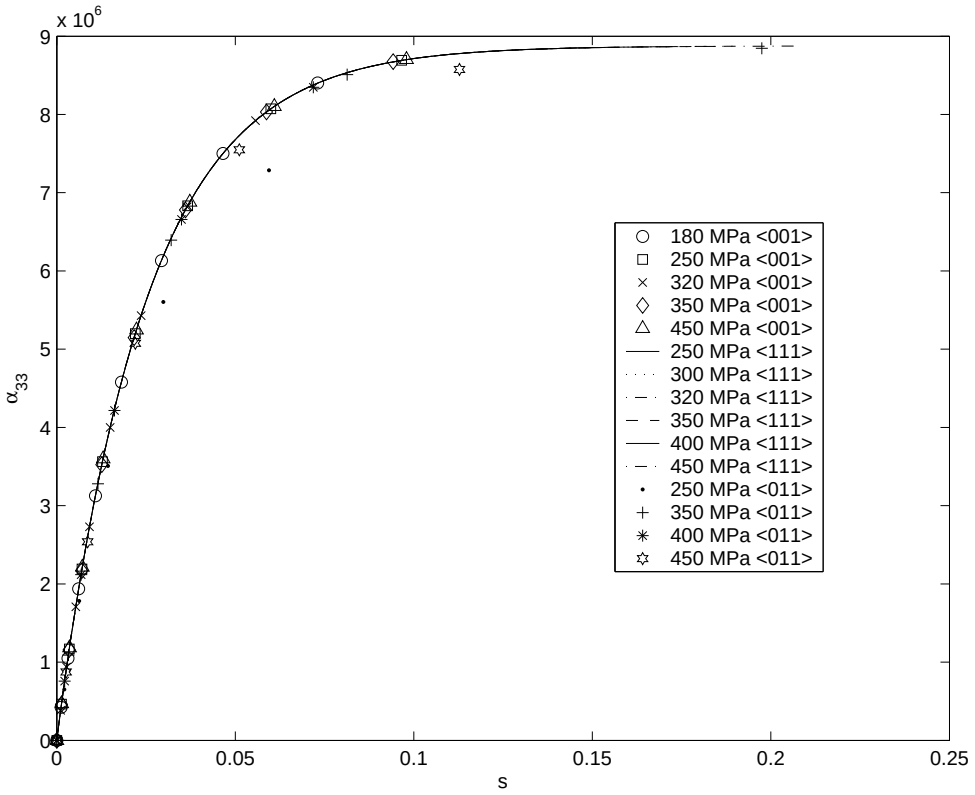

Fig. 26. Third component of backstress vs. inelastic strain pathlength for CMSX-4 , $\theta = 950\ ^{o}$C: Predictions of the model.

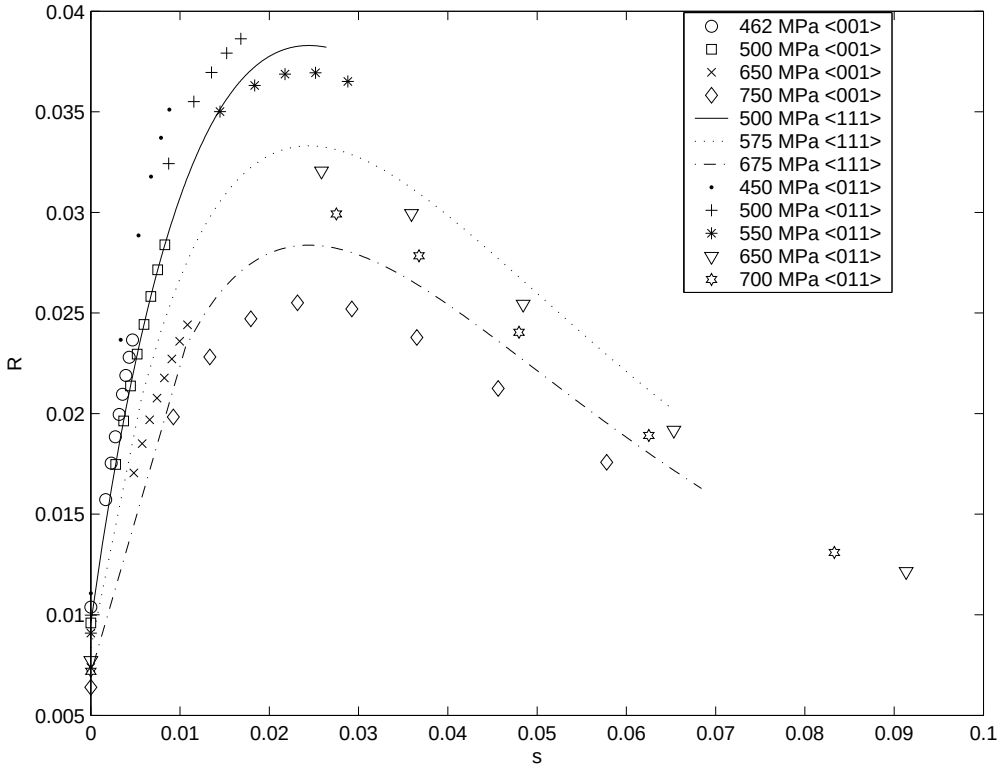

Fig. 27. Instantaneous rate of energy storage vs. inelastic strain pathlength for CM-SX-4 , $\theta = 800\ ^{o}$C: Predictions of the model.

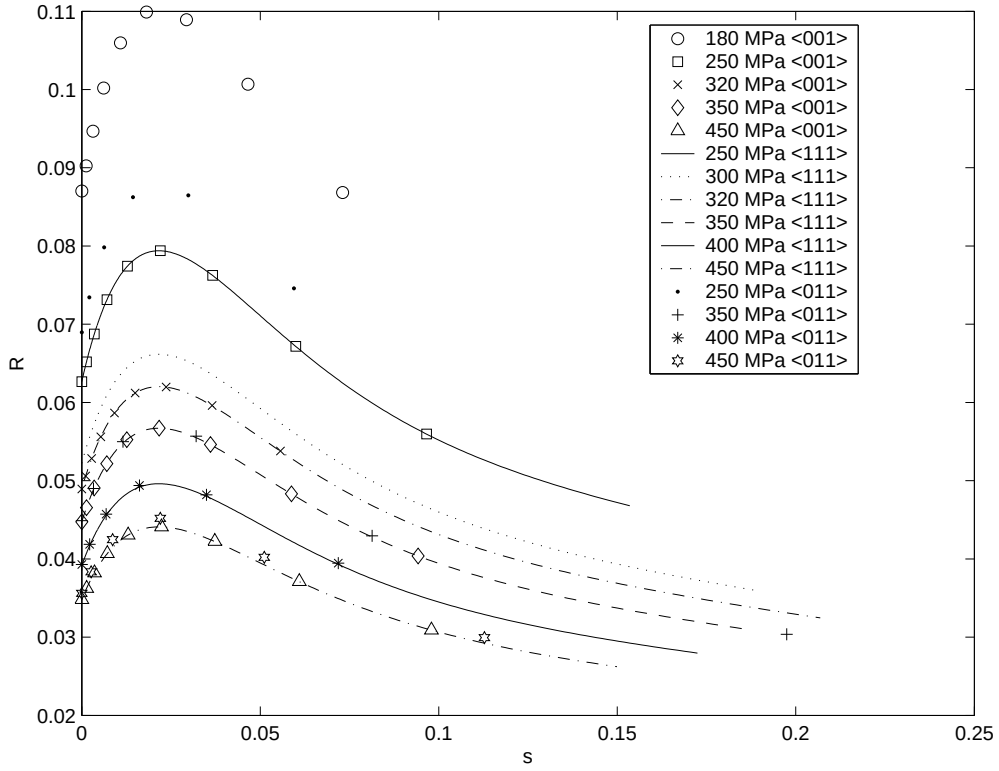

Fig. 28. Instantaneous rate of energy storage vs. inelastic strain pathlength for CM-SX-4 , $\theta = 950\ ^{o}$C: Predictions of the model.

CHAPTER V

IMPLEMENTATION IN FINITE ELEMENT SOFTWARE ABAQUS

The constitutive model that has been developed is implemented in finite element software ABAQUS/STANDARD through a user subroutine (UMAT).

Table VIII. Schematic of the user subroutine UMAT in ABAQUS/STANDARD.

ABAQUS	
(1) Solves the equilibrium equation at every time step (quasi-static problem).	
(2) Large deformation analysis is carried out.	
$\Downarrow\ \mathbf{F}(t),\ \mathbf{F}(t+\Delta t)$	$\Uparrow\ \mathbf{F}_e(t+\Delta t),\ \mathbf{T}(t+\Delta t)$
$\Downarrow\ \mathbf{F}_e(t),\ \mathbf{T}(t),\ s(t),\ \mathbf{G}(t)$	$\Uparrow\ s(t+\Delta t),\ \mathbf{G}(t+\Delta t)$
UMAT	
(1) Evaluates various quantities at time $t+\Delta t$ using their values at time t.	
(2) Uses an implicit scheme based on backward difference (backward Euler method).	
(3) Solves the resulting non-linear algebraic equation using Newton-Raphson method.	
(4) Provide the jacobian $\mathbf{J}_1 = \frac{\partial \Delta \mathbf{T}}{\partial \Delta \mathbf{E}}$,where $\mathbf{E}$ is the strain measure.	

User MATerial or UMAT is the user subroutine that is written in FORTRAN programming language and is used for incorporating the user defined material model in ABAQUS/STANDARD. This feature makes it possible to define any constitutive model of arbitrary complexity into ABAQUS. The user defined material models can be used with any ABAQUS element type. The structure of UMAT also allows one to incorporate multiple user materials at the same time. Table VIII shows the schematic of the interaction between ABAQUS/STANDARD and UMAT for large deformation analysis based on continuum formulation.

For the large deformation analysis based on continuum formulation, ABAQUS

sends, for each integration point, the values of total deformation gradient, $\mathbf{F}$ at the current time t, the deformation gradient from the current natural configuration, $\mathbf{F}_e$ at current time t, current value of the Cauchy stress, $\mathbf{T}$ and the state variables such as s and $\mathbf{G}$ at the current time step. It also sends an estimate of the total deformation gradient at the next time step $(t + \Delta t)$. The UMAT supplies the values of the state variables such as s, $\mathbf{F}_e$ and $\mathbf{G}$ and Cauchy stress at time step $t+\Delta t$ and return it back to the ABAQUS. This process continues until the a converged solution is obtained at time step $t + \Delta t$. In estimating the value of total deformation gradient at time $t + \Delta t$, ABAQUS uses the value of the jacobian, $\mathbf{J}_1$ which is specified in the UMAT. An exact definition of the consistent jacobian is necessary to ensure quadratic convergence however the jacobian is often approximated in favor of a simpler algorithm and computational speed. This may result in the loss of quadratic convergence. In the current work, we have also used an approximate jacobian which is the same as the elasticity matrix for a face centered cubic crystal.

A. Numerical scheme

In this section, the numerical scheme for the creep of superalloys loaded along the <001> orientation is developed and implemented in UMAT. For this case, the rate of dissipation can be assumed to be isotropic. However, the UMAT developed with an isotropic rate of dissipation can not capture the anisotropy in the creep behavior. Such an approach will enable the analysis of gas turbine blades loaded along the <001> direction. This is especially relevant in the analysis of turbine blades because the <001> orientation is the natural grain growth direction of single crystal superalloys and creep resistance of such components is the best along the <001> orientation. The implementation of anisotropic creep in ABAQUS is completely different from the

isotropic case, since the way ABAQUS handles the anisotropic problem is entirely different from the isotropic case in that the specification of orientation of crystal lattice in UMAT requires using additional user subroutines. Also, specifying the orientation of crystal lattice using such user routines alters the way in which variables such as stresses and strains are handled by UMAT. For example, when the orientation of crystal lattice is specified using the user subroutine ORIENT in ABAQUS/STANDARD, the stresses and strains components will be in the local basis (that is, the basis specifying the crystal axes) and this basis also rotates with the material in finite strain analysis. A more general implementation of UMAT for anisotropic creep has not been carried out in this work.

1. UMAT for creep along the <001> orientation

Let us now develop the numerical scheme based on implicit first order backward difference formula (backward Euler method). For the sake of completeness let us now list the equations describing the constitutive model. For the case when the rate of dissipation is assumed to be isotropic, the equations describing the constitutive model reduces to

$$\begin{aligned} \mathbf{D}_p &= \frac{\dot{s}}{h + 2k_{44}\dot{s}} \Big(\mathbf{A} - \frac{1}{3} tr(\mathbf{A})\mathbf{I} - \boldsymbol{\alpha} \Big) \ , \\ &:= \frac{\dot{s}}{h + 2k_{44}\dot{s}} \bar{\mathbf{A}} \ . \end{aligned} \tag{5.1}$$

Using the definition for $\dot{s}$ $(= \sqrt{\mathbf{D}_p \cdot \mathbf{D}_p})$, we can get an explicit expression for $\dot{s}$:

$$\dot{s} = \frac{1}{2k_{44}} \Big(\sqrt{\bar{\mathbf{A}} \cdot \bar{\mathbf{A}}} - h \Big) \ . \tag{5.2}$$

Using Eqs. (5.1) and (5.2), equations for the evolution of inelastic stored energy and backstress (Eqs. (3.20) and (3.22), respectively) reduce to

$$\dot{\tilde{\psi}} = \frac{1}{\rho}\Big(h + \frac{\boldsymbol{\alpha}\cdot\bar{\mathbf{A}}}{\sqrt{\bar{\mathbf{A}}\cdot\bar{\mathbf{A}}}}\Big)\dot{s} \ . \tag{5.3}$$

$$\dot{\boldsymbol{\alpha}} = \Big(\rho\psi_2\frac{\bar{\mathbf{A}}}{\sqrt{\bar{\mathbf{A}}\cdot\bar{\mathbf{A}}}} - \eta\boldsymbol{\alpha}\Big)\dot{s} \ , \tag{5.4}$$

Discreatizing Eqs (5.2), (5.3) and (5.4) using first order backward difference, we arrive at the following algebraic non-linear equations.

$$f_1 := {}^{t+\Delta t}s - {}^{t}s - \frac{\Delta t}{2^{t+\Delta t}k_{44}}\Big(\sqrt{{}^{t+\Delta t}\bar{\mathbf{A}}\cdot{}^{t+\Delta t}\bar{\mathbf{A}}} - {}^{t+\Delta t}h\Big) = 0 \ , \tag{5.5}$$

$$f_2 := {}^{t+\Delta t}\tilde{\psi} - {}^{t}\tilde{\psi} - \frac{({}^{t+\Delta t}s - {}^{t}s)}{\rho}\left({}^{t+\Delta t}h - \frac{\Delta t\,{}^{t+\Delta t}\boldsymbol{\alpha}\cdot{}^{t+\Delta t}\bar{\mathbf{A}}}{{}^{t+\Delta t}h\Delta t + 2^{t+\Delta t}k_{44}({}^{t+\Delta t}s - {}^{t}s)}\right) = 0 \ , \tag{5.6}$$

$$\mathbf{f}_3 := {}^{t+\Delta t}\boldsymbol{\alpha} - {}^{t}\boldsymbol{\alpha} + \eta^{t+\Delta t}\boldsymbol{\alpha}({}^{t+\Delta t}s - {}^{t}s) - \frac{\rho\psi_2\Delta t^{t+\Delta t}\bar{\mathbf{A}}({}^{t+\Delta t}s - {}^{t}s)}{{}^{t+\Delta t}h\Delta t + 2^{t+\Delta t}k_{44}({}^{t+\Delta t}s - {}^{t}s)} = \mathbf{0} \ . \tag{5.7}$$

Eqs (5.5), (5.6) and (5.7) are set of non-linear algebraic equations which need to be solved for ${}^{t+\Delta t}s$, ${}^{t+\Delta t}\tilde{\psi}$ and ${}^{t+\Delta t}\boldsymbol{\alpha}$.

The set of equations (5.5)-(5.7) is solved using Newton-Raphson method. For the sake of convenience, the second order symmetric tensors are written as a column vector (Voigt notation). Lets define the vector $\mathbf{H}$ and $\mathbf{Y}$ such that

$$[\mathbf{H}] = \begin{pmatrix} f_1 \\ f_2 \\ \mathbf{f}_3 \end{pmatrix}, \quad [\mathbf{Y}] = \begin{pmatrix} {}^{t+\Delta t}s \\ {}^{t+\Delta t}\tilde{\psi} \\ {}^{t+\Delta t}\boldsymbol{\alpha} \end{pmatrix} \ . \tag{5.8}$$

The equation $\mathbf{H}(\mathbf{Y}) = \mathbf{0}$ is solved for $\mathbf{Y}$ in order to get the solution using Newton-Raphson scheme:

$$\mathbf{Y}^{k+1} = \mathbf{Y}^{k} - [\mathbf{J}]^{-1}\mathbf{H}(\mathbf{Y}^{k}) \ , \tag{5.9}$$

where

$$\mathbf{J} = \begin{pmatrix} \frac{\partial f_1}{\partial s} & \frac{\partial f_1}{\partial \tilde{\psi}} & \frac{\partial f_1}{\partial \boldsymbol{\alpha}} \\ \frac{\partial f_2}{\partial s} & \frac{\partial f_2}{\partial \tilde{\psi}} & \frac{\partial f_3}{\partial \boldsymbol{\alpha}} \\ \frac{\partial \mathbf{f}_3}{\partial s} & \frac{\partial \mathbf{f}_3}{\partial \tilde{\psi}} & \frac{\partial \mathbf{f}_3}{\partial \boldsymbol{\alpha}} \end{pmatrix} , \tag{5.10}$$

and k is the iteration number. The solution at time t for the variables s, $\mathbf{G}$ and $\boldsymbol{\alpha}$ is used as the initial guess for the Newton-Raphson scheme in order to find their values at time step $t + \Delta t$.

The derivatives appearing in the jacobian are evaluated as follows:

$$\frac{\partial f_1}{\partial s} = 1 - \frac{\Delta t}{2}\frac{\partial (k_{44})^{-1}}{\partial s}\left(\sqrt{\bar{\mathbf{A}} \cdot \bar{\mathbf{A}}} - h\right) + \frac{\rho \Delta t (k_{44})^{-1}}{2}(\psi_1 a'' + \psi_1 \eta a') \ , \tag{5.11a}$$

$$\frac{\partial f_1}{\partial \tilde{\psi}} = -\rho \eta \Delta t \frac{(k_{44})^{-1}}{2} \ , \tag{5.11b}$$

$$\frac{\partial f_1}{\partial \boldsymbol{\alpha}} = \frac{\Delta t (k_{44})^{-1}}{2} \frac{\bar{\mathbf{A}}}{\sqrt{\bar{\mathbf{A}} \cdot \bar{\mathbf{A}}}} \ , \tag{5.11c}$$

$$\begin{aligned} \frac{\partial f_2}{\partial s} = &- \frac{\partial h}{\partial s}\left(\frac{s - {}^t s}{\rho}\right) - \frac{h}{\rho} - \frac{1}{\rho}\left(\frac{\Delta t \boldsymbol{\alpha} \cdot \bar{\mathbf{A}}}{h\Delta t + 2k_{44}(s - {}^t s)}\right) \\ &+ \frac{1}{\rho}\frac{(\Delta t)^2 (s - {}^t s)\boldsymbol{\alpha} \cdot \bar{\mathbf{A}}}{(h\Delta t + 2k_{44}(s - {}^t s))^2}\left(\frac{\partial h}{\partial s} + \frac{2k_{44}}{\Delta t} + \frac{2(s - {}^t s)}{\Delta t}\frac{\partial k_{44}}{\partial s}\right) \ , \end{aligned} \tag{5.11d}$$

$$\frac{\partial f_2}{\partial \tilde{\psi}} = 1 + \eta(s - {}^t s)\left(1 - \frac{(\Delta t)^2 (s - {}^t s)\boldsymbol{\alpha} \cdot \bar{\mathbf{A}}}{(h\Delta t + 2k_{44}(s - {}^t s))^2}\right) \ , \tag{5.11e}$$

$$\frac{\partial f_2}{\partial \boldsymbol{\alpha}} = -\frac{(s - {}^t s)}{\rho}\left(\frac{\bar{\mathbf{A}} - \boldsymbol{\alpha}}{h\Delta t + 2k_{44}(s - {}^t s)}\right) \ , \tag{5.11f}$$

$$\begin{aligned} \frac{\partial \mathbf{f}_3}{\partial s} = &- \rho \psi_2 \Delta t \left(\frac{\bar{\mathbf{A}}}{h\Delta t + 2k_{44}(s - {}^t s)}\right) \\ &+ \frac{\rho \psi_2 (\Delta t)^2 (s - {}^t s)\bar{\mathbf{A}}}{(h\Delta t + 2k_{44}(s - {}^t s))^2}\left(\frac{\partial h}{\partial s} + \frac{2k_{44}}{\Delta t} + \frac{2(s - {}^t s)}{\Delta t}\frac{\partial k_{44}}{\partial s}\right) \ , \end{aligned} \tag{5.11g}$$

$$\frac{\partial \mathbf{f}_3}{\partial \tilde{\psi}} = -\frac{\rho^2 \eta \psi_2 (\Delta t)^2 (s - {}^t s)\bar{\mathbf{A}}}{(h\Delta t + 2k_{44}(s - {}^t s))^2} \ , \tag{5.11h}$$

$$\frac{\partial \mathbf{f}_3}{\partial \boldsymbol{\alpha}} = \left(1 + \frac{\rho\psi_2 \Delta t(s - {}^t s)}{h\Delta t + 2k_{44}(s - {}^t s)} + \eta(s - {}^t s)\right)\mathbf{I}_4 \ , \tag{5.11i}$$

where

$$a'(s) = \beta_2\alpha_1 e^{-\alpha_1 s} \ , \tag{5.12a}$$

$$a''(s) = -\beta_2\alpha_1^2 e^{-\alpha_1 s} \ , \tag{5.12b}$$

$$\frac{\partial (k_{44})^{-1}}{\partial s} = \beta_1 e^{\kappa_1 p} a' e^{-\alpha_2 s} - \alpha_2\beta_1 a e^{\kappa_1 p} e^{-\alpha_2 s} + \beta_3\alpha_3 e^{\kappa_2 p} e^{\alpha_3 s} \ , \tag{5.12c}$$

$$\frac{\partial k_{44}}{\partial s} = -k_{44}^2\Big(\beta_1 e^{\kappa_1 p} a' e^{-\alpha_2 s} - \alpha_2\beta_1 a e^{\kappa_1 p} e^{-\alpha_2 s} + \beta_3\alpha_3 e^{\kappa_2 p} e^{\alpha_3 s}\Big) \ , \tag{5.12d}$$

$$p = \frac{1}{3} tr(\mathbf{A}) \ , \tag{5.12e}$$

and $a(s)$ and h are as defined in equations (3.19) and (3.20), respectively. All the quantities that appear in the terms which constitute the jacobian are determined at the iteration level k.

2. Validation of UMAT for creep along the <001> orientation

The numerical scheme developed in the previous section is implemented in UMAT to study the creep behavior of single crystal superalloys loaded along the <001> orientation. The UMAT is validated by using it to obtain the results already obtained in previous sections using the semi-inverse approach. The results obtained through the UMAT is compared with the results obtained using the semi-inverse approach and the experimental results. Figs. 29, 30 and 31 show a comparison of strain versus time curves for loading along <001> orientation at temperatures $\theta = 750, 982$ and 1000 ^{o}C obtained using the UMAT and the semi-inverse method and experimental results. Figs. 32, 33 and 34 show a comparison for the inelastic stored energy at temperatures $\theta = 750, 982$ and 1000 ^{o}C. A similar comparison is shown for third component of the backstress tensor in Figs. 35, 36 and 37. Figs. 38, 39 and 40 show the same comparison for instantaneous rate of energy storage.

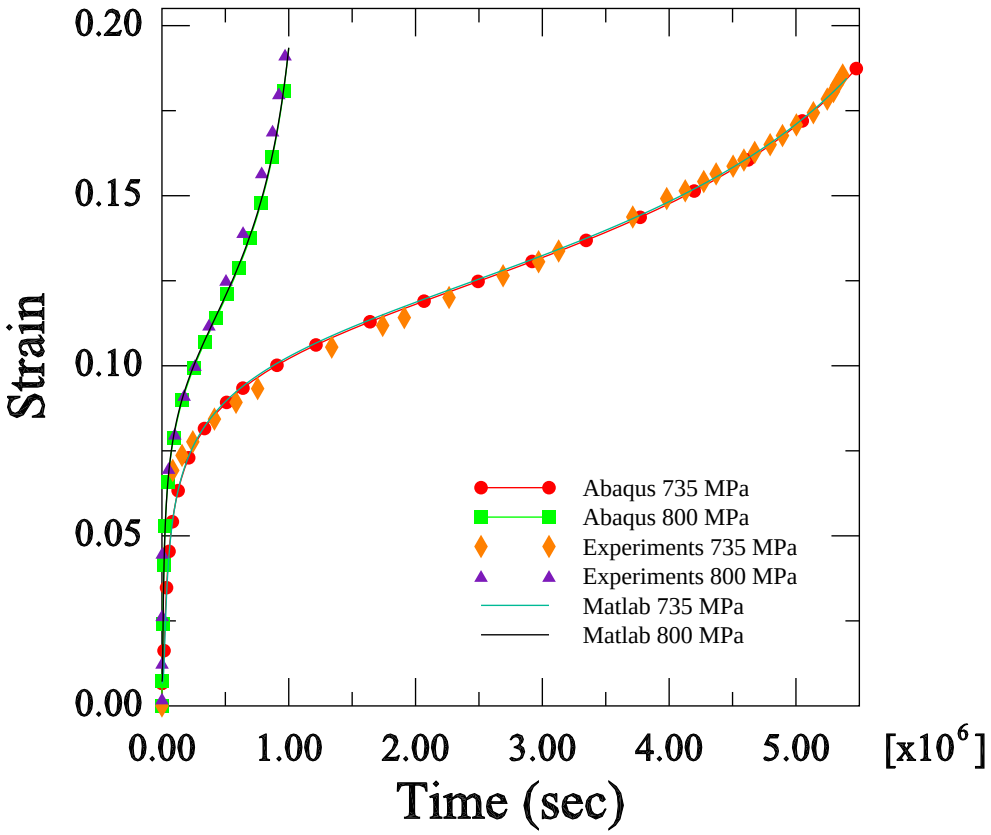

Fig. 29. Strain vs. time for CMSX-4 for loading along the <001> orientation, $\theta = 750$ ^{o}C: Comparison of the results obtained from User Material in ABAQUS with results obtained in MATLAB and experimental results of Svoboda and Lucas [90] and Henderson and Lindblom [32].

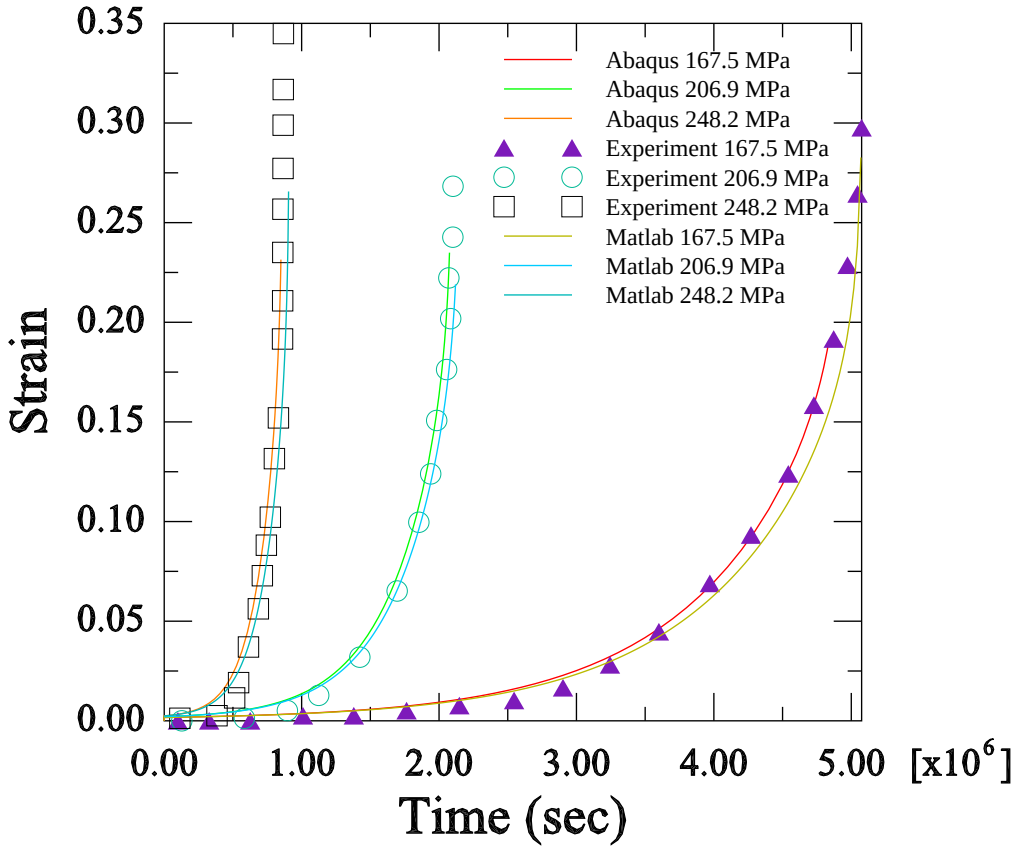

Fig. 30. Strain vs. time for CMSX-4 for loading along the <001> orientation, $\theta = 982$ ^{o}C: Comparison of the results obtained from User Material in ABAQUS with results obtained in MATLAB and experimental results of Svoboda and Lucas [90] and Henderson and Lindblom [32].

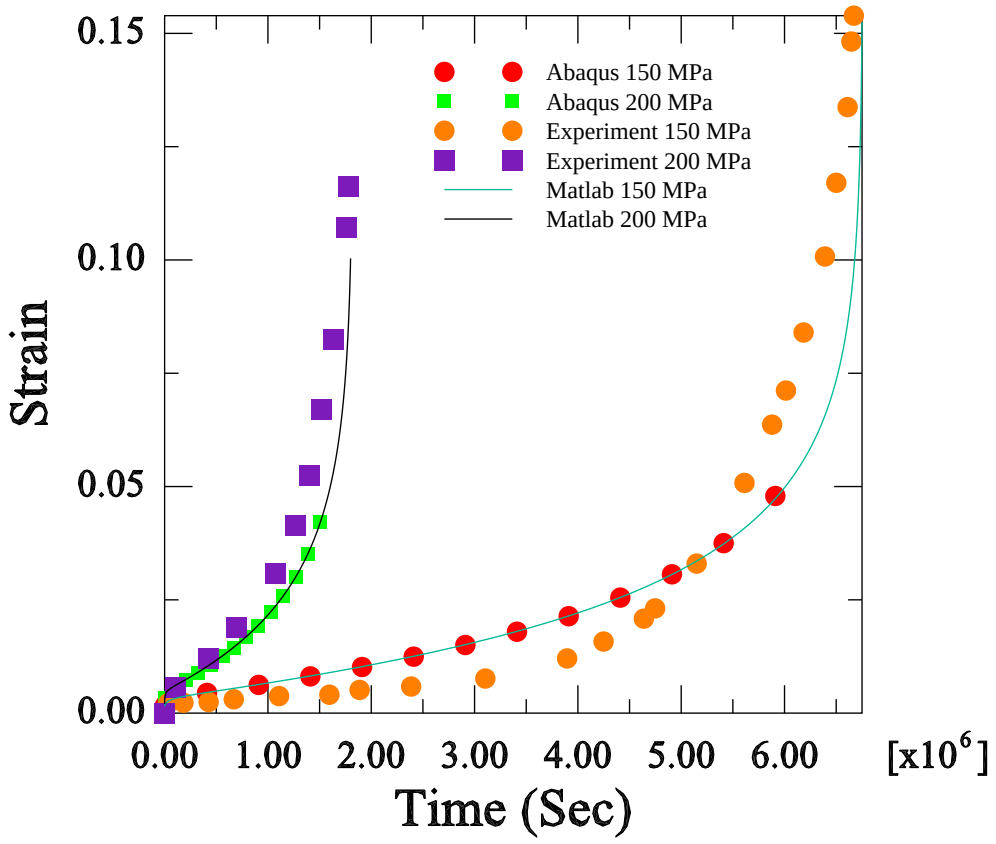

Fig. 31. Strain vs. time for CMSX-4 for loading along the <001> orientation, $\theta = 1000\ ^{o}$C: Comparison of the results obtained from User Material in ABAQUS with results obtained in MATLAB and experimental results of Svoboda and Lucas [90] and Henderson and Lindblom [32].

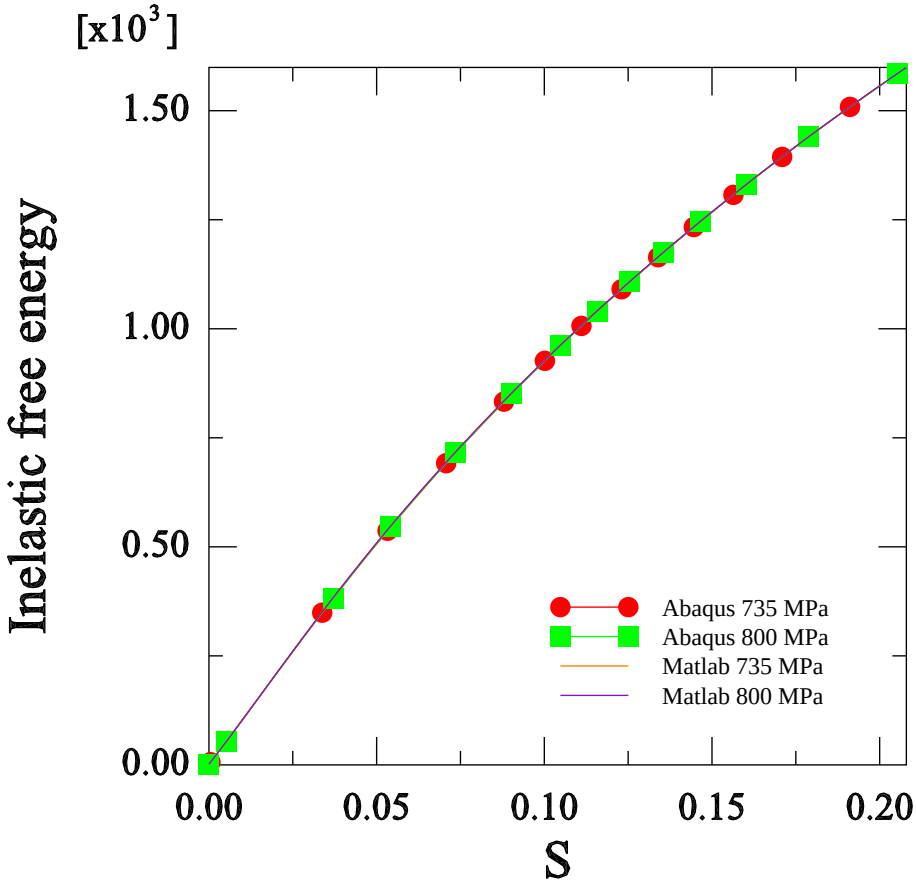

Fig. 32. Inelastic stored energy vs. inelastic strain pathlength for CMSX-4 for loading along the <001> orientation, $\theta = 750\ ^{o}$C: Comparison of the results obtained from User Material in ABAQUS with results obtained in MATLAB.

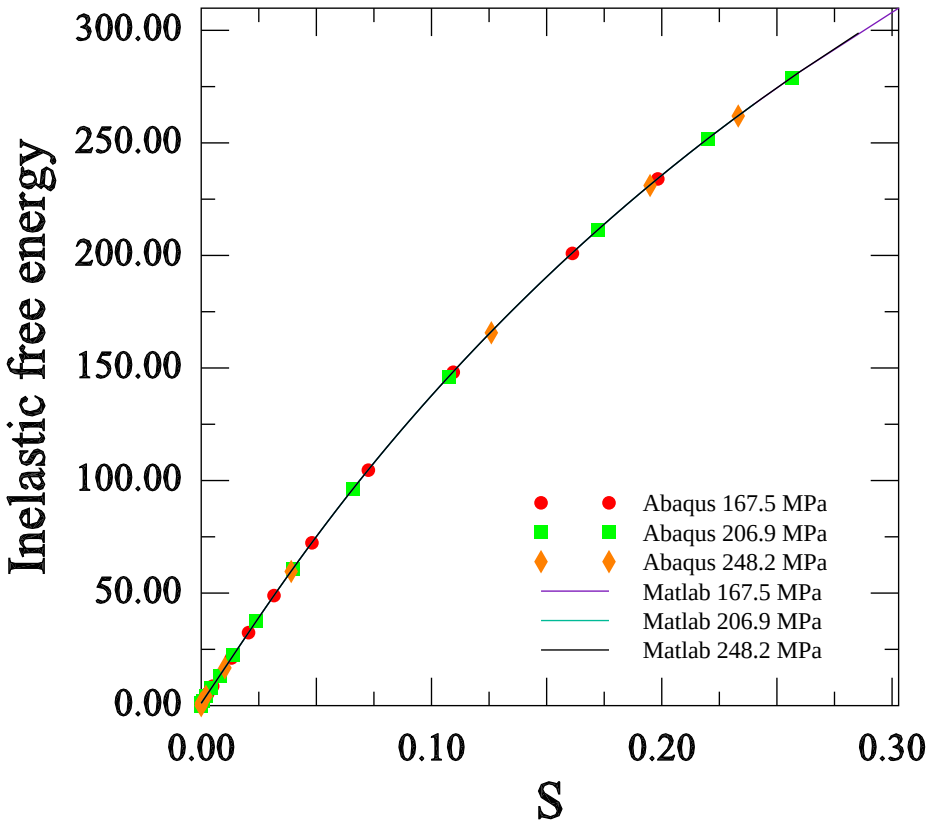

Fig. 33. Inelastic stored energy vs. inelastic strain pathlength for CMSX-4 for loading along the <001> orientation, $\theta = 982\ ^{o}$C: Comparison of the results obtained from User Material in ABAQUS with results obtained in MATLAB.

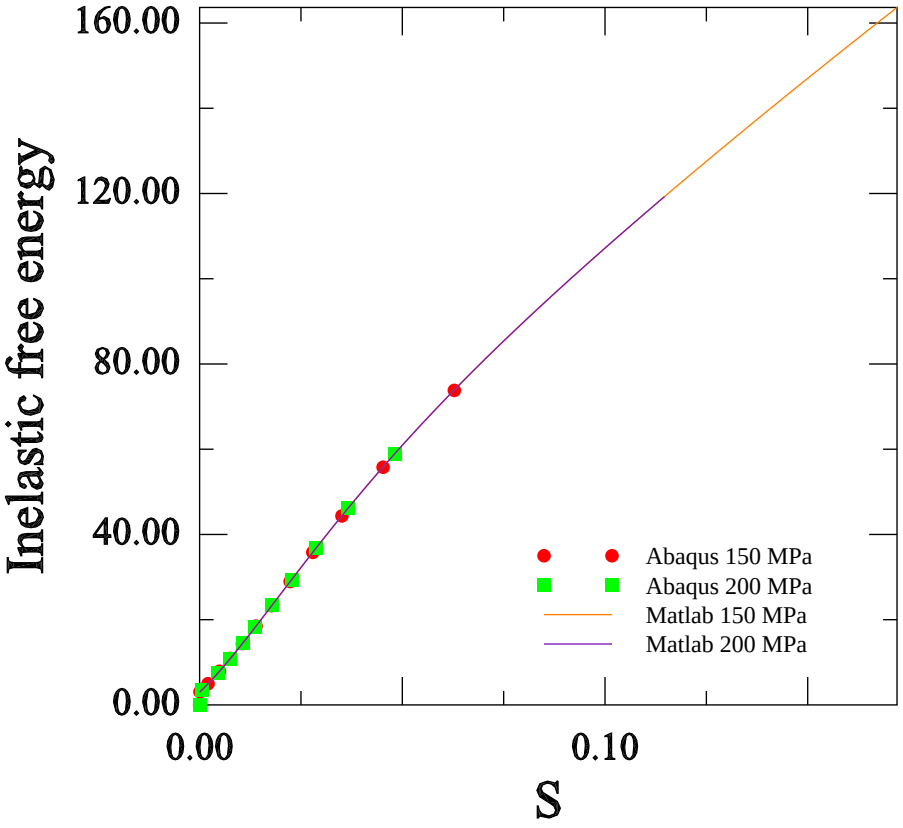

Fig. 34. Inelastic stored energy vs. inelastic strain pathlength for CMSX-4 for loading along the <001> orientation, $\theta = 1000\ ^{o}$C: Comparison of the results obtained from User Material in ABAQUS with results obtained in MATLAB.

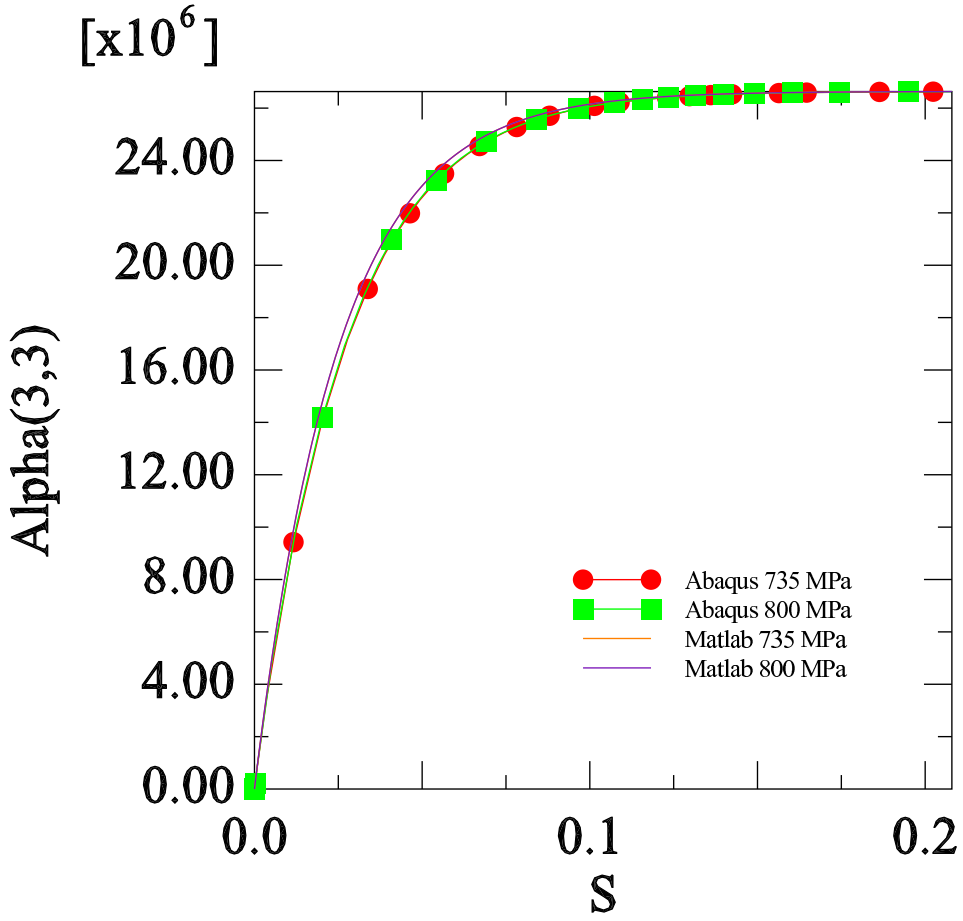

Fig. 35. Third component of backstress vs. inelastic strain pathlength for CMSX-4, $\theta = 750$ ^{o}C: Comparison of the results obtained from User Material in ABAQUS with results obtained in MATLAB.

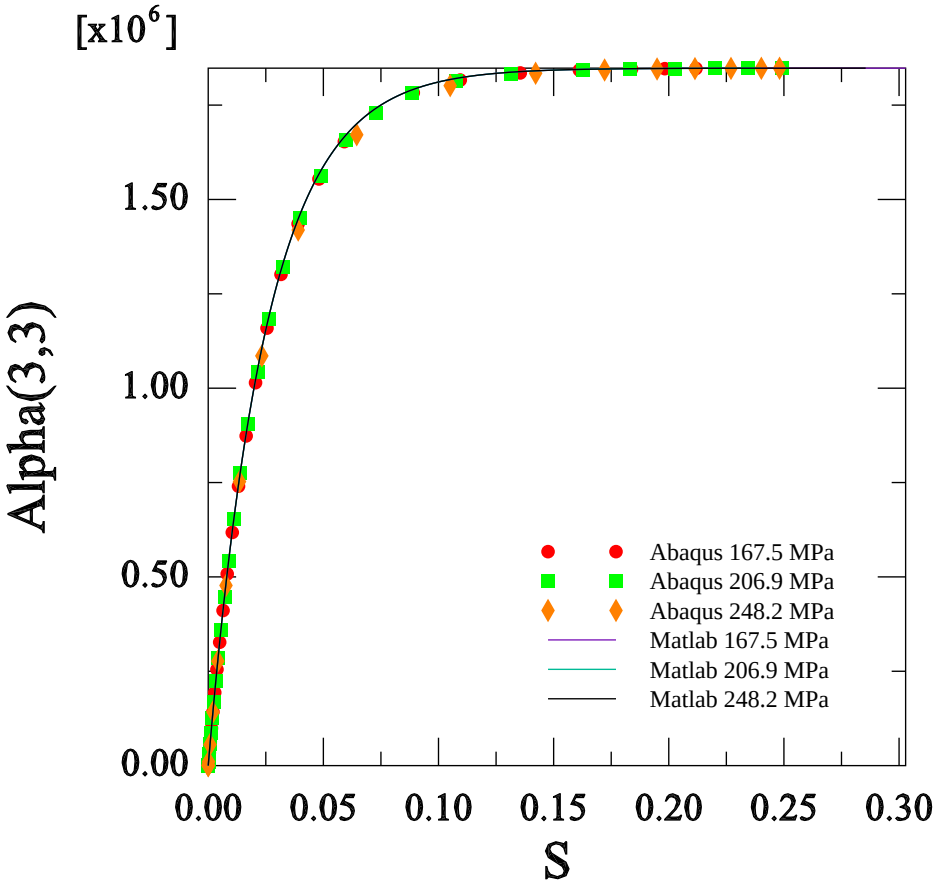

Fig. 36. Third component of backstress vs. inelastic strain pathlength for CMSX-4, $\theta = 982$ ^{o}C: Comparison of the results obtained from User Material in ABAQUS with results obtained in MATLAB.

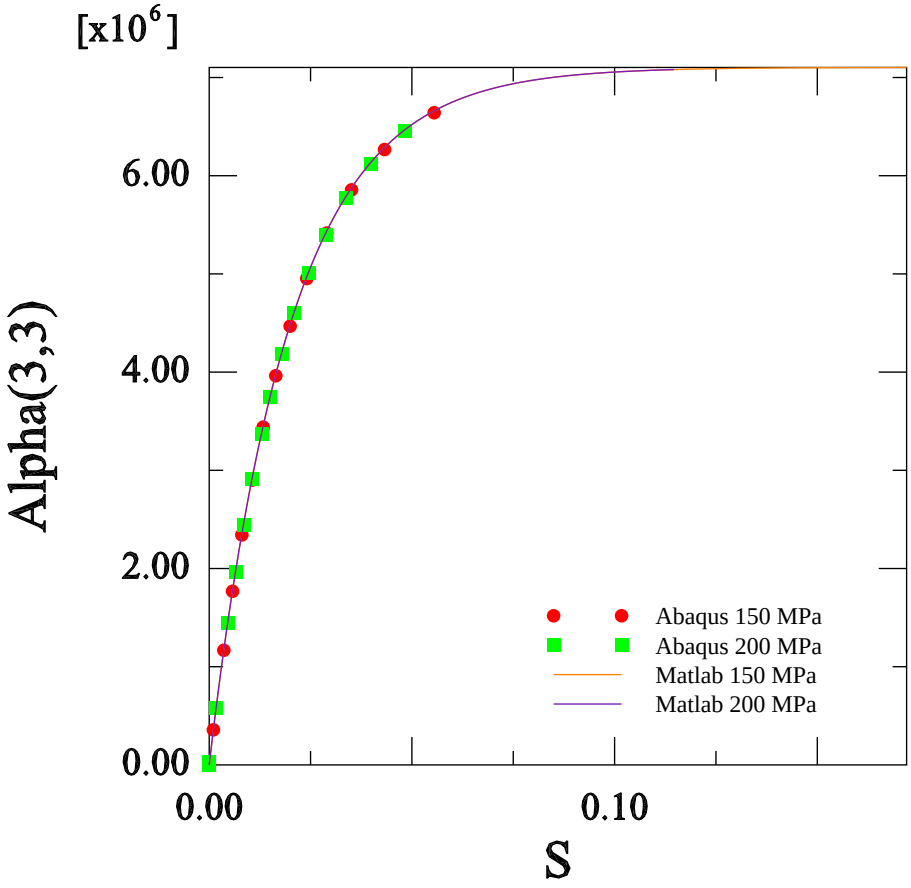

Fig. 37. Third component of backstress vs. inelastic strain pathlength for CMSX-4, $\theta = 1000\ ^{o}$C: Comparison of the results obtained from User Material in ABAQUS with results obtained in MATLAB.

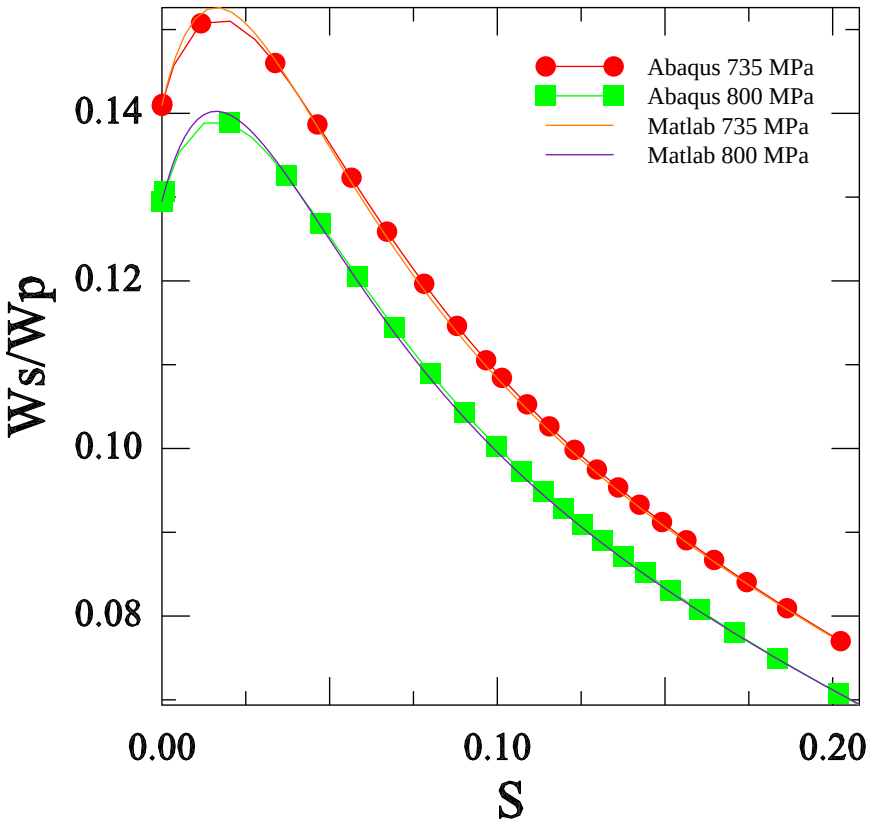

Fig. 38. Instantaneous rate of energy storage vs. inelastic strain pathlength for CM-SX-4 for loading along the <001> orientation, θ = 750 ^{o}C: Comparison of the results obtained from User Material in ABAQUS with results obtained in MATLAB.

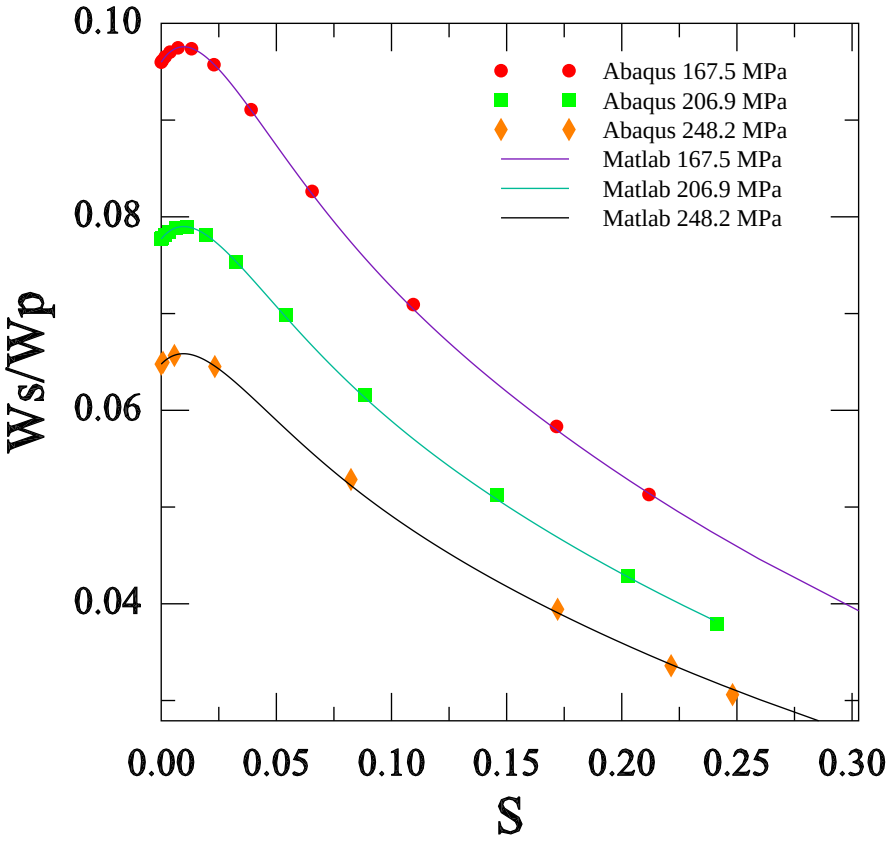

Fig. 39. Instantaneous rate of energy storage vs. inelastic strain pathlength for CM-SX-4 for loading along the <001> orientation, θ = 982 ^{o}C: Comparison of the results obtained from User Material in ABAQUS with results obtained in MATLAB.

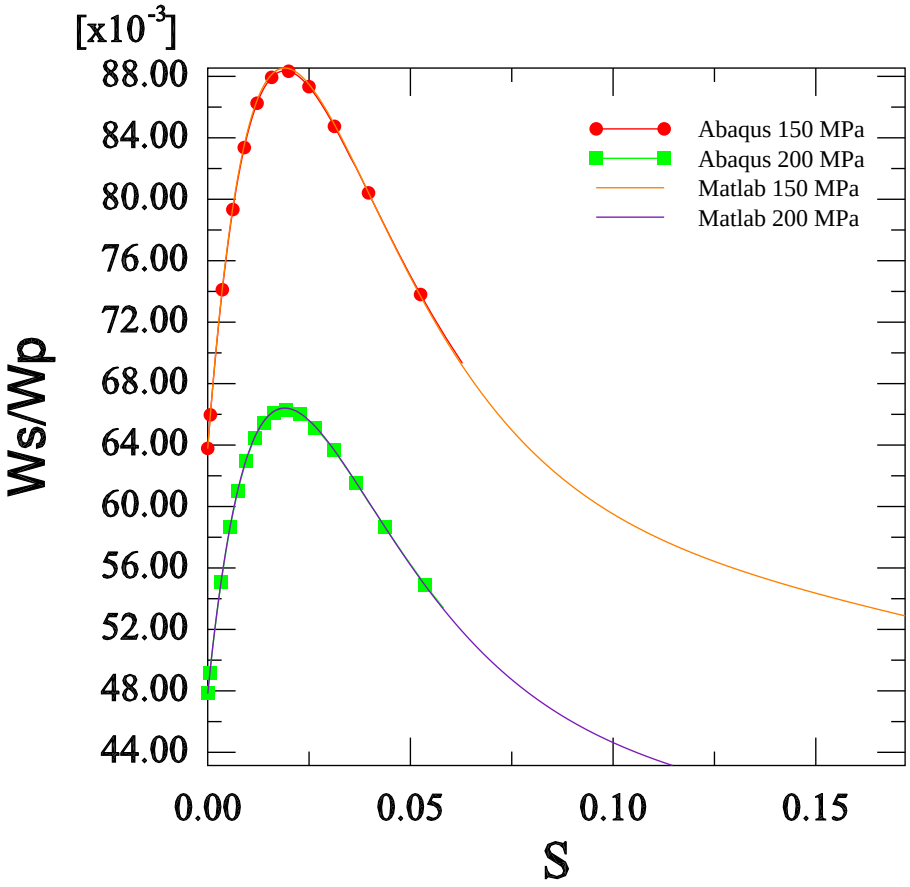

Fig. 40. Instantaneous rate of energy storage vs. inelastic strain pathlength for CM-SX-4 for loading along the <001> orientation, θ = 1000 ^{o}C: Comparison of the results obtained from User Material in ABAQUS with results obtained in MATLAB.

CHAPTER VI

A THERMOMECHANICAL MODEL FOR THE CREEP OF SUPERALLOYS

In this chapter, a thermomechanical model for creep of single crystal superalloys will be developed. Although, complete constitutive prescriptions for stored energy and rate of dissipation function is not provided, the outline of such a model is delineated. An evolution equation for the evolution of rafts with creep strain is also incorporated within the thermodynamical framework.

A. Development of non-isothermal model

Let us now again start with the reduced dissipation equation (Eq. (3.2)):

$$\mathbf{T} \cdot \mathbf{L} - \rho\dot{\psi} - \rho\eta\dot{\theta} = \zeta \geq 0 \ , \tag{6.1}$$

wherein the term associated with the rate of dissipation due to conduction ($-\frac{\mathbf{q}\cdot grad(\theta)}{\theta}$) has already been additively split from the rate of dissipation term on the right hand side.

We will assume that the Helmholtz potential for a single crystal superalloy is of the form

$$\psi(\mathbf{F}_{\kappa_{p(t)}}, \mathbf{G}, \varphi, \theta) = \bar{\psi}(\theta) + \hat{\psi}(\mathbf{F}_{\kappa_{p(t)}}, \theta) + \tilde{\psi}(\mathbf{G}, \varphi, \theta) \ , \tag{6.2}$$

where φ is a measure of the extent of rafting. Although there is no robust way of measuring the extent of rafting in modern single crystal superalloys, experiments carried out by Matan *et al.* [48] seems to be the only effort towards this goal. Matan *et al.* [48] used a stereological procedure utilizing techniques based on digital image analysis to characterize the extent of rafting.

The form for the $\bar{\psi}(\theta)$ is assumed to be

$$\bar{\psi}(\theta) = b_o - \frac{1}{2} b_2 (\theta - \theta_o)^2 \ , \tag{6.3}$$

and the form for the elastic stored energy for a crystal having cubic symmetry is given by

$$\begin{aligned} \hat{\psi} = \frac{1}{2\rho}\Big\{ & c_{12}(\theta)(\text{tr } \mathbf{E}_{\kappa_{p(t)}})^2 + 2c_{44}(\theta)(\text{tr } \mathbf{E}^2_{\kappa_{p(t)}}) + (c_{11}(\theta) - c_{12}(\theta) - 2c_{44}(\theta)) \\ & \Big((\mathbf{a} \cdot \mathbf{E}_{\kappa_{p(t)}} \mathbf{a})^2 + (\mathbf{b} \cdot \mathbf{E}_{\kappa_{p(t)}} \mathbf{b})^2 + (\mathbf{c} \cdot \mathbf{E}_{\kappa_{p(t)}} \mathbf{c})^2\Big)\Big\} - b_1 (\text{tr } \mathbf{E}_{\kappa_{p(t)}})(\theta - \theta_o) \ . \end{aligned} \tag{6.4}$$

$\tilde{\psi}(\mathbf{G}, \varphi, \theta)$ denoted the inelastic stored energy which is a function of temperature, inelastic strain and the extent of rafting.

Substituting the form for the stored energy into reduced dissipation equation (Eq. (6.1)) and collecting like terms will lead to

$$\begin{aligned} \left(\mathbf{T}\mathbf{F}^{-T}_{\kappa_{p(t)}} - \rho \frac{\partial \hat{\psi}}{\partial \mathbf{F}_{\kappa_{p(t)}}}\right) \cdot \dot{\mathbf{F}}_{\kappa_{p(t)}} + \left(\mathbf{F}^T_{\kappa_{p(t)}} \mathbf{T}\mathbf{F}^{-T}_{\kappa_{p(t)}} - \frac{\partial \tilde{\psi}}{\partial \mathbf{G}} \mathbf{G}^T\right) \cdot \mathbf{L}_p \\ - \rho \left(\eta + \frac{\partial \bar{\psi}}{\partial \theta} + \frac{\partial \hat{\psi}}{\partial \theta} + \frac{\partial \tilde{\psi}}{\partial \theta}\right) \dot{\theta} - \rho \frac{\partial \tilde{\psi}}{\partial \varphi} \dot{\varphi} = \zeta \ . \end{aligned} \tag{6.5}$$

We are only looking for sufficient conditions to satisfy Eq. (6.5). Towards such a goal, we will assume the Cauchy stress to be of the form given by

$$\begin{aligned} \mathbf{T} &= \rho \frac{\partial \hat{\psi}}{\partial \mathbf{F}_{\kappa_{p(t)}}} \mathbf{F}^T_{\kappa_{p(t)}} = \rho \mathbf{F}_{\kappa_{p(t)}} \frac{\partial \hat{\psi}}{\partial \mathbf{E}_{\kappa_{p(t)}}} \mathbf{F}^T_{\kappa_{p(t)}} \\ &= \big(c_{12}(\theta)(\text{tr } \mathbf{E}_{\kappa_{p(t)}}) - \rho b_1 (\theta - \theta_o)\big) \mathbf{F}_{\kappa_{p(t)}} \mathbf{F}^T_{\kappa_{p(t)}} + 2c_{44}(\theta) \mathbf{F}_{\kappa_{p(t)}} \mathbf{E}_{\kappa_{p(t)}} \mathbf{F}^T_{\kappa_{p(t)}} \\ &+ (c_{11}(\theta) - c_{12}(\theta) - 2c_{44}(\theta)) \mathbf{F}_{\kappa_{p(t)}} (\boldsymbol{\mathcal{N}} \mathbf{E}_{\kappa_{p(t)}}) \mathbf{F}^T_{\kappa_{p(t)}} \ , \end{aligned} \tag{6.6}$$

where fourth order tensor $\boldsymbol{\mathcal{N}}$ has the form

$$\mathcal{N}_{ijkl} = a_i a_j a_k a_l + b_i b_j b_k b_l + c_i c_j c_k c_l \ . \tag{6.7}$$

a_i, b_i and c_i are the components of the orthogonal unit vectors $\mathbf{a}$, $\mathbf{b}$ and $\mathbf{c}$ along

the crystal axes. It should be noted here that Eq. (6.6) when linearized under the assumption of small elastic strain gives the usual relation for linear thermoelasticity:

$$\begin{aligned}\mathbf{T} \approx c_{12}(\theta)(\text{tr } \boldsymbol{\epsilon}_{\kappa_{p(t)}})\mathbf{I} + 2c_{44}(\theta)\boldsymbol{\epsilon}_{\kappa_{p(t)}} + (c_{11}(\theta) - c_{12}(\theta) - 2c_{44}(\theta))(\boldsymbol{\mathcal{N}}\boldsymbol{\epsilon}_{\kappa_{p(t)}}) \\ -\rho b_1(\theta - \theta_o)\mathbf{I} \ ,\end{aligned} \tag{6.8}$$

where $\boldsymbol{\epsilon}_{\kappa_{p(t)}}$ is the linearized strain tensor from the natural configuration $\kappa_{p(t)}$.

We also suppose that

$$\begin{aligned}\eta &= -\left(\frac{\partial\bar{\psi}}{\partial\theta} + \frac{\partial\hat{\psi}}{\partial\theta} + \frac{\partial\tilde{\psi}}{\partial\theta}\right) \\ &= b_1(\text{tr } \mathbf{E}_{\kappa_{p(t)}}) + b_2(\theta - \theta_o) - \frac{1}{2\rho}\Big\{c_{12}^o(\text{tr } \mathbf{E}_{\kappa_{p(t)}})^2 + 2c_{44}^o(\text{tr } \mathbf{E}^2_{\kappa_{p(t)}}) \\ &+ (c_{11}^o - c_{12}^o - 2c_{44}^o)\Big((\mathbf{a}\cdot\mathbf{E}_{\kappa_{p(t)}}\mathbf{a})^2 + (\mathbf{b}\cdot\mathbf{E}_{\kappa_{p(t)}}\mathbf{b})^2 + (\mathbf{c}\cdot\mathbf{E}_{\kappa_{p(t)}}\mathbf{c})^2\Big)\Big\} - \frac{\partial\tilde{\psi}}{\partial\theta} \ ,\end{aligned} \tag{6.9}$$

where we have assumed, following the experimental observations of Siebörger *et al.* [88] that the elastic constants c_{11}, c_{12} and c_{44} depend on temperature in a linear fashion:

$$c_{11}(\theta) = c_{11}^o\theta + c_{11}^1 \ , \quad c_{12}(\theta) = c_{12}^o\theta + c_{12}^1 \ , \quad c_{44}(\theta) = c_{44}^o\theta + c_{44}^1 \ . \tag{6.10}$$

Substituting Eqs. (6.6) and (6.9) into Eq. (6.5) will lead us to

$$\left(\mathbf{F}^T_{\kappa_{p(t)}}\mathbf{T}\mathbf{F}^{-T}_{\kappa_{p(t)}} - \frac{\partial\tilde{\psi}}{\partial\mathbf{G}}\mathbf{G}^T\right)\cdot\mathbf{L}_p - \rho\frac{\partial\tilde{\psi}}{\partial\varphi}\dot{\varphi} = \zeta \ . \tag{6.11}$$

We will assume that the rate of dissipation ζ can be split into two parts. The first part ζ_m relates to the entropy production due to mechanical working while the other part ζ_R is the entropy production due to rafting, i.e.,

$$\zeta(\mathbf{G}, \mathbf{L}_p, \varphi, \dot{\varphi}, \theta) = \zeta_m(\mathbf{G}, \mathbf{L}_p, \varphi, \theta) + \zeta_R(\mathbf{G}, \mathbf{L}_p, \varphi, \dot{\varphi}, \theta) \ . \tag{6.12}$$

Inserting Eq. (6.12) into Eq. (6.11) and appealing to sufficiency condition again, we

arrive at

$$\begin{aligned} \mathbf{A}\cdot\mathbf{L}_p &= \zeta_m(\mathbf{G},\mathbf{L}_p,\varphi,\theta)\ , \\ \mathbf{A} &:= \left(\mathbf{F}^T_{\kappa_{p(t)}}\mathbf{T}\mathbf{F}^{-T}_{\kappa_{p(t)}} - \frac{\partial\tilde{\psi}}{\partial\mathbf{G}}\mathbf{G}^T\right)\ , \end{aligned} \tag{6.13}$$

and

$$-\rho\frac{\partial\tilde{\psi}}{\partial\varphi}\dot{\varphi} = \zeta_R(\mathbf{G},\mathbf{L}_p,\varphi,\dot{\varphi},\theta)\ . \tag{6.14}$$

Equation (6.14) is the equation governing the rafting kinetics.

We will further assume that the rate of dissipation due to mechanical working takes the following form:

$$\begin{aligned} \zeta_m &= \zeta_m^1 + \zeta_m^2 \\ &= \mathbf{D}_p\cdot\mathbf{K}\mathbf{D}_p + \eta_2\mathbf{W}_p\cdot\mathbf{W}_p\ , \end{aligned} \tag{6.15}$$

Combining Eq. (6.13) with Eq. (6.15) lead us to

$$\begin{aligned} \mathbf{A}_{sym}\cdot\mathbf{D}_p &= \zeta_m^1\ , \\ \mathbf{A}_{skew}\cdot\mathbf{W}_p &= \zeta_m^2\ , \end{aligned} \tag{6.16}$$

where *sym* and *skew* denotes the symmetric and skew parts of the tensor $\mathbf{A}$.

Maximizing the rate of dissipation subject to the constraint $tr(\mathbf{D}_p) = 0$ lead us to following equations for $\mathbf{D}_p$ and $\mathbf{W}_p$:

$$\begin{aligned} \mathbf{D}_p &= \mathbf{K}^{-1}\left(\mathbf{A}_{sym} - \frac{tr(\mathbf{K}^{-1}\mathbf{A}_{sym})}{tr(\mathbf{K}^{-1}\mathbf{I})}\mathbf{I}\right)\ , \\ \mathbf{W}_p &= \frac{\mathbf{A}_{skew}}{\eta_2}\ . \end{aligned} \tag{6.17}$$

Equations (6.17) and (6.14) give us the complete set of equations for determining the evolution of natural configurations.

The framework developed in this chapter is general enough to develop models to describe the thermomechanical response of single crystal superalloys. A equation

describing the rafting kinetics has also been incorporated from a thermodynamical perspective. Forms for the rate of dissipation associated with rafting and the inelastic stored energy as a function of inelastic strain, temperature and extent of rafting need to be developed to develop specific models.

CHAPTER VII

CONCLUSIONS

A. Summary

The current work was focussed on developing a constitutive model for describing the creep of single crystal superalloys at high temperatures in the range of 700 ^{o}C to 1000 ^{o}C with emphasis on microstructure, dissipation of energy and material symmetry. The framework that has been used is general enough in that a plethora of constitutive models can be developed to describe a diverse range of material behavior. The framework is rooted in a robust thermodynamical setting and hence it is the choice to model the high temperature creep behavior of single crystal superalloys. Some of the salient features of the constitutive model and the modeling approach that has been used and the major accomplishments are as follows:

1. The constitutive model that has been developed is within a thermodynamical framework that has been put in place to describe the mechanics of bodies capable of existing in multiple stress free configurations or natural configurations. The framework is built on the idea of evolving natural configurations and maximization of the rate of dissipation. Specific choice for stored energy function and the rate of dissipation function give rise to different constitutive models which capture diverse range of material behavior. The constitutive model complies with the second law of thermodynamics through the requirement that the rate of entropy production be non negative.

2. The framework recognizes the fact that single crystals are not simple materials in the sense of Noll and takes into account the appropriate symmetry of single crystals and its evolution. For the case of single crystals, the symmetry remains

the same as the crystal is sheared since the underlying crystal lattice remains the same. This rules out modeling single crystals using the theory of simple materials. The current framework fills this lacunae and takes into account the fact that the symmetry of single crystals remains the same as the crystal undergoes inelastic deformations.

3. The current approach has definitive advantage over theories based on the notion of directors, which has certain inherent difficulties such as introduction of new balance laws containing terms which are not physically motivated. Moreover, there are difficulties with regard to specifying boundary conditions for quantities such as directors. Current approach appeals to thermodynamical quantities such as stored energy and rate of dissipation functions which can be readily measured using experiments based on calorimetry. No additional balance laws need to be introduced here and ideas associated with dislocation motion, which are very physical, are used.

4. Appropriate forms for the stored energy and the rate of dissipation function are developed in order to describe the creep behavior of single crystal superalloys. The form for the stored energy has two parts, one due to the elastic part of the deformation and the other due to the inelastic part. The form for the inelastic stored energy captures the part of mechanical work that is trapped in the dislocation networks. As pointed out earlier, models due to Lee [40], Brown *et al.* [5] and Mason *et al.* [46] account for this kind of energy storage mechanism in the body by multiplying the "plastic work" by an ad hoc factor whose value is approximately 0.8. The current work accounts for this energy storage mechanism explicitly and adopts the rigorous ideas developed by Mollica *et al.* [50]. Such an approach is especially relevant to single crystal superalloys which are

strengthened by the presence of various alloying elements (solid solution hardening) and other hardening phases such as γ' phase (precipitation hardening). A form for the rate of dissipation function is developed based on the idea of energy dissipation during a thermo-mechanical process through the movement of dislocations which are mobile.

5. The form for elastic stored energy reflects the fact that the elastic response exhibits cubic symmetry. The rate of dissipation function is chosen to be anisotropic, in that it reflects invariance to transformations that belong to the cubic symmetry group. Such a choice captures the anisotropy in the creep behavior of single crystal superalloys. Also, the symmetry of the single crystal does not change as the natural configuration is evolving.

6. The results of the model corroborate well with the experimental data for a range of temperatures and different loading orientations. The model needs to be corroborated with experimental data for the <001> and the <111> orientations. Once corroborated, the model predicts the creep strain versus time behavior for other orientations. One such comparison at 950 ^{o}C showed that the predictions of the model are reasonably close to the experimental results.

B. Recommendations for future work

The current work was first of its kind wherein creep behavior of single crystal superalloys was modeled within a three dimensional continuum mechanics based thermodynamical framework. While the model captures the creep deformation of single crystal superalloys reasonably well, there is a need to utilize the model to solve problems in a wide range of operating conditions which gas turbine blades are subject to.

Following are specific recommendations to improve or utilize the model for solving

various problems:

1. The model is used to describe the creep strain versus time behavior for different temperatures and loading orientations such as the <001>, <111> and <011> orientations. In such orientations, there is no associated rotation of crystal lattice. The model should be used to predict the creep strain versus time behavior for arbitrary orientations. Such results are of interest because manufacturing limitations does not allow the specimen to be perfectly oriented along the <001> orientation which is the desired orientation. A study of creep behavior of single crystal superalloys as a function of small misorientations away from the <001> orientation needs to be carried out. Since the deformation is such cases is three dimensional, solution using a semi-inverse method seems infeasible. However, the user subroutine developed herein can be used to carry out such an analysis.

2. The components such as gas turbine blades are manufactured in the <001> orientation since <001> is the natural grain growth direction for single crystal superalloys. The current user subroutine can be used to study the creep response of gas turbine blades loaded along the <001> orientation. These components usually have a complex shape with lot of intricate cooling channels built in to facilitate cooling of components. Such problems can be studied in commercial finite element software ABAQUS using the user defined material subroutine formulated in the current work. Also an analysis can be carried out when the loading condition is more complicated.

3. The constitutive model that has been developed in the current work is an isothermal model. The material parameters that appear in the model need to be changed with temperature. The motivation for such a constitutive model is the fact that the creep experiments are carried out at constant temperature.

While we have presented a general thermo-mechanical model for capturing the creep behavior as a function of temperature, orientation and applied stress, we have not corroborated the model. A corroboration of such a thermo-mechanical model will lead to a unified model which can capture the creep behavior as a function of temperature, loading orientation and applied stress with a single set of material parameters. Such a thermo-mechanical model can also be incorporated in ABAQUS through a user defined material subroutine to enable three dimensional thermo-inelastic analysis of gas turbine blades.

4. The current model captures the behavior of single crystal superalloys reasonably well in the temperature range 700 ^{o}C to 1000 ^{o}C. The effect of high temperature rafting has not been explicitly incorporated by specifying an evolution equation for rafting. There are several road blocks towards such a goal. One needs to have a credible way to quantify the amount of rafting that has taken place, something which has not been done. The other limitation is that the effect rafting has on dislocation motion is not clearly understood although the rule of thumb is that at temperatures beyond 1000 ^{o}C, rafting improves the creep strength in single crystal nickel based superalloys. The current thermodynamical framework is well suited to come up with an evolution equation for rafting and its effect on dislocation motion. Although we have presented a theoretical framework to incorporate the effect of rafting and the evolution of rafts, specific models need to be developed.

REFERENCES

[1] R. J. Asaro, "Micromechanics of cyrstals and polycrystals," *Advances in Applied Mechanics*, vol. 23, pp. 1–115, 1983.

[2] A. Bertram and J. Olschewski, "Anisotropic creep modelling of the single crystal superalloy SRR99," *Computational Materials Science*, vol. 5, pp. 12–16, 1996.

[3] M. B. Bever, D. L. Holt, and A. L. Tichener, "Stored energy of cold work," *Progress in Materials Science*, vol. 17, pp. 5–177, 1972.

[4] B. A. Bilby, "Continous distribution of dislocations," in *Solid Mechanics*, I. Sneddon and R. Hill, Eds. Amsterdam: North-Hollands, 1960.

[5] S. B. Brown, K. H. Kim, and L. Anand, "An internal variable constitutive model for hotworking of metals," *International Journal of Plasticity*, vol. 5, pp. 95–130, 1989.

[6] G. Bruno, B. Schonfeld, and G. Kostorz, "Lattice misfit in CMSX-4 like Nickel-base superalloys and its temperature dependence," *Zeitschrift Fur Metallkunde*, vol. 94, no. 1, pp. 12–18, Jan. 2003.

[7] J. Y. Buffiere and M. Ignat, "A dislocation based criterion for the raft formation in nickel-based superalloys single-crystals," *Acta Metallurgica et Materialia*, vol. 43, no. 5, pp. 1791–1797, May 1995.

[8] P. Caron and T. Khan, "Improvement of creep strength in a Nickel-base single-crystal super-alloy by heat-treatment," *Materials Science and Engineering*, vol. 61, no. 2, pp. 173–184, 1983.

[9] P. Caron, T. Khan, and Y. G. Nakagawa, "Effect of orientation on the intermediate temperature creep behavior of Ni-base single crystal superalloys," *Scripta Metallurgica*, vol. 20, pp. 499–502, 1986.

[10] C. Carry and J. L. Strudel, "Apparent and effective creep parameters in single-crystals of a Nickel-base superalloy .1. incubation period," *Acta Metallurgica*, vol. 25, no. 7, pp. 767–777, 1977.

[11] C. Carry and J. L. Strudel, "Apparent and effective creep parameters in single-crystals of a Nickel-base super-alloy .2. secondary creep," *Acta Metallurgica*, vol. 26, no. 5, pp. 859–870, 1978.

[12] J. L. Chaboche, "Time-independent constitutive theories for cyclic plasticity," *International Journal of Plasticity*, vol. 2, no. 2, pp. 149–188, 1986.

[13] J. L. Chaboche, "Cyclic viscoplastic constitutive equations. part i: A thermodynamically consistent formulation," *Journal of Applied Mechanics*, vol. 60, pp. 813–821, 1993.

[14] J. L. Chaboche, "Cyclic viscoplastic constitutive equations. part ii: Stored energy - comparison between models and experiments," *Journal of Applied Mechanics*, vol. 60, pp. 822–828, 1993.

[15] J. C. Chang and S. M. Allen, "Elastic energy changes accompanying γ' rafting in Nickel-base superalloys," *Journal of Materials Research*, vol. 6, no. 9, pp. 1843–1855, Sep. 1991.

[16] A. Coujou, M. Benyoucef, M. Legros, and N. Clement, "Role of the γ/γ' interface on the mechanical properties of single crystals Nickel base superalloys," *Solid State Phenomena*, vol. 60, pp. 185–200, 1998.

[17] M. J. Donachie and S. J. Donachie, *Superalloys*. Materials Park, Ohio: ASM International, 2002.

[18] M. Durand-Charre, *The Microstructure of Superalloys*. Amsterdam: Gordon and Breach Science Publishers, 1997.

[19] B. F. Dyson, "Creep and fracture of metals: mechanisms and mechanics," *Revue de Physique Appliquee*, vol. 23, pp. 605–613, 1988.

[20] B. F. Dyson and M. Mclean, "Particle-coarsening, σ_o and tertiary creep," *Acta Metallurgica*, vol. 31, pp. 17–27, 1983.

[21] C. Eckart, "The thermodynamics of irreversible processes. iv. the theory of elasticity and anelasticity," *Physical Review*, vol. 73, pp. 373–382, 1948.

[22] J. D. Eshelby, "The continuum theory of lattice defects," in *Solid State Physics*, F. Seitz and D. Turnbull, Eds. New York: Academic Press, 1956.

[23] J. A. Ewing and W. Rosenhain, "The crystalling structure of metals," *Philosophical Transactions of the Royal Society, London. Series A*, vol. 193, pp. 353–375, 1920.

[24] J. Gayda and R. A. Mackay, "Analysis of γ' shape changes in a single-crystal Ni-base superalloy," *Scripta Metallurgica*, vol. 23, no. 11, pp. 1835–1838, Nov. 1989.

[25] J. Gayda and D. J. Srolovitz, "A monte-carlo-finite element model for strain-energy controlled microstructural evolution - rafting in superalloys," *Acta Metallurgica*, vol. 37, no. 2, pp. 641–650, Feb. 1989.

[26] R. N. Ghosh, R. V. Curtis, and M. Mclean, "Creep deformation of single crystal superalloys-modeling the crystallographic anisotropy," *Acta Metallurgica et Materialia*, vol. 38, no. 10, pp. 1977–1992, Oct. 1990.

[27] R. N. Ghosh and M. Mclean, "Modeling the orientation dependence of tertiary creep in single crystal superalloy," *Scripta Metallurgica*, vol. 23, pp. 1301–1306, 1989.

[28] J. J. Gilman, *Micromechanics of Flow in Solids*. New York: McGraw-Hill, 1969.

[29] A. E. Green and P. M. Naghdi, "On thermodynamics and the nature of the second law," *Proceedings of the Royal Society of London Series A*, vol. 357, pp. 253–270, 1977.

[30] S. S. K. Gunturi, D. W. Maclachlan, and D. M. Knowles, "Anisotropic creep in CMSX-4 in orientations distant from <001>," *Materials Science and Engineering*, vol. A289, pp. 289–289, 2000.

[31] K. S. Havner, *Finite Plastic deformation of crystalline solids*. Cambridge: Cambridge University Press, 1992.

[32] P. J. Henderson and J. Lindblom, "High temperature creep in a <001> single crystal Nickel-base superalloy," *Scripta Materialia*, vol. 37, no. 4, pp. 491–496, 1997.

[33] M. Ignat, J. Y. Buffiere, and J. M. Chaix, "Microstructures induced by a stress gradient in a Nickel-based superalloy," *Acta Metallurgica et Materialia*, vol. 41, no. 3, pp. 855–862, Mar. 1993.

[34] W. C. Johnson, "On the elastic stabilization of precipitates against coarsening under applied load," *Acta Metallurgica*, vol. 32, no. 3, pp. 465–475, 1984.

[35] W. C. Johnson, M. B. Berkenpas, and D. E. Laughlin, "Precipitate shape transitions during coarsening under uniaxial-stress," *Acta Metallurgica*, vol. 36, no. 12, pp. 3149–3162, 1988.

[36] M. Kamlah and P. Haupt, "On the macroscopic description of stored energy and self heating during plastic deformation," *International Journal of Plasticity*, vol. 13, no. 10, pp. 893–911, 1998.

[37] B. H. Kear and B. J. Piearcey, "Tensile and creep properties of single crystals of nickel-base superalloy MAR-M200," *Transactions of the Metallurgical Society of AIME*, vol. 239, no. 8, pp. 1209–1215, 1967.

[38] K. Kondo, "On the analytical and physical foundation of the theory of dislocations and yielding by the differential geometry of continua," *International Journal of Engineering Science*, vol. 2, pp. 219–251, 1964.

[39] E. Kröner, "Alleganeine kontinuumstheorie der verzetsmugen and eigenspannuugen," *Archive for Rational Mechanics and Analysis*, vol. 4, pp. 273–334, 1960.

[40] E. H. Lee, "Elastic-plastic deformation at finite strains," *Journal of Applied Mechanics*, vol. 36, pp. 1–6, 1969.

[41] G. R. Leverant and H. B. Kear, "The mechanism of creep in gamma prime precipitation-hardened nickel-base alloys at intermediate temperatures," *Metallurgical Transactions*, vol. 1, no. 2, pp. 491–498, 1970.

[42] G. R. Leverant, H. B. Kear, and J. M. Oblak, "Creep of precipitation-hardened Nickel-base alloy single-crystals at high-temperatures," *Metallurgical Transactions*, vol. 4, no. 1, pp. 335–362, 1973.

[43] R. A. MacKay and R. D. Maier, "The influence of orientation on the stress rupture properties of nickel-base superalloy single crystals," *Metallurgical Transactions A*, vol. 13A, pp. 1747–1754, 1982.

[44] D. W. Maclachlan and D. M. Knowles, "The effect of material behaviour on the analysis of single crystal turbine blades: Part I-material model," *Fatigue and Fracture of Engineering Materials and Structures*, vol. 25, pp. 385–398, 2002.

[45] D. W. Maclachlan, L. W. Wright, S. Gunturi, and D. M. Knowles, "Constitutive modelling of anisotropic creep deformation in single crystal blade alloys SRR99 and CMSX-4," *International Journal of Plasticity*, vol. 17, pp. 441–467, 2001.

[46] J. J. Mason, A. J. Rosakis, and G. Ravichandran, "On the strain and strain rate dependence of the fraction of plastic work converted to heat: an experimental study using high speed infrared detectors and the Kolsky bar," *Mechanics of Materials*, vol. 17, pp. 135–145, 1994.

[47] N. Matan, D. C. Cox, P. Carter, M. A. Rist, C. M. F. Rae, and R. C. Reed, "Creep of CMSX-4 superalloy single crystals: Effects of misorientation and temperature," *Acta Materialia*, vol. 47, no. 5, pp. 1549–1563, 1999.

[48] N. Matan, D. C. Cox, C. M. F. Rae, and R. C. Reed, "On the kinetics of rafting in CMSX-4 superalloy single crystals," *Acta Materialia*, vol. 47, no. 7, pp. 2031–2045, 1999.

[49] M. McLean, *Directionally Solidified Materials for High Temperature Service*. London: The Metals Society, 1983.

[50] F. Mollica, K. R. Rajagopal, and A. R. Srinivasa, "The inelastic behavior of metals subject to loading reversal," *International Journal of Plasticity*, vol. 17, pp. 1119–1146, 2001.

[51] J. Murali Krishnan and K. R. Rajagopal, "Thermodynamic framework for the constitutive modeling of asphalt concrete: Theory and applications," *Journal of Materials in Civil Engineering*, vol. 16, no. 2, pp. 155–166, 2004.

[52] F. R. N. Nabarro, *Theory of Crystal Dislocations*. New York: Dover Publications, 1987.

[53] F. R. N. Nabarro, "The superiority of superalloys," *Materials Science and Engineering A*, vol. 184, no. 2, pp. 167–171, Aug. 1994.

[54] F. R. N. Nabarro, C. M. Cress, and P. Kotschy, "Thermodynamic driving force for rafting in superalloys," *Acta Materialia*, vol. 44, no. 8, pp. 3189–3198, Aug. 1996.

[55] F. R. N. Nabarro and H. L. De Villers, *The Physics of Creep*. London: Tylor & Francis, 1995.

[56] P. M. Naghdi and A. R. Srinivasa, "A dynamical theory of structured solids. i. Basic developments," *Philosophical Transactions of the Royal Society, London. Series A*, vol. 345, pp. 425–458, 1993.

[57] P. M. Naghdi and A. R. Srinivasa, "Characterization of dislocations and their influence on plastic deformation in single crystals," *International Journal of Engineering Science*, vol. 32, no. 7, pp. 1157–1182, Jul. 1994.

[58] M. V. Nathal, R. A. Mackay, and R. G. Garlick, "Temperature-dependence of γ-γ' lattice mismatch in Nickel-base superalloys," *Materials Science and Engineering*, vol. 75, no. 1-2, pp. 195–205, 1985.

[59] D. W. Nicholson, "Large deformation theory of coupled thermoplasticity including kinematic hardening," *Acta Mechanica*, vol. 136, pp. 223–241, 1999.

[60] W. Noll, "On the foundations of the mechanics of continous media," Carnegie Institute of Technology, Department of Mathematics, Report Volume 17, 1957.

[61] G. R. Piercy, R. W. Cahn, and A. H. Cottrell, "A study of primary and conjugate ship in crystals of alpha-brass," *Acta Metallurgica*, vol. 3, pp. 332–338, 1955.

[62] G. R. Piercy, R. W. Cahn, and A. H. Cottrell, "Polyslip in polycrystals," *Acta Metallurgica*, vol. 6, pp. 85–94, 1958.

[63] A. Pineau, "Influence of uniaxial stress on morphology of coherent precipitates during coarsening - elastic energy considerations," *Acta Metallurgica*, vol. 24, no. 6, pp. 559–564, 1976.

[64] T. M. Pollock and A. S. Argon, "Directional coarsening in Nickel-base single crystals with high volume fractions of coherent precipitates," *Acta Metallurgica et Materialia*, vol. 42, no. 6, pp. 1859–1874, 1994.

[65] S. C. Prasad, I. J. Rao, and K. R. Rajagopal, "A continuum model for the creep of single crystal nickel-base superalloys," *Acta Materialia*, vol. 53, no. 3, pp. 669–679, 2005.

[66] W. Qi and A. Bertram, "Damage modeling of the single crystal superalloy SRR99 under monotonous creep," *Computational Materials Science*, vol. 13,

no. 4-5, pp. 132–141, 1998.

[67] K. R. Rajagopal, "Multiple configurations in continuum mechanics," Institute for Computational and Applied Mechanics, University of Pittsburgh, Pittsburgh, Pa, Report Volume 6, 1995.

[68] K. R. Rajagopal, "Art, craft and philosophy of modeling," In preperation.

[69] K. R. Rajagopal and N. Chandra, "A thermodynamic framework for the superplastic response of materials," *Materials Science Forum*, vol. 357, pp. 261–271, 2001.

[70] K. R. Rajagopal and A. R. Srinivasa, "On the inelastic behavior of solids-part i: Twinning," *International Journal of Plasticity*, vol. 11, pp. 653–678, 1995.

[71] K. R. Rajagopal and A. R. Srinivasa, "Inelastic behavior of materials-part ii: Energetics associated with discontinuous deformation twinning," *International Journal of Plasticity*, vol. 13, pp. 1–35, 1997.

[72] K. R. Rajagopal and A. R. Srinivasa, "Mechanics of the inelastic behavior of materials. part i. theoretical underpinnings," *International Journal of Plasticity*, vol. 14, pp. 945–967, 1998.

[73] K. R. Rajagopal and A. R. Srinivasa, "Mechanics of the inelastic behavior of materials. part ii. inelastic response." *International Journal of Plasticity*, vol. 14, pp. 969–995, 1998.

[74] K. R. Rajagopal and A. R. Srinivasa, "On the thermodynamics of shape memory wires," *International Journal of Plasticity*, vol. 50, pp. 459–496, 1999.

[75] K. R. Rajagopal and A. R. Srinivasa, "A thermodynamic framework for rate type fluid models," *Journal of Non-Newtonian Fluid Mechanics*, vol. 88, pp. 207–227, 2000.

[76] K. R. Rajagopal and A. R. Srinivasa, "Modeling anisotropic fluids within the framework of bodies with multiple natural configurations," *Journal of Non-Newtonian Fluid Mechanics*, vol. 99, pp. 109–124, 2001.

[77] K. R. Rajagopal and A. R. Srinivasa, "On the thermomechanics of materials that have multiple natural configurations. part i: Viscoelasticity and classical plasticity," *Zeitschrift Fur Angewandte Mathematik Und Physik*, vol. 55, pp. 861–893, 2004.

[78] K. R. Rajagopal and A. R. Srinivasa, "On the thermomechanics of materials that have multiple natural configurations. part ii: Twinning and solid to solid phase transformation," *Zeitschrift Fur Angewandte Mathematik Und Physik*, vol. 55, pp. 1074–1093, 2004.

[79] K. R. Rajagopal and A. R. Srinivasa, "On thermomechanical restrictions of continua," *Proceedings of the Royal Society of London Series A*, vol. 460, pp. 631–651, 2004.

[80] K. R. Rajagopal and L. Tao, *Mechanics of Mixtures*. Singapore: World Scientific, 1996.

[81] K. R. Rajagopal and A. S. Wineman, "A constitutive equation for non-linear solids which undergo deformation induced microstructural changes," *International Journal of Plasticity*, vol. 8, pp. 385–395, 1992.

[82] I. J. Rao, J. D. Humphrey, and K. R. Rajagopal, "Biological growth and remodeling: A uniaxial example with application to tendon and ligaments," *CMES-Computer Modeling in Engineering & Sciences*, vol. 4, no. 3-4, pp. 439–455, Jun. 2003.

[83] I. J. Rao and K. R. Rajagopal, "Thermomechanical framework for the crystallization of polymers," *Zeitschrift Fur Angewandte Mathematik Und Physik*, vol. 53, pp. 365–406, 2002.

[84] R. C. Reed, N. Matan, D. C. Cox, M. A. Rist, and C. M. F. Rae, "Creep of CMSX-4 superalloy single crystals: Effects of rafting at high temperature," *Acta Materialia*, vol. 47, no. 12, pp. 3367–3381, 1999.

[85] R. E. Reed-Hill and R. Abbaschian, *Physical Metallurgy Principles*. Boston: PWS-KENT, 1992.

[86] V. Sass, U. Glatzel, and M. Feller-Kniepmeier, "Creep anisotropy in the monocrystalline Nickel-base superalloy CMSX-4," in *Superalloys 1996*, R. D. Kissinger, D. J. Deye, D. L. Anton, A. D. Cetel, M. V. Nathal, T. M. Pollock, and D. A. Woodford, Eds. Warrendale, PA: The Minerals, Metals and Materials Society, 1996, pp. 283–290.

[87] F. Schubert, G. Fleury, and T. Steinhaus, "Modeling of the mechanical behavior of the single- crystal turbine alloy CMSX-4 during thermomechanical loading," *Modelling and Simulation in Materials Science and Engineering*, vol. 8, pp. 947–957, 2000.

[88] D. Siebörger, H. Knake, and U. Glatzel, "Temperature dependence of the elastic moduli of the nickel-base superalloy CMSX-4 and its isolated phases," *Materials Science and Engineering A*, vol. 298, pp. 26–33, 2001.

[89] S. Socrate and D. M. Parks, "Numerical determination of the elastic driving force for directional coarsening in Ni-superalloys," *Acta Metallurgica et Materialia*, vol. 41, no. 7, pp. 2185–2209, Jul. 1993.

[90] J. Svoboda and P. Lukas, "Model of creep in <001>-oriented superalloy single crystals," *Acta Materialia*, vol. 46, no. 10, pp. 3421–3431, 1998.

[91] G. I. Taylor, "The mechanisms of plastic deformation of crystals," *Philosophical Transactions of the Royal Society, London. Series A*, vol. 145, pp. 362–387, 1926.

[92] G. I. Taylor and C. F. Elam, "The distortion of an aluminum crystal during tensile test," *Philosophical Transactions of the Royal Society, London. Series A*, vol. 102, pp. 643–667, 1923.

[93] G. I. Taylor and C. F. Elam, "The plastic extension and fracture of aluminum crystals," *Philosophical Transactions of the Royal Society, London. Series A*, vol. 108, pp. 28–51, 1925.

[94] G. I. Taylor and C. F. Elam, "The distortion of iron crystals," *Philosophical Transactions of the Royal Society, London. Series A*, vol. 112, pp. 337–361, 1926.

[95] J. K. Tien and S. M. Copley, "Effect of orientation and sense of applied uniaxial stress on morphology of coherent γ' precipitates in stress annealed Nickel-base superalloy crystals," *Metallurgical Transactions*, vol. 2, no. 2, pp. 543–553, 1971.

[96] J. K. Tien and S. M. Copley, "Effect of uniaxial stress on periodic morphology of coherent gamma-prime precipitates in Nickel-base superalloy crystals," *Metallurgical Transactions*, vol. 2, no. 1, pp. 215–219, 1971.

[97] C. Truesdell and W. Noll, *The Non-Linear Field Theories of Mechanics*, 1st ed. Berlin: Springer-Verlag, 1965.

[98] H. G. Van Buereu, *Imperfections in crystals*, 2nd ed. Amsterdam: North Holland, 1961.

[99] M. Veron, Y. Brechet, and F. Louchet, "Directional coarsening of Ni-based superalloys: Computer simulation at the mesoscopic level," *Acta Materialia*, vol. 44, no. 9, pp. 3633–3641, Sep. 1996.

[100] G. A. Webster and C. P. Sullivan, "Some effects of temperature cycling on creep behaviour of a Nickel-base alloy," *Journal of Institute of Metals*, vol. 95, pp. 138–142, 1967.

[101] R. O. Williams, "Stored energy and release kinetics in Lead, Aluminum, Silver, Nickel, Iron and Zirconium after deformation," *Transactions of the Metallurgical Society of AIME*, vol. 224, pp. 719–726, 1962.

[102] A. S. Wineman and K. R. Rajagopal, "On constitutive theory for materials undergoing microstructural changes," *Archives of Mechanics*, vol. 42, pp. 53–75, 1990.

VITA

Sharat Chand Prasad was born on March 22, 1979 in Mumbai (erstwhile Bombay), India. He obtained his Bachelor of Technology degree in mechanical engineering from the prestigious Indian Institute of Technology at Kanpur, India. He came to College Station, Texas in the fall of 2001 to pursue his graduate studies at Texas A&M University. He received his Master of Science degree in mechanical engineering in December 2002. The title of his Master of Science thesis was "A study of the effect of boundary conditions and drag force on the diffusion of a Newtonian fluid through a non-linearly elastic solid". During his stay in the graduate school, he has worked on a diverse range of engineering projects and has submitted/published several research publications in reputed journals. He can be reached at the following Email address: sharat_cp@yahoo.com

His permanent address is:

c/o Shri Moti Chand Prasad

House # 3, Mangalam Vihar

Arrah Garden Road, Jagdeo Path

Patna, Bihar, India

Pin: 800014

The typist for this thesis was Sharat Chand Prasad.